Master's thesis

NTNU
Norwegian University of Science and Technology
Department of Marine Technology

Tor Magnus Konradsen Aarskog

Analysis of Full Scale Structural Vibrations on S.A. Agulhas II

Master's thesis in Nordic Master In Maritime Engineering - Ocean Construction

Supervisor: Amir R. Nejad

August 2020

NTNU
Norwegian University of Science and Technology

Tor Magnus Konradsen Aarskog

Analysis of Full Scale Structural Vibrations on S.A. Agulhas II

Master's thesis in Nordic Master In Maritime Engineering - Ocean Construction
Supervisor: Amir R. Nejad
August 2020

Norwegian University of Science and Technology
Department of Marine Technology

NTNU
Norwegian University of
Science and Technology

NTNU – Trondheim
Norwegian University of
Science and Technology
Department of Marine Technology

MSC THESIS IN MARINE TECHNOLOGY
SPRING 2020

Modelling and Analysis of Full Scale Structural Vibration of S.A. Agulhas II

Tor Magnus Konradsen Aarskog

Background:

During July 2019 full scale measurements on the S.A. Agulhas II. was performed. The data collected consists of 28 accelerometers at various locations in the hull and superstructure of the vessel.

The aim of the project is to improve our understanding of structural responses and vibration propagation due to different environmental excitations (wave, ice impact), slamming, and propeller harmonics. Investigate the relationship between peak acceleration levels, wave state, ship velocity and heading. Develop a technique for investigations when dealing with big data. The candidate is expected to employ state-of-the art tools and methods for data analysis and further build a model (physical or data driven) to estimate the responses.

Assignment:

The following tasks should be addressed in the thesis work:
1. Carry out a literature review on ship vibration, measurement techniques, and state-of-the-art analysis methods.

2. Carry out a literature review on signal processing techniques.

3. Select a set of data in different environmental conditions (calm sea, medium to high and severe) and carry both time and frequency domain analysis to investigate the responses at different measurement points.

4. Evaluate and discuss possible correlations.

5. Develop a model for slamming detection.

6. Discuss the results, conclude the work and give recommendations for future work.

7. Write the MSc thesis report.

In the thesis the candidate shall present his/her personal contribution to the resolution of problem within the scope of the thesis work.

Theories and conclusions should be based on mathematical derivations and/or logic reasoning identifying the various steps in the deduction.

The candidate should utilize the existing possibilities for obtaining relevant literature.

The thesis should be organized in a rational manner to give a clear exposition of results, assessments, and conclusions. The text should be brief and to the point, with a clear language. Telegraphic language should be avoided.

The thesis shall contain the following elements: A text defining the scope, preface, list of contents, summary, main body of thesis, conclusions with recommendations for further work, list of symbols

Dedicated to my family, friends and inspirational professors for their support and motivation through my studies.

Summary

A ship is exposed to external and internal forces, exciting the ship with a variety in force magnitude and frequency. The oscillatory forces inflict vibrations trough the structure which can lead to fatigue and reduce the operational life of the vessel. As ship design is becoming more complex so does the task of mapping and monitoring the vibrations. Hull condition monitoring allows ship owners to better protect their assets and ship masters to make decisions based on the reality of situations. Methods for controlling and reporting vibrations has been developed by International standards. The standards are applied by classification societies in their guidelines and in issuing class notation.

Full scale measurements were subjected to frequency and time domain analysis. The analysis was performed on the basis of improving our understanding of structural response from environmental and internal excitation sources. The relationship between acceleration levels, wave state, ship velocity and relative heading towards waves was examined. The largest acceleration levels was experienced in the bow, followed by the aft-body. A clear correlation was observed between acceleration amplitude and vessel velocity. Further on the largest mitigating for bow slamming was seen to be relative heading, although certain heading changes could increase stern slamming in stationary conditions.

To understand how slamming events affected the structure, an algorithm for detecting slamming events was developed and applied for a variety of study cases. A comparison between results and previous studies on the vessel was made. Results showed that the structure was excited by higher vibration modes. Differences in structural excitation between open water navigation and ice navigation was made clear, observing that ice navigation excited higher vibration modes with a larger degree.

Sammendrag

Et skip er utsatt for eksterne og interne krefter som eksiterer skipet med en variasjon av kraft størrelse og frekvens. Den oscillerende kraften medfører vibrasjoner gjennom strukturen som kan lede til utmattelse gjennom sprekkpropagasjon og på den måten redusere den operative levetiden til fartøyet. Å begrense vibrasjoner starter med design og skipsbyggingssektoren er i konstant søking etter forbedrede metoder for å forutsi vibrasjonsnivået. Ettersom design av skip blir mer kompleks, gjelder tilsvarende for kartlegging og overvåking av vibrasjoner. Internasjonale standarder har blitt utviklet, innpasset i protokoller fra klassifikasjonsselskap som utsteder klassenotasjon. Nye metoder for skrogbetinget overvåking gjør det mulig for skipseiere å bedre beskytte sine verdier og mulig for skipskapteiner å fatte beslutninger basert på situasjonsrealiteter.

Fullskala målinger ble underkastet frekvens- og tidsdomeneanalyse. Overføringen av målinger ble presentert via nødvendig maskinvare og programvare. Analysen ble utført med det mål å oppnå forbedret forståelse av strukturelle responser fra indre eksiterende krefter og eksiterende krever fra omgivelsene. Forbindelsen mellom akselleras jonsnivået, bølgetilstand, skipets fart og relative kurs mot bølger ble undersøkt basert på toppverdiene. For å kunne forstå hvordan slamminghendelser påvirket strukturen, ble det utviklet en algoritme for å oppdage slamminghendelser og det ble gjennomført casestudier. Deretter ble det uført en sammenligning av resultat og tidligere studier av fartøyet.

Forskjeller i eksitering mellom navigering i åpent farvann og is, ble det observert hvordan navigering i is eksiterte høyere vibrasjonsmoduser. Akselleras jonsnivået mellom seksjoner var i visse tilfeller mistolket uten spesifikke mønstre. Litteraturstudier om den adverse effekten av slamming understreker behovet for en forbedret forståelse av slammingpåkjenninger og resulterende responser.

Preface

This thesis serves as the graduating assignment of the joint double master degree program ”Maritime Engineering - Ocean Construction” between Aalto University and the Norwegian University of Science and Technology (NTNU). The topic of this thesis is full scale measurements conducted onboard the polar supply and research vessel, S.A. Agulhas II. The thesis was enabled by the collaboration between NTNU and Stellenbosch University sound and vibration group. The author would like to emphasize a special gratitude to Prof. Annie Bekker, for the invitation onboard the vessel. Furthermore I would like to thank the sound and vibration group for the unique experiences shared. I would also thank my supervisors from Aalto university, Prof. Spyros Hirdaris, and NTNU, Prof. Amir R. Nejad, for their support and motivation trough my research endeavour.

Finally, I would like to thank my family and friends for all their support during my academic pursuit.

Table of Contents

List of Tables

List of Figures

Abbreviations

CDF	=	Cumulative Density Function
EEDI	=	Energy Efficiency Design Index
FFT	=	Fast Fourier Transformation
FIR	=	Finite Impulse Response
Hp	=	High-pass filtered signal
IACS	=	International Association of Classification Societies
Lp	=	Low-pass filtered signal
OMA	=	Operational Modal Analysis
PDF	=	Probability Density Function
PSD	=	Power Spectral Density
rpm	=	Rotations Per Minute
r.m.s	=	Root Mean Square
VIBR	=	DNV GL Vibration class notation

Chapter 1

Introduction

The topic of this thesis is about hull condition monitoring and the analysis of acceleration data gathered from the South African polar supply and research vessel, S.A. Agulhas II on her round trip voyage from Cape Town to the coast of Antarctica. The following sections explains the research motivation, objectives and structure of the report.

1.0.1 Background

A ship is exposed to external and internal oscillatory forces forces. These forces cause structural vibrations through the structure which can lead to fatigue failure thus reducing the operational life of the vessel. Other complications relate to failure of essential structural components which may impair structural integrity and lead to hazardous situations. They may in addition impair the functionality of systems required to safely operate the vessel. Uncontrolled vibrations and the accompanying noise can be disturbing to crew and passengers, leading to human fatigue, operator mistakes and poor decision making.

Ship specifications are given by costumers, usually in relation to mission and main dimensions. The contractors role is to deliver a ship that meets the described demand and fulfills the necessary requirements given by regulations and Classification Societies. Emphasis is placed on the design in ways to meet these requirements. The usage of reference ships is common, where the design from previously constructed ships is altered to meet the desired ship specifications. Ship construction methods have been established through decades of trial and error leading to efficient construction techniques, maximizing the structural integrity in terms of material usage. As the energy efficiency design index, $EEDI$, gives stricter requirements in the decades to come, alterations to construction methods are probable. High strength steel introduces benefits in this regard, as less steel is required to gain necessary strength. In addition, experiments have shown a significant increased fatigue

life of high strength steel (Lillemäe-Avi et al., 2018). The use of high strength steel is however considered as a significant contributing factor to fatigue. Beghin (2010) explains it as the fatigue of welded components doesn't improve with material property. High strength steel can also introduce problems in terms of vibration and noise, as they are closer related to the geometry of structural components, i.e, thinner structures, can lead to increased displacement. Vibration requirements is an important factor to include in the design of ships. Thus an important factor to be included in the contract between purchaser and ship builder, justifying the necessity of a vibration class notation. International standards regarding ship vibrations originating from machinery and propulsion has been established and are used by Classification Societies as a guideline in establishing their regulations.

Vibration response can be divided into global, sub-structure and local vibrations. The international standard for shipboard vibration, ISO 20283-2, defines global vibrations as deflection shapes of the entire structure. Sub-structures involve parts of the superstructure, such as the wheelhouse but also deck equipment such as cranes and masts. They includes sub-systems such as the main engines and its subsystems, e.g. propulsive engines and shaft line. Local vibrations are seen on the individual structural elements, which combined make up the hull girder, sub-structure or sub-systems (Soal and Bekker, 2014). Lloyds register (2006) states in their guidance notes for ship vibration and noise, that investigation of hull girder vibration is fundamental to identification of the possible causes of high shipboard vibration.

Accelerometers can be used to capture a vessels global and local vibrations levels. Specifying acceleration design values, either for structure, equipment or for human comfort. The data can be monitored in real time by the ship master in order to manage/maintain acceleration levels under certain limits. Ship master use the information to adjust relative ship heading to mitigate acceleration levels during dynamic positioning. In rough weather velocity and course adjustments may be necessary to reduce slamming probability. In the world of shipping, where time is a scarce commodity, such course adjustments may reduce operation time. Furthermore, cargo and container vessels can take mitigating measures based on cargo fragility. Such big data along with environmental monitoring of wave state could prove valuable in our further understanding of ship design and technology (Shan Wang, 2015).

1.0.2 Objectives

The objective of the thesis has been to study and improve our understanding of ship structural response from external and internal excitation sources. Analysis has been conducted on accelerometer data gathered from full scale measurements on the S.A. Agulhas II. To achieve these goals, the following steps have been taken.

1. literature review on ship vibration, measurement techniques and state-of-the-art analysis methods and its industry applications.
2. Investigations on processing methods to interpret data.
3. Selection of data in different environmental conditions, including ice and open water navigation in wave states deemed as calm, medium and severe. Frequency and time domain analysis have been performed to investigate structural responses at different measurement points.
4. Study the affect of wave state, ship velocity and ship heading on structural response.
5. Develop a slamming detection algorithm for dealing with big data. Furthermore, structural response to slamming has been investigated.

1.0.3 Structure of the Report

Chapter 2 contains a literature review on slamming and investigates current methods developed for measuring structural response. Two case studies are presented, one of which include previous investigations conducted on the S.A Agulhas II. International standards and Classification Societies approach for handling vibrations are reviewed and including the benefits of condition monitoring.

Chapter 3 explains the basic theory of vibrations, presenting the equation of motion in different states. Typical ship vibration sources are identified and explained. For statistical analysis the term stochastic process is introduced. Theory that lay the foundation for frequency analysis is explained along with important theorems for signal processing that has been applied.

Chapter 4 introduces the case study which is to be analysed. A brief introduction is given to the vessel and the voyage. The sensor layout for accelerometers is shown. Chapter 5 continues with the analysis. Explaining the signal processing steps taken and how frequency and time domain analysis was performed. Results are presented separately for frequency and time domain. The results are presented with comparison to previous investigations performed on the vessel. Three slamming cases are investigated in detail and discussed. Peak analysis investigated further the relation between vessel velocity, wave state and the affect of ship heading on acceleration amplitudes. Peak analysis lays the basis for a localized damping evaluation. The last section of chapter 5 discusses statistical features seen before concluding remarks and further work is made in chapter 6.

Chapter 2

Literature review

Whipping is classified as a transient response, with decrementale decay of the response due to structural damping. It occurs as a result from slamming or wave impacts. Whipping is identified as it excites higher order of vibration modes, where 2-node vertical bending mode is predominant (Faltinsen, 2005). Magnitude and duration of whipping is dependent on the pressure time history and damping of the structure. Whipping can cause both global and local damages to the structure. Faltinsen (2005) discussed the importance of hydro elasticity for global vibrations, but includes that it may also be important for the local occurring vibrations. Therefor for proper analysis of slamming must be analysed in terms of hydrodynamics and structural mechanics.

Springing is a conventionally defined as a stationary resonance vibration. It is caused by linear and non-linear excitation, where the frequency of passing waves are close to the 2-node bending mode of the hull girder (Faltinsen, 2005). The Vibration amplitude will vary correspondingly with the waves characteristics. Whipping and springing rarely occur alone, and due to low damping of the structure, they are hard to distinguish from another. Their combined effect can be detrimental to the ships fatigue life. However, quantifying their contribution to the extent of sensible implementation to the design process is still in need for further research (Hirdaris and Temarel, 2009).

Faltinsen (2005) showed that ships navigating in head seas, exposed to slamming are dominated by the 2-node vertical bending, termed whipping. Slamming was seen to be dependent on vessel velocity, therefor recommending to reduce velocity in conditions where three slams occur for every 100 passing wave. There is a need to establish certain criterion's for a ship master to make voluntary speed reductions. Storhaug (2007a) referees in his dissertation to the classification society, American Bureau of Shipping, guidance notes of hull condition monitoring. Where stated that a significant slam can be classified as standard deviation of acceleration exceeding $0.4g$ (ABS, 1995). Storhaug applied this

criterion and although no recordings exceeded the threshold value, severe slamming events was registered. An argument was made that a new criterion should be developed founded on peak values compared to a design value unique to the ship .

Soares (2015) investigated the transient response of ship hulls to wave impact. From his studies he proposed that slamming is the sum of two contributions. One from impact of the hull with the ocean surface, containing characteristics of a large pressure peak with a duration of milliseconds. The second contribution comes from the rate of change of hydrodynamic momentum as the hull enters into the water. (Shan Wang, 2015)

Shan Wang (2015) studied the probability of slamming occurrence on a chemical tanker in an irregular sea-state using numerical data and comparing with experimental models. Ship motions was calculated in three irregular sea-states using a fully nonlinear time domain strip theory approach. The irregular waves were described by a sea spectra, assuming that maximum vertical velocity relative to sea surface follows a Rayleigh distribution, the probability of slamming was calculated by a joint probability between bow emergence and exceedance of threshold velocity. The numerical data were compared to experimental results for statistical analysis. In the study, bottom slamming occurred in extreme sea-states, and the magnitude of the slamming pressure increased with wave amplitude. Slamming pressures was greatest near the keel for non-flare bows. Slamming probability increased with increased forward velocity, as also identified by Faltinsen (2005). The momentum component of the slam was seen to be of great importance in stern slamming. Numerical and experimental data did not correspond for slamming probability, attributed to deviations in ship motion velocity. However a clear trend between peak immersion velocity and peak pressure was observed for both cases. In addition it was observed that the largest factor on the slamming pressure was caused by the rate of change of momentum as the hull immerses into the water.

This was also observed by Fonseca and Soares (2006) who studied the whipping response of vessels with large amplitude wave motions. It was seen that for a ship section with a small deadrise keel angle and a big flare, the second contribution, i.e., momentum played a larger role in the slamming pressure. The large pressure peak inflicted from a slam will in most instances give rise to a peak in acceleration.

Icebreakers slamming behavior is not as well documented as that of open water designs, naturally. But it can be speculated that the blunt bow section will behave similarly to that of an chemical tanker, i.e. greater contribution from bottom slamming. In addition, the large volume body doesn't cleave through the water as more hydrodynamic bow sections would. Therefor it is expected that it would experience large rate of change of momentum from water intrusion.

The high pressure forces from a slamming event can lead to localized structural damages. It has also been shown that the whipping response can lead to damages in the mid ship section from the resulting high stresses. From full scale measurements it has been observed that stresses resulting from whipping can attain the same level as obtained from wave induced bending stress. Despite, whipping being an transient event, long term predictions has been

observed to attain the same values of stress as still-water and bending stresses (Aertssen, 1968).

Storhaug (2007b) investigated the effect of wave induced vibration on an ore carriers 277 effective days at sea. The stress signal was filtered as:

- Noise above 2Hz was removed
- Wave damage: Constitutes signal between 0 up to 0.35Hz
- Vibration damage: constitutes signal between 0.35Hz and 2Hz

A 20 year prediction was extrapolated. During the 20 year lifespan, stresses resulting from waves was estimated up to $60 * 10^6$ cycles. The contribution from Springing and whipping could potentially add up to $300 * 10^6$. Storhaug points this out as problematic as whipping and springing is not considered to fatigue and extreme loading contributions. The study identified 56 % of fatigue damage was attributed to vibration, while the remaining damage was attributed to wave damage. Furthermore from the vibration damage, 24 % was attributed to ringing. Storhaug suggests that vibration damage should be included in the design of vessel and particularly if a ships fatigue strength is optimized for a operational area or trade. A need for more conservative rules may be justified by these findings as well as P. Lacey (1995) findings of wave bending with effects of whipping can exceed IACS bending moments requirements at wave heights of 9m.

Gunnar Lian (2016) analysed the stochastic nature of slamming loads measured under model tests from breaking waves on offshore structures. Slamming loads with a q-annual probability of exceedance were estimated using short term distribution of slamming loads and long term distribution of sea states. The study showed a large scatter between measurements and a large short term variability. Although the study was performed on a stationary structure, the relevance for applying to ships can be argued in the variability of slamming loads and its stochastic nature.

2.1 State of Art

2.1.1 Operational modal analysis

Operational modal analysis (OMA) is an efficient way of acquiring structural dynamic characteristics properties. It is developed on the principle of experimental modal analysis, where the structure is subjected to an input of known properties and measuring system response. However, due to the complexity and interaction between structure and subjected environmental load, the input is not easily quantifiable. This motivated researchers to develop techniques that identifies structure characteristics based on the response output alone. One of many benefits is that Operational modal analysis is performed in-situ and does not interfere with the daily operations. Therefore it is ideal to be used in hull condition

monitoring for vessels. Operational modal analysis is a fairly recent discipline, developed in the 1990's and the first book that specifically discussed OMA was released in 2014 (Ghalishooyan and Shooshtari, 2015).

The equations for OMA assumes a excitation of stochastic nature, that is also smooth and broad banded. The procedure is categorized into time domain, implementing correlation functions and frequency domain evaluating the relation between specified input and output power spectral densities (Ghalishooyan and Shooshtari, 2015).

One of the earliest algorithms for OMA, NExT, was developed in the 1990's and was an extension from experimental modal analysis algorithms. For identifying modal parameters NeXT applies several system identification methods such as, Ibrahim time domain, Eigensystem realization Algorithm, Polyreference time domain and Least square complex estimation. The last for mentioned is commercially known as polyMAX, a common approach used in engineering for operational modal analysis (Ghalishooyan and Shooshtari, 2015). Peeters and Van der Auwerer (2005) gives a thorough review of PolyMAX modal parameter estimation in developing stabilization diagrams for identifying modal parameters.

Bosei Maru

Gianpiero et al. (2016) performed an operational modal analysis on the vessel, Bosei Maru. Three situations was analysed; Anchor drop test, wave induced vibrations, run up and stationary speed maneuvers. A spectrogram of engine and shaft harmonic frequencies were plotted vs rotational speed of the main engines. The run-up and stationary speed maneuvers allows for plotting vibration amplitude at different frequencies against *rpm* levels of the engines in a waterfall diagram. The diagram can thereby reveal potential resonance frequencies. structural response to stochastic excitation was identified using a spectrum based OMA. The modal parameters was estimated based on cross-correlation and cross-spectra between the accelerometers. PolyMAX was applied for constructing the stabilization diagram. Attention should be placed in interpretation of modes as they be may influences by end of order effects. An example is given where the frequency of the engines at 11.3Hz may be interpreted as the 5 bending mode which is located at 11.1Hz. The results from the three different test are compared below displaying a fairly good agreement.

Table 2.1: Natural frequency comparison from test performed on Bosei Maru (Gianpiero et al., 2016)

Vibration mode	OMA run-up test [Hz]	Peak-picking anchor drop test[Hz]	Peak-picking wave impacts[Hz]
2 nodes vibration	3.36	3.67	3.24
3 nodes vibration	6.08	6.35	5.79
4 nodes vibration	9.06	9.4	8.57

S.A. Agulhas II

Omer (2016) Performed a full scale slamming investigation on the S.A. Agulhas and identified vertical operational deflection shapes, *ODS*, from both stern and bow slamming.

Slamming location was determined by identifying sensors which peaked first in time, thus being closer to the impact site. A stern slam was identified in a sea state corresponding to a wave height of 8m, resulting in a peak acceleration amplitude of $5m/s^2$. Bow sensor accordingly registered the same magnitude. Vibration modes was identified at 2.1Hz in the stern and for 2.1 and 3.7 Hz in the bow. Operational deflection shapes decayed to normal values after 20 seconds. These frequencies has been identified by the shipbuilder, STX Finland, by finite element analysis as the first and second bending modes(Omer, 2016).

The bow slam occurred with a wave height 2.5m. The peak acceleration amplitude measured in bow was $16m/s^2$. Accordingly a $7m/s^2$ was registered in the stern. The ODS returned to normal values after approximately 40 seconds. Acceleration levels in the superstructure and cargo hold was significantly lower, which Omer attributed to the stiffening effect of the superstructure.

Soal et al. (2019) performed a operational modal analysis of the S.A. Agulhas II. The ship was only subjected to excitation from ripple waves and wind. The analysis identified the first and second bending mode at frequencies of 1.94Hz and 3.4Hz which is a large

deviation to what the ODS identified in Omer (2016). This could be attributed to a change in draft. In the analysis the vessel had a draft of 6.8m while FEM analysis assumed a draft of 7.7m. The effect of added mass and wave forces are not considered. Another influence is how mooring lines would affect the measurements.

2.1.2 ISO standard

Technical committees create standards for procedures in an international collaboration. Standards are created on the basis of collecting knowledge and experience. The technical committees work is later adopted by ISO, The international organization for standardization, as standards to be followed as guidelines. Standards enable improvement through systematic comparison against theoretical predictions. In addition, standards adopt learning through previous engineering errors, and therefore allows for improved engineering. (ISO 20283-2)

ISO 20283-2 focuses on mechanical vibration originating from the power plant. The vibrations may be of local and global order. The standard however, focuses on global vibrations. The standard gives an overview to how the structures vibration behavior is collected by measurements at different locations and under different loading conditions. The goal for measurements is to determine global deflection shapes and to identify dominant excitation frequencies arising from machinery. It is recommended to perform measurements in order to validate theoretical predictions. As this is done, the results can be compared with similar reference ship based on their measurements and theoretical predictions. This allows for validation and to determine vibration deficiencies.

The measurements should be done in as similar conditions to that of the operational profile. ISO 20283-2 states that the water depth shall be at least more than 5 times the ship draught. presumably to avoid hydrodynamic and blockage effects experienced at low water depths. Furthermore it is stated that sea state shall be under a Beaufort scale of 3. If the ladder requirement is not met, this must be reported consequently with a signal analysis section with high-pass filtered measurement data. To accurately depict natural frequencies, ship loading should be close to the operational condition. For ships with large deviations in mass, separate measurements should be done for the various loading conditions. The natural vibration frequency and mode shape will change with velocity of the vessel, therefore it is recommended to to perform measurements between $30 - 100$ % of maximum continuous power. A sequence is recommended in ISO 20283-4 to determine main operational vibration deflection shapes.

Vibrations can be measured by displacement, acceleration and velocity. The international standards tends to measure vibrations in velocity with mm/s, correspondingly adopted by many of the classification societies. For measurements on structural components the frequency can give an indication on what kind of measurements that should be performed. In the low frequency range, accelerations are usually low but higher displacements are expected. In a higher frequency range, displacements are expected to be lower, thus measuring acceleration can be better suited. However, it depends on the limiting criteria and the functionality of the component being measured, as the overall aim is to limit structural

vibration to limit fatigue propagation (DNVGL, 2011).

Velocity and acceleration requirements are given as the root mean square of the signal, *r.m.s*. The relationship between *r.m.s* and the average value is found by the relation seen in Equation 2.1 (Lloyds register, 2006).

$$r.m.s = \frac{\pi}{2 * \sqrt{2}} * average\,value = \frac{1}{\sqrt{2}} * peak\,value \tag{2.1}$$

Measurement position

Specific measurement positions must depict the goal of accurately describing vibrations arising from machinery and propeller. Depending on the vessels general arrangement, the positions can deviate substantially. Propeller excitation on the hull due to cavitation can be measured by pressure pulses mounted on the outside hull. Typical measurement positions for a vessel equipped with medium speed engine is shown in Figure 2.1. The numbers indicate location and orientation of sensor as seen in Table 2.2.

Rina (2019) gives a review of recent ISO meetings. It was concluded that future study is needed to evaluate the basis for acceptable vibration limits in regard to human response. Statistics presented by membering countries showed higher vibration limits for crew accommodation and for the wheel house compared to values specified in ISO 20283-5, the standard for habitability onboard merchant ships. Speculations regarding the standards credibility is raised as it is reformed based on standards established for merchant ship build in 1960's. it can be argued that there is a necessity to establish new standards based on current construction methods and habitability requirements (Rina, 2019).

Table 2.2: Global vibration measurement position for merchant ships with medium speed engine

No.	Location	Direction
1	Stern, port	Transverse
2	Stern, port	Vertical
3	Navigation bridge deck forward, port	Longitudinal
4	Navigation bridge deck forward, port	Transverse
5	Navigation bridge deck forward, starboard	Longitudinal
6	Navigation bridge deck forward, port	Vertical
7	Supersliucture fore, foundation, centre line	Vertical
8	Main engine top, aft cylinder frame	Transverse
9	Main engine top, fore cylinder frame	Transverse
10	Main engine top, fore cylinder frame	Longitudinal
11	Main mast top	Longitudinal
12	Main mast top	Transverse

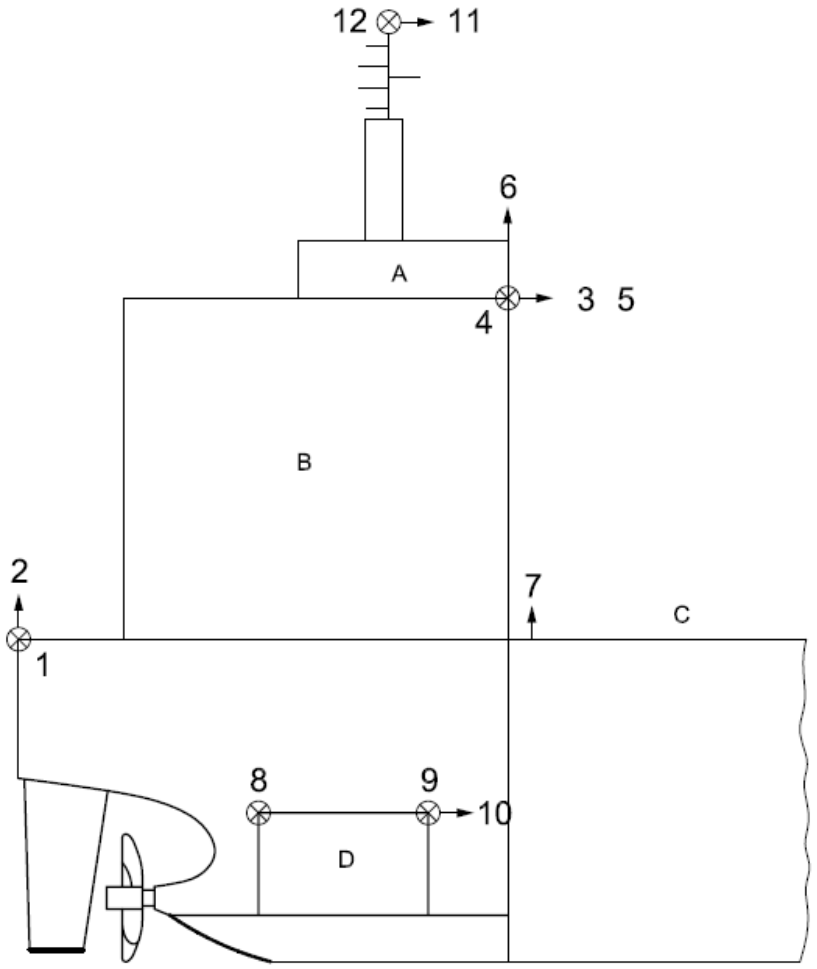

Figure 2.1: Typical measurement positions for a vessel equipped with a medium speed engine. gathered from ISO 20283-2

2.1.3 Vibration class, VIBR

DNVGL (2011) specifies requirements for newbuildings to achieve DNV's vibration class, *VIBR*. "The objective of the vibration class notation is to reduce the risk of failure in machinery, components and structures on board ships, caused by excessive vibration" (Sec.1 A100). The class notation can be applied to machinery, equipment and components, as-well as the structure in where machinery components and equipment are in the proximity of the vessels propellers. A protocol is established based on ISO 20283-2, setting vibration limits to measurement positions. If measurements are within specified limit, the class notation is granted.

In general, structural vibration should be restricted as much as possible, but there are different limits given to the compartmentalisation of the ship, as seen in Table 2.3. The specific rooms and structural component in each compartment class is given in Table 2.4

Table 2.3: Compartment class and vibration limits, gathered from DNVGL (2017) Section 5, 2.8

Class	Location	Frequency range	Amplitude	Acceleration amplitude
A	Control rooms, accommodation, bridge, local equipment room, central equipment room	2-100Hz	1mm below 13.2 Hz	0.7g above 13.2Hz
B	Machinery space	2-100Hz	1.6mm below 25Hz	4.0g above 25Hz
C	Open deck, masts, below floor plates in machinery space	2-50Hz	2.5mm below 15Hz	2.3g above 25Hz

Table 2.4: Components and location to conduct measurements deepening on compartment class. Gathered from DNVGL (2017), Section 5. Table 1

Compartment class	Location
A	Bulkheads, beams, deck, bridge, engine control room
B	On machinery, such as internal combustion engines, compressors, pumps, including piping on such machinery
C	Masts, cranes

A risk assessment shall be performed on each component in order to evaluate the vibration limit (DNVGL, 2011). Rules specified by DNV GL can deviate from from the assessment.

DNVGL (2011) states that positions with high vibration levels not predefined in the protocol, must be included. This gives an indication of the complexity and difficulty in establishing the protocol. As many measurements are performed during ship fabrication, the natural frequency can change as further attachments are mounted to structural components, or machinery components. e.g. clamps on pipes alter the effective length and consequently the natural frequency. Due to the complexity of the task, it should be performed by vibration experts, accompanied by experienced surveyors. The data shall be analysed by Fast Fourier

transformation.

2.1.4 Hull monitoring systems

DNV GL class notation *HMON*, applies for ships which have installed a system for hull response monitoring. The system is said to give better safety related to maintenance of ships. The systems will give warnings when stress levels, frequency and magnitude of ship accelerations approach levels that require corrective action. Ship's in transit are often required to make detours based on weather conditions (Naess et al., 2019). The Monitoring system can in these instances function as a decision tool.

Digital twin

DNV GL, "Nerves of Steel Extraordinary Innovation Project" (DNVGL, 2019) investigates the possibilities of using hull condition monitoring in combination with the vessels digital twin for maintenance purposes. Hull condition monitoring can prove useful for continuous surveying of the vessel during operation. Important components for structural integrity can be instrumented, thus allowing for a better prediction of the vessels health. Considering the complexity of modern ships and the inter-dependencies between all their components, comprehensive instrumentation can provide crucial insights. In essence, to provide a improved overall picture of the structural health, more instrumentation is required.

Symmetric design can reduce the number of instruments required. Identifying and instrumenting key structural components to be representative to the global health condition. This would require fundamental understanding of structural damping and dependence between structural components. A problem with structural monitoring is that structural characteristics are maintained until fracture (Randall, 2011).

Chapter 3

Basic Theory

3.0.1 Vibration

A vibrating system comprises of kinetic and potential energy. Kinetic energy is stored in the mass set in motion, while the potential energy assumes a spring pulling the mass towards its equilibrium position. Vibrations can be distinguished between free and forced vibration (Braun et al., 2002). Free vibrations are described as a system excited to an initial position and left to oscillate without influence of external excitation sources. Forced vibrations are essentially the opposite, where a force is causing the oscillations. A mode of vibration can be interpreted as a pattern of vibration with spatial and time variations. Free vibrations modes will represent inherent vibration properties of the structure, i.e., natural modes. For large movements non-linear affects must be considered, a difficult process still in need for development due to the complexity of damping and elastic properties for complicated structures (Braun et al., 2002). For smaller motions linearity can be assumed, often neglecting damping contributions. The vibrations are thereby described by applying the principle of superposition. Vibrations will propagate through the medium and are determined by the density and elastic properties of the materiel. Vibration signals propagate in the form of waves with individual characteristics, such as, amplitude, velocity and frequency. For periodic signals this is visible as distinctive patterns over the vibration time history. As the wave propagates through the structure the signal will be transferred through primary, secondary and teriatary structural components. Reverberation of the signal at the finite ends are causing the vibration modes. Damping is the attenuation of the signal, it is introduced by scattering, absorption and leakage. Scattering occurs from inhomogeneities seen from welding, inclusion and surface roughness. Absorption is here refereed to material hysteresis, where the energy is transferred to heat. Lastly, leakage is where the energy is transferred from the structure to its surrounding medium, i.e, the ocean. Due to the material properties seen in steel and water, the effect of leakage can be neglected (Braun et al., 2002)

3.0.2 Equation of Motion

A system is discretized for a finite number of lump masses, M_k, distributed over the length, x, being elastically interconnected. A continuous system is approximated by approaching the continuous limit. The equation of motion for a continuous system is partial differential equations governed by spatial boundary and initial time conditions. The mathematical expressions describing vibrations are derived from Newtons law of motion, with an equation of motion for each of its degrees of freedom. The general equation of motion for an undamped system is given by Equation 3.1, where M and K is a $n-by-n$, mass and stiffness matrix with n degrees of freedom.

$$M\ddot{x}(t) + Kx(t) = f(t) \tag{3.1}$$

Free Vibration

Free vibrations are seen without influence from external sources, where the displacement is assumed to be described as $x(t) = Ae^{\lambda t}$. The system is excited and released from its initial conditions. By setting initial conditions equal to zero, the system is evaluated for all mode shapes by introducing the eigenvector, u, in the expression for displacement, seen as $x(t) = ue^{i\omega t}$. Equation 3.1 results in Equation 3.2

$$\omega^2 Mu = Ku \tag{3.2}$$

$$det(-\omega^2 M + K) = 0 \tag{3.3}$$

where ω_n, the eigenvalues are the solution to the expression corresponding to the systems natural circular frequencies. Given that one oscillation occurs every 2π, the frequency of oscillation, termed natural frequency is defined as $f_n = \omega_n/2\pi$. For a multi body system the solution contains n eigenvalues, giving equal number of natural frequencies. Furthermore the systems mode shape is described by Equation 3.4, where the coefficients A_k and B_k are solved from applying the initial conditions. The full vibration behavior of the system is estimated by superposition. A technique applied to linear systems, yielding in simplified mathematical expressions for estimating outcome (Braun et al., 2002).

$$x_k(t) = A_k \sin(\omega_n t + B_k \cos \omega_n t) * u_k \tag{3.4}$$

Furthermore it be shown from Equation 3.3 that the natural frequency can be described by the relationship seen in Equation 3.5.

$$\omega_n = \sqrt{\frac{k}{m}} \tag{3.5}$$

Damping

Damping of ships is a complex phenomenon and mainly created by two reasons, hysteresis and viscous damping. By each deformation cycle some of the energy is lost due to material

damping where the mechanical energy is turned into thermal energy. Important parameters regarding structural damping are the type of materiel used, stress amplitude, internal forces, number of cycles, geometry features, surface and temperature. Ship structures are mainly fabricated with steel due to its strength properties and workability, making it the desirable construction element. Steel vibration attenuation is low, i.e. energy is easily transmitted through the material. Damping analysis is often confined to machinery compartments vulnerable to vibration. The damping contribution is seen in the equation of motion as the C matrix. It can be seen from the equation that damping is dependent to the velocity, however, damping force is opposite to the velocity gradient (Braun et al., 2002)

$$M\ddot{x}(t) + C\dot{x}(t) + Kx(t) = f(t) \tag{3.6}$$

Setting the input excitation to zero and assuming the vibration is described by $x(t) = Ae^{\lambda t}$. The free response is given by:

$$x(t) = e^{-\zeta\omega_n t}(A\sin(\omega_d t) + B\cos(\omega_d t)) \tag{3.7}$$

where ω_d is given by $\sqrt{1-\zeta^2}\omega_n$, and ζ is the damping ratio given by $C/(2m\omega_n)$. The effect of ζ is detrimental to how the vibration decays. The effect is illustrated in Figure 3.1. Ship structures are in underdamped systems.

- Overdamped, $\zeta > 1$
- Critically damped, $0 < \zeta < 1$
- Underdamped, $\zeta < 1$

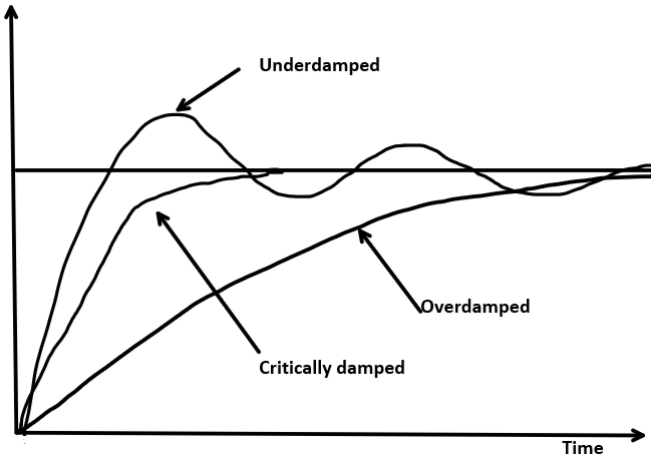

Figure 3.1: How vibration decays with different values for the damping ratio, ζ. When damping is present the vibration will move towards equilibrium position seen as the horizontal line.

A method of calculating damping ratio is explained by Casiano (2016). The method involves approximating a curve based on peak values. By calculating the decremental decay between each peak from oscillations a generalized logarithmic decrement can be estimated. Equation 3.8 is correctly applied to free vibrations, but an approximation using this technique has been made for acceleration values in chapter 5.

$$\delta = \frac{1}{n} * ln(\frac{P_1}{P_2}) \tag{3.8}$$

where P_1 and P_2 are peak values and n is the number of cycles between the peak values. The relationship between decremental decay and damping ratio is given by Equation 3.9

$$\zeta = \frac{\delta}{\sqrt{(2\pi)^2 + \delta^2)}} \tag{3.9}$$

Forced vibration

As opposed to free vibrations, forced vibrations result from external excitation sources seen as either transient or steady state response. For a periodic exiting force given by $F_0 \sin(\omega t)$, the steady state response is defined as in Equation 3.10, where ϕ is the phase alignment and ω is the frequency, assumed to be equal for exciting force and response.

$$x_{ss}(t) = X_0 \sin(\omega t + \phi) \tag{3.10}$$

The expression in Equation 3.10 is the particular solution to the differential equation. The full solution includes the homogeneous part as seen in Equation 3.7

Resonance

For forced vibration conditions where the excitation frequency coincides with one of the natural frequency of the system, resonance occurs. With resonance the displacement is seen to increase significantly and is therefore an important phenomenon to consider in many engineering applications. In the design of ship structures, such investigations should be performed on structural components and equipment in vulnerable positions (see Table 2.3. Resonance analysis is also applied in the design of whole substructures, e.g. design of the aft ship and control of resonance with propeller pulse. Impact test and artificial excitation's can be performed on structural components to map vibration characteristics in the design phase (ITTC, 2017).

Impulse

Ships are exposed to large waves, leading to large magnitude loads over a short duration. Quantifying the magnitude of slamming events are commonly performed by pressure sensors or strain gauges. A method of calculating impulse force is to apply principles from

momentum theory. By calculating the integral seen in Equation 3.11 the impulse force is given.

$$I_0 = \int_0^{\varepsilon} F(t)dt = m\dot{x}(0^+) - m\dot{x}(0) \tag{3.11}$$

Where the duration of the impact is between 0 and $\varepsilon = 0^+$.

3.0.3 Excitation sources

Propeller excitation

Propeller induced vibrations are caused by the fluctuating pressure field created and from the cavitation volume on propellers. The pressure field is translated through the shaft and through the water acting on the hull surface and rudder (Bertram, 2012). In general terms the exciting frequency is evaluated as:

$$\frac{rpm}{60} * number\,of\,blades \tag{3.12}$$

When designing the aft of the ship, it is necessary to keep the natural frequency of the structure in between one of these orders of excitation frequencies to avoid resonance. Analysis of the pressure forces can be made by computational fluid dynamics, but model testing is usually applied to accurately depict the forces and frequencies.

Wave excitation on the propeller change the hydro-static pressure and cause disturbances. There is also the effect of inflow angle and wake effects from appendage disturbance on the inflow which act on the propeller and translate through the shaft (Bertram, 2012).

Shaft whirling

A rotating shaft can tend to start a whirling motion, classified as self-exciting motion. The exciting forces on the shaft are controlled by the motions. According to Randall (2011) a number of phenomena cause the centre of the shaft to whirl (either forwards or backwards) at a frequency different from the rotation speed. These disturbances can be caused by, among others, unbalanced mass, hysteresis damping in the shaft, gyroscopic forces and fluid friction from the bearings.

Oil whirl is caused by the interaction between shaft and the fluid film in the bearing. It can cause a forward whirling of the shaft, approximately at half the frequency of the rotating shaft. This is explained by the fluid film's boundary layer's velocity profile. As the rotational speed towards the shaft is equal to the shaft rotation and the boundary layer towards the bearing casing has a velocity of zero. (Randall, 2011)

Hysteresis whirl is characterized by the whirl frequency being at the shaft's critical speed independent of the actual rotation speed Randall (2011). Thus the whirling is initiated by

the exciting frequency of rotation resonating with the natural frequency of the shaft and then being ”locked in” as the rotating speed increases.

Figure 3.2 illustrates measurements conducted on the bearing housing. The relative motion, measured by the X and Y probe is closely related to the oil film thickness, and thus to the oil film distribution. The dynamics of the fluid film bearing can be idealised by a highly nonlinear spring. An increase in static load causes the film to become thinner, and the bearing stiffer, which reduces the vibration motion amplitude, despite the fact that forces acting upon it may be higher. The bearing house structure however possesses linear elastic properties, so even though the static properties on the film changes, the motion on the housing, measured by the accelerometer in Figure 3.2 would be representative for the acting forces. A disadvantage from the ladder is that it will not depict the absolute position of the shaft vibration inside of the bearing. The type of accelerometers used are typically ICP, measuring acceleration fluctuations around a zero mean value (Randall, 2011).

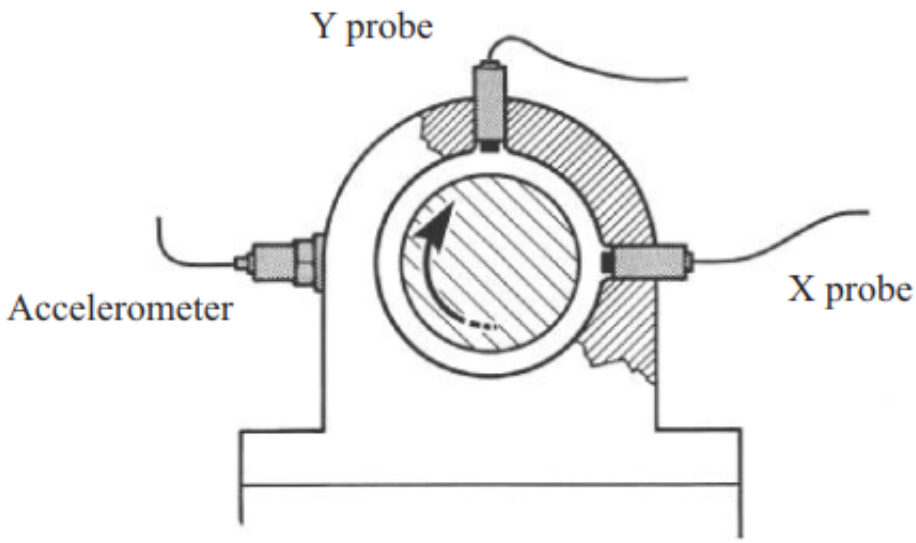

Figure 3.2: Measurements of shaft and bearing housing. Gathered from Randall (2011).

Engine excitation

Engines consists of many rotating components, such as shafts, electric fields and meshing gearteeth. Gear teeth deform under loads which leads to transmission error where teethes don’t perfectly align. During the lifetime of the gear the deformation continues and the transmission error may increase. The transmission error between teeths is not necessarily the same, and thus the vibrations amplitude at the tooth meshing frequency can vary (Randall, 2011). Generators will induce vibrations not exclusively to its rotating parts, they will in addition induce electromagnetic forces which will cause vibrations (Randall, 2011).

Engine excitation's are repetitive during the engine cycle, e.g., for medium internal combustion engines we have 4 strokes for each engine cycle. There are in turn additional vibration sources linked to fluid flow, although their contribution to hull girder excitation is considered to be low (Randall, 2011). Usually a order of excitation for engines is introduced as follows:

$$order = \frac{Exciting\ frequency}{rpm} \tag{3.13}$$

Engine vertical vibrations are dominant. However, if the engines are located off center from the centreplane of the vessel they may excite horizontal and torsional vibrations. This problem can be avoided if two engines are arranged symmetrically and arranged in rpm and phase to counter balance each other. (Bertram, 2012)

The forces transmitted from the engine to the foundation can be classified into H, X, and L, as seen in Figure 3.3. X and L moments only contribute to hull girder vibration through engine housing deformation and are negligible compared to H moment, which is fully introduced to the foundation. Measurements by Asmussen and Muller-Schmerl (1995) has revealed that cases where resonance between ignition frequency and H-type vibrations drastically magnify the transmitted vibrations. It is therefore necessary to acquire accurate estimates of engine excitation frequencies before designing the foundation floor of engine compartments. A method for estimating the natural frequency of the H-mode vibration by considering the stiffness of the engine housing is presented in Asmussen and Muller-Schmerl (1995).

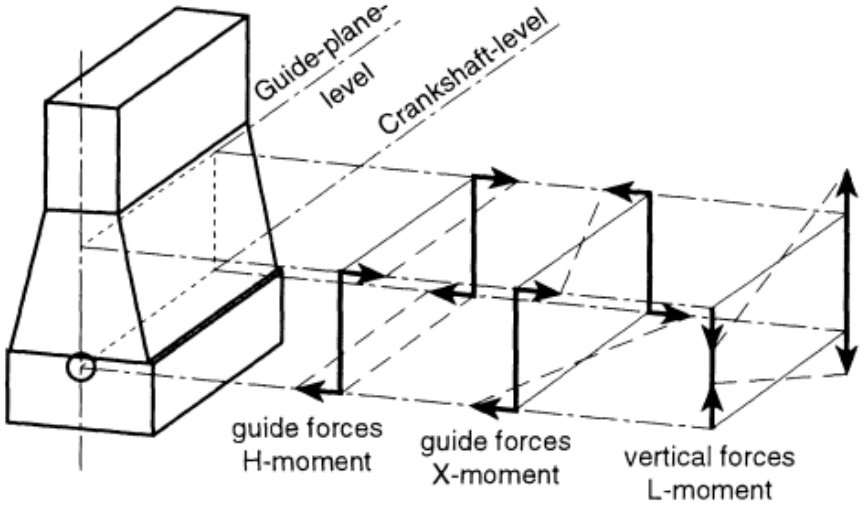

Figure 3.3: Excitation forces and moments of engines. (Asmussen and Muller-Schmerl, 1995)

Wave induced vibrations

Slamming is the event of high pressure forces acting on the structure, usually caused by bottom re-entry or sudden large wave impacts. There are two criterion necessary for slamming to occur. The relative vertical motion between the vessel and sea surface must be larger than the draft for ship section considered. Secondly the vertical velocity must exceed a threshold velocity. Statistical analysis has lead to empirical formulas for estimating the threshold velocity as the forward part of the vessel emerges from the still water. The critical threshold velocity is given by Equation 3.14, where l denotes length of vessel and g is gravitational constant.

$$V_{cr} = 0.093 * (gl)^{\frac{1}{2}} \tag{3.14}$$

As surface elevation and ship motion is a stochastic process and random in nature, slamming occurrence can best be described by an statistical approach. The initial study of slamming statistics was performed by Ochi (1964), where it was assumed that vertical motion and velocity of ship relative to sea surface follows a gaussian and narrow-banded distribution (Wang and Soares, 2017). The vertical velocity can be estimated by Equation 3.15

$$V_r = \frac{d\xi_3}{dt} - x\frac{d\xi_5}{dt} - U\xi_5 - w \tag{3.15}$$

where w is the vertical velocity of the undisturbed wave; ξ_3 is the heave motion; ξ_5 account for the pitching motion x meters away from centre of rotation, and ξ_a is the sea surface elevation. Ochi (1964)

3.0.4 Stochastic process

The outcome of a stochastic process can not be determined, only predicted by probabilistic methods based on experience and its statistical values. Naess and Moan (2012) defines a stochastic process as; $The quantity$X(t)$is called a stochastic process if$X(t)$is a random variable for each value of t$

The surface elevation of the ocean can be described as an infinite collection of deterministic sinusoidal waves superimposed. The result is a truly random and stochastic process. The probability distribution can be estimated by counting the number of occurrences where the surface elevation is larger than a specific value. Performed for all values of x, results in the cumulative probability distribution denoted by CDF.

$$F_{X(t)}(x) \approx \frac{N[X(t) \leq x]}{N} \tag{3.16}$$

where the numerator of Equation 3.16 represents the number of occurrences where the surface elevation is equal to or less than a wave height and the denominator; N, is the total number of surface elevations in the timeseries observed. For the equation to be valid it is imperative that N is of sufficiently high value. From the cumulative probability distribution, the probability density function, PDF, is derived by differentiating CDF with respect to x:

$$f_x = \frac{dF_x(x)}{dx} \tag{3.17}$$

where f_x is the probability density function.

Another important principle within probability calculation is stationarity. By assuming stationarity it is assumed that the physical processes responsible for the surface elevation does not change within given time of three hours. Stationarity implies that the mean value is equal to zero, and that the standard deviation and variance of the process are constants.

The mean value, or expected value of a stochastic process can be estimated with the probability density function as shown in Equation 3.18 or by Equation 3.19.

$$m_x = E[X] = \int_{-\infty}^{\infty} x f_x(x) dx \tag{3.18}$$

$$m_x = \lim_{N \to \infty} \frac{1}{N} \sum_{j=1}^{N} x_j \tag{3.19}$$

3.0.5 Skewness and kurtosis

Statistical analysis can reveal important features off the data. Assuming a stochastic ergodic process will follow a Gaussian distribution the mean vibrations value would be equal to zero.

Skewness S_x is defined in Equation 3.20. The amplitude is raised to the power of three, thus making it more sensitive to large values, but suppressing lower values. Brandt (2011).

$$S_x = \frac{M_3}{\sigma_x^3} \tag{3.20}$$

Where σ_x is the standard deviation and M_3 is the 3rd central moment. The skewness gives an indication of how the signal is symmetric around the mean value. For example a true Gaussian distribution have a skewness level of 0.

On the other hand, Kurtosis is defined by Equation 3.21. Kurtosis is calculated by raising the values of the time signal to the power of four it will be more sensitive to larger values and suppress lower values. A Gaussian distribution has a kurtosis value of 3. Positive deviation indicates more data in the tails.

$$K_x = \frac{M_4}{\sigma_x^4} \tag{3.21}$$

3.0.6 Frequency analysis theory

By applying Fourier transform a signal can be shifted from time to frequency domain. A signal in time domain is describe as the sum of sine waves. However, when shifted to

frequency domain the signal is decomposed into its individual components. An example of this is depicted in Figure 3.4

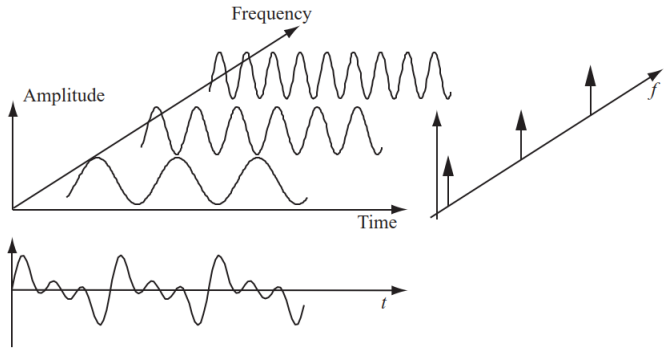

Figure 3.4: Fourier transform transfers the signal from time to frequency domain. This forms the basis for a spectrum, which can be seen as the plane created by the amplitude and frequency axis. (Brandt, 2011)

Vibrations from a stochastic ergodic processes, as opposed to periodic signals are excited by an infinite amount of frequencies. A distinct amplitude or root mean square, *RMS* value can not be displayed for a single frequency. Instead, the density of a frequency interval is calculated, i.e, power spectral density, *PSD*. The area under the *PSD* curve is equal to the mean square value of the signal in that frequency range. Newland (1993) derives the double sided power spectral density from the forward Fourier transform of the autocorrelation function.

$$S_{xx}(f) = \int_{-\infty}^{\infty} R_{xx}(\tau) * e^{-j2\pi f\tau} d\tau \tag{3.22}$$

Welch's Method

There are several methods for estimating the *PSD* of a signal, although Welch's method is virtually the only method commercially available in noise and vibration analysis systems (Brandt, 2011). The method is mathematically described by Equation 3.23

$$\hat{G_{xx}}^{W}(k) = \frac{S_p}{M}\sum_{m=1}^{M} X^*_{w,m}X_{w,m} = \frac{S_P}{M}\sum_{m=1}^{M}|X_{w,m}(k)|^2, k = 1,2...,N/2 \tag{3.23}$$

where, $\hat{G_{xx}}^{W}(k)$ is welch's power spectral density; $X_{w,m}$ is the averaged discrete Fourier transform; M, is the segments which the signal $x(n)$ is divided into, and N is the length of each segment. S_P is the scaling factor, ensuring Parseval's theorem is withheld, i.e., *r.m.s* value equivalence between frequency and time domain. Each segment is windowed before the discrete Fourier transform is calculated. A common procedure is to apply a Hanning

window with a 50 % overlap between segments Brandt (2011). Due to averaging between segments the *PSD* created is different from the true power spectrum (Matlab, 2019).

Spectral leakage can occur if the frequency increment is undesirably high, where two closely spaced signals aren't distinguished and resulting in spectral content being leaked to adjacent frequencies. Leakage is minimized by decreasing the frequency increment

Root mean square, r.m.s

The *r.m.s* for a discrete spectra is simply calculated as the sum of the *r.m.s* for each discrete frequency, equated by Equation 3.24, where the term being summed is the mean square value for each discrete frequency represented by k.

$$x_{rms} = \sqrt{\sum R_{xk}^2} \tag{3.24}$$

The *r.m.s* within a frequency interval for a continuous spectra is calculated by:

$$x_{rms}(k_1, k_2) = \sqrt{\Delta f \sum_{k_1}^{k_2} \hat{G_{xx}}^{W}(k)} = \sqrt{area\, under\, curve} \tag{3.25}$$

3.0.7 Sampling theorem

The theorem states that the sampling frequency must be twice the bandwidth of the signal to capture all information present in the signal. Often refereed to the Nyquist frequency. If the theorem is not withhold the signal will affected by be aliasing and folding (Brandt, 2011). An interpretation of the theorem is that there should be no frequency above half the sampling frequency which is of interest. For clarification, a sampling frequency of 50Hz, will contain all information in a signal between 0 to 25Hz. However, with a sampling frequency of 50Hz, Transient events with a time period less than $1/50s$ would be completely missed. Therefor higher sampling frequencies is necessary to capture slamming events.

3.0.8 Signal filtering

Design of suitable filters requires deep understanding from many aspects of signal processing to be applied correctly. Digital filters and their design is a discipline of its own in the field of digital signal processing (Brandt, 2011). A general definition of the relationship between the input and output of a filter is described by Equation 3.26, where x and y denotes input and output, respectively.

$$a_0 y_n = \sum_{k=0}^{N_b} b_k x_{n-k} - \sum_{l=1}^{N_a} a_l y_{n-1} \tag{3.26}$$

a_l and b_k are filter coefficients defining the characteristics of the filter. The signal used for analysis in this thesis been filtered with a so-called Finite Impulse Response filter FIR. For

this type of filter, N_a is set to zero and only old input values are used to compute the output. FIR filters are often preferred when linear phase characteristics are wanted, i.e avoiding peak distortions in time domain. Cascade coupling is quite common where the output of one filter is the input to another Brandt (2011).

Chapter 4

Case study, S.A. Agulhas II

On the 18. Of July 2019, the South African research and polar supply ship, S.A. Agulhas II, started her journey from Cape Town, South Africa, to the marginal ice zone off the coast of Antartica. The operational goal of the journey was strictly scientific where teams of multiple disciplines were invited to conduct research. The vessel has been designed to facilitate module laboratories in form of containers on its aft deck. To facilitate this, the vessel has a wide transom stern. This makes the stern prone to slamming, often causing work and operations to be interrupted. Stern slamming was particularly frequent during dynamic positioning. The intended course can be seen in Figure 4.1. The ship was accompanied by a meteorological team which tracked the dynamic behavior of the ice.

The vessel has a diesel electric power supply and propulsive system, as is preferred among icebreakers because of maximum torque available at low rpm. Vessel specifications are shown in Table 4.1.

Table 4.1: Main dimensions, engine and propulsion details.

Length over all [LOA]	133.9 m
Length between perpendiculars	121.8 m
Beam	21.7 m
Ice-classification	PC 5
Breaking capability	5knots in 1m thick ice.
VCG	8.81 m
Total weight	11914.8 tonnes
Installed power	4 x Wartsila 6L32, 3000 kW
Propulsion	Diesel-electric, 2 x 4500kW, with CPP.
Speed	14 knots, service speed 17 knots, max speed

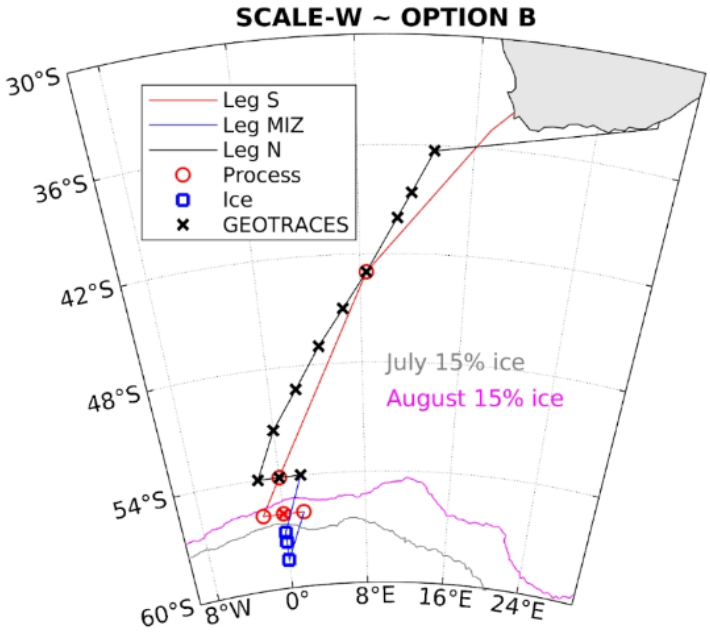

Figure 4.1: The map describes the intended course of the ship. The red line indicates the route going south, originating from Cape Town. The black line indicates the route going north, stopping in East London. The crosses on the route going north indicate positions where stationary operations are performed. The grey and purple line indicates the extent of the marginal ice zone, for each of the months. The marginal ice zone is defined as where there is a 15% probability of ice coverage.

4.0.1 Instrumentation

The S.A Agulhas II was instrumented with a total of 28 accelerometers to capture the ship's local and global accelerations. The instrumentation was done in collaboration with students from Stellenbosch University, sound and vibration team. There were two types of accelerometers installed. The ICP accelerometers were used to capture local accelerations. The other kind, DC, accounted for the static gravitational acceleration, thereby making it possible to capture rigid body motions of the ship, as well as global accelerations of the hull girder. The specifications of the instruments is seen in 4.2.

Table 4.2: Accelerometer hardware.

Accelerometer Type	Brand/model	Numbers installed	Sample rate [Hz]	Sensitivity
ICP	PCB-333B32	18	2048	100mV/g
DC	PCB-3711B111OG	10	2048	200mV/g

The ICP accelerometers are based on piezoelectric technology. They consists of certain crystals, functioning as a spring that generate an electric charge proportional to the strain exhibited on them. The electric charge is measured by picocoulombs and is converted to voltage by a charge amplifier, thus the voltage is proportional to the acceleration. The voltage signal is transferred to a data acquisition system, *DAQ*, through coaxial cables that protects the signal from interference by electromagnetic radiation. The data acquisition system were of the kind LMS SCADAS. There were in total three *DAQ* onboard. Two located at the central measurment unit, *CMU*, and the third located in starboard steering gear room. The *DAQ* were setup in a master-slave configuration connected by fibre optic cables.

There were 20 coaxial cables installed on the ship, originating from the *CMU* to various locations, indicated by the squares in Figure 4.2. The coaxial cables were installed during the construction of the vessel by STX Finland 2012, and are permanently installed on the vessel (Bekker et al., 2019). Each coaxial cable is connected to either the master *DAQ* or slave 1. The additional eight sensors were located in the steering gear room. These sensors was connected to slave 2 which in return was connected to the master *DAQ*, (see Figure 4.2). From the master *DAQ* an Ethernet cable was connected to a laptop running the recording software LMS test lab turbine testing. The software used has two main functionalities. (a), Communicate with the *DAQ*, to either start or stop recording. (b), Configure the channel setup on the master-slave DAQ system. This includes adjusting the bandwidth sensitivity according to vibration levels expected by the respective accelerometers.

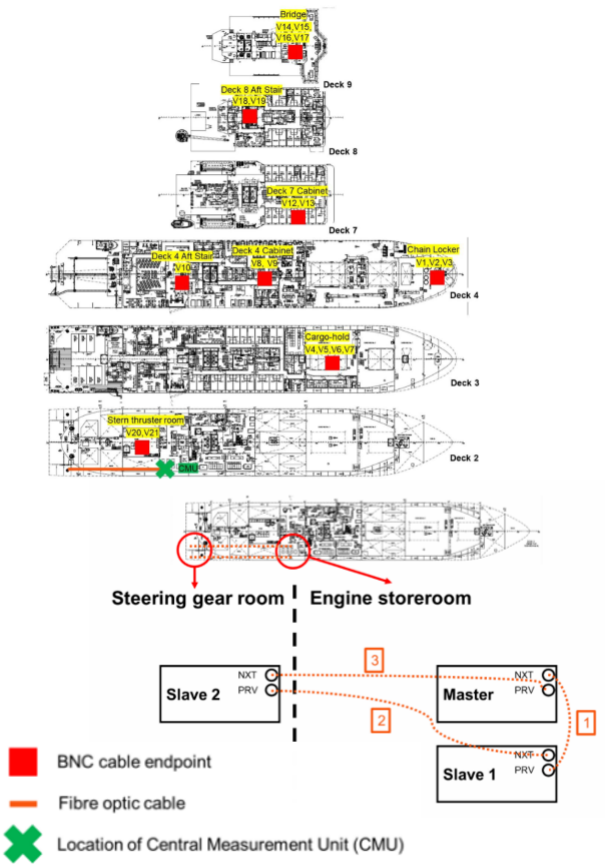

Figure 4.2: Red squares indicate end location of coaxial cables. The cables are originating from the *CMU*. Lower part of figure shows configuration of data acquisitions system as a Master-slave setup. Master and slave 1 is located at the *CMU*, in the engine storeroom. Slave 2 is located at starboard steering gear room.

The placement of accelerometers are seen in Figure 4.3 to 4.6. Green dots, indicate a transverse direction, i.e, Y-direction. Red dot indicates a vertical, meaning Z direction. Lastly, purple dots indicated a tri-axial accelerometer. A smaller black dot represents a DC accelerometer.Sensors are summarized in Table 4.3.

Table 4.3: Sensor location and sensor ID, as seen in Figure 4.3 to4.6

Deck	Sensor location	Sensor ID
2	Steering gear room	SG
	Stern thruster room	ST
	Engine store room	ES
	Fresh water tank	FW
3	Cargo hold	CH
4	Aft stairwell, deck 4	XX
	Chefsroom	CR
	Chain locker	CL
7	Deck 7	D7
8	Deck 8	D8
9	Bridge	B

Figure 4.3: Sensor layout on deck 2. from aft to bow: Tri axle DC accelerometers on starboard, and one DC accelerometer in vertical direction on port. ICP in Y direction and Z direction. Two ICP accelerometers are located on the centre line at the stern thruster room. One ICP accelerometer , vertically oriented in the engine store room and fresh water room, star/port, respectively.

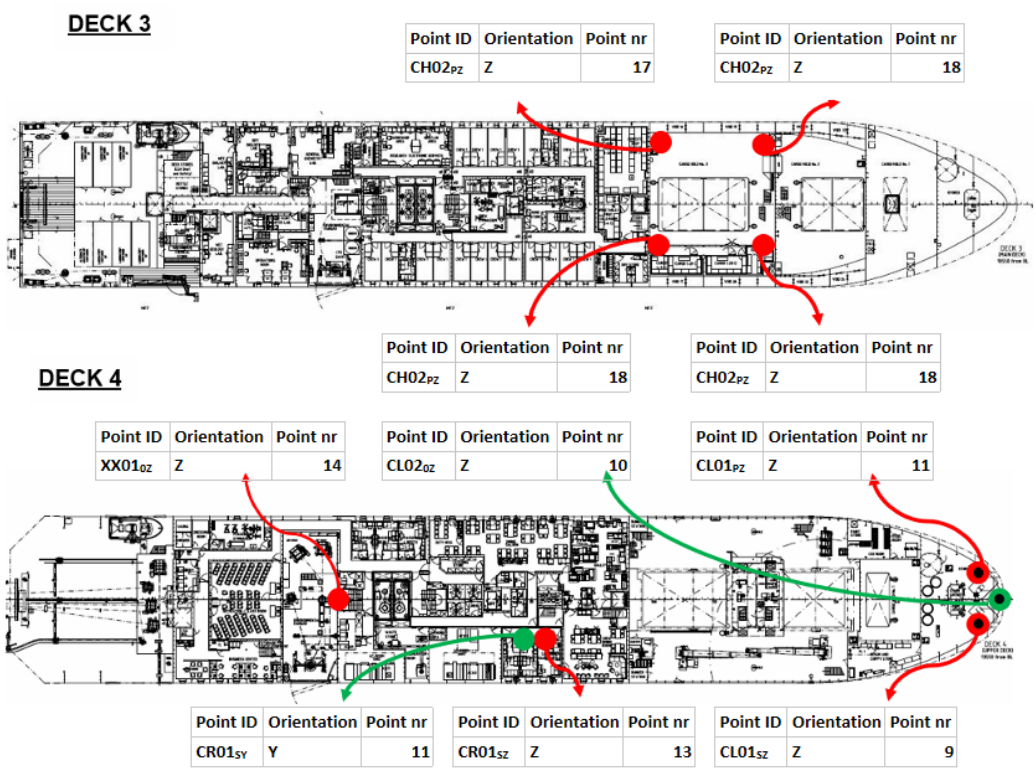

Figure 4.4: Sensor layout of deck 3, Four ICP accelerometers in the cargo hold, measuring in Z-direction. Deck 4, from aft to bow: Vertical ICP on the centre line. Two ICP on starboard, crew accommodation area, one in Y and Z direction. In the bow, there are three DC accelerometers in the chain locker, DC measuring in Z-direction on port and starboard and a DC accelerometer on the centre line.

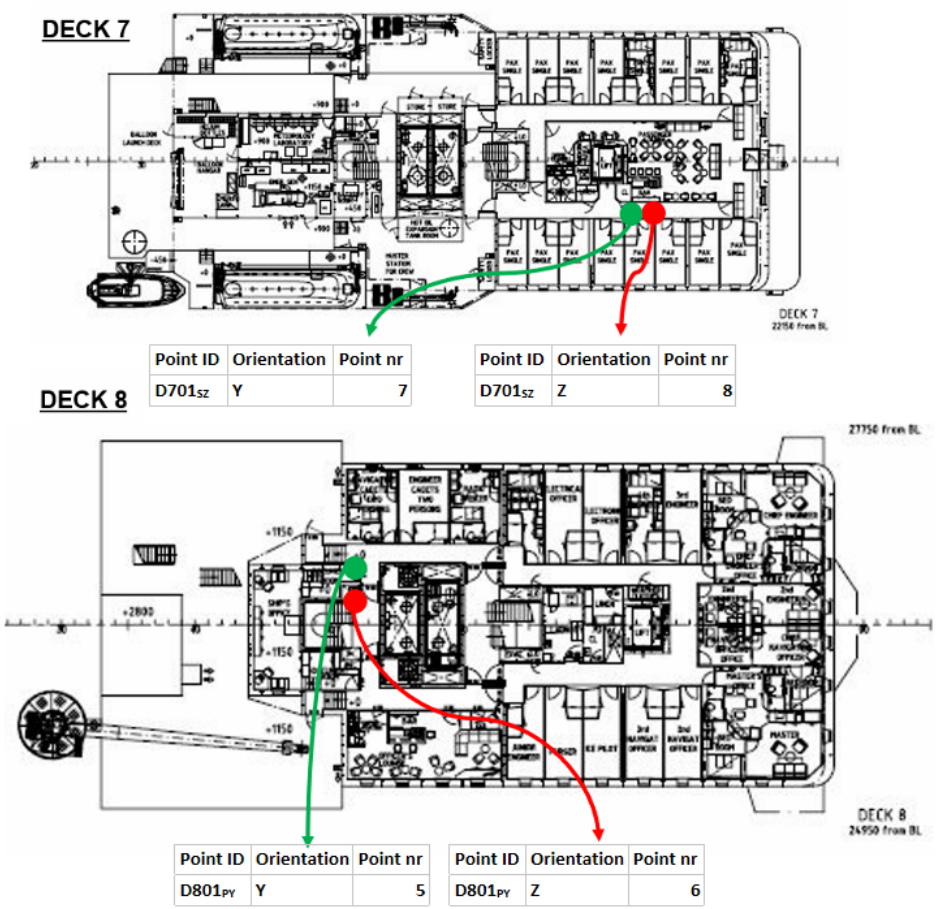

Figure 4.5: Sensor layout of deck 7 and 8. On deck 7, there is one ICP in both vertical and transverse direction, both located on starboard. Deck 8 conceits of same configuration, but located closer to the centre line of the ship.

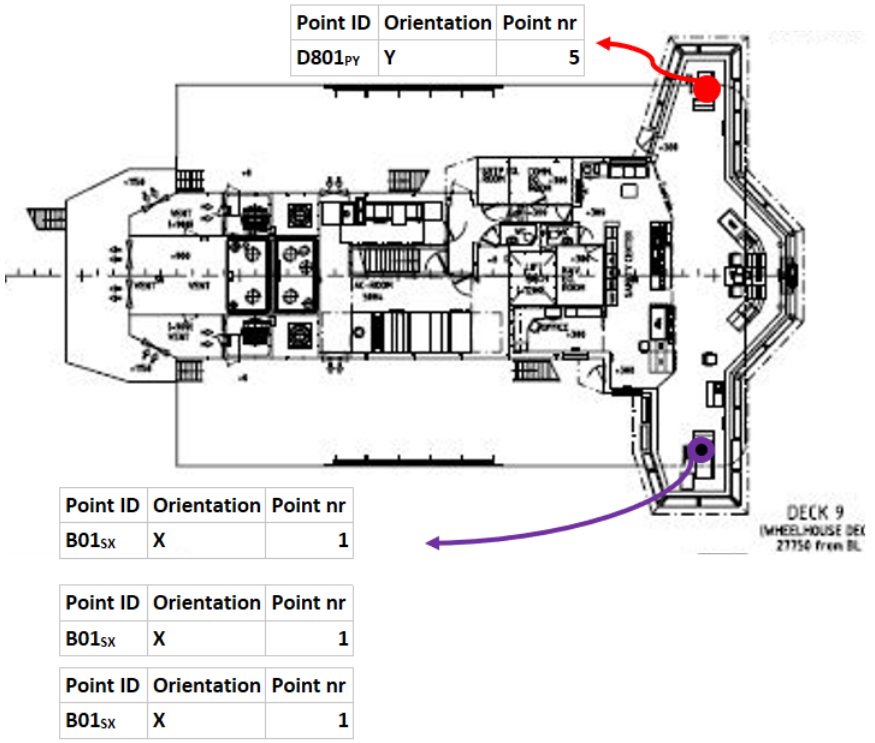

Figure 4.6: Sensor layout on the bridge. A tri axle DC accelerometer is located on starboard side and one ICP accelerometer vertically oriented on portside.

Figure 4.7 shows instrumentation in the chain locker, located in the bow. Only the DC accelerometer in the image is connected, as there was a limited amount of coaxial cables. The accelerometer was connected to the charge amplifier via an optic fibre cable. The signal was converted to voltage and transferred to the data acquisition system via the coaxial cables. Figure 4.8 shows three DC accelerometers glued to a small metal box, thus creating a tri axle accelerometer.

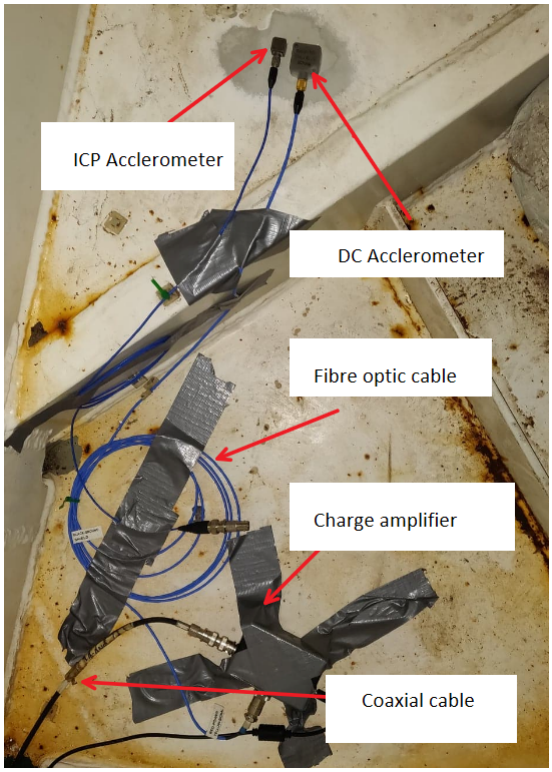

Figure 4.7: Picture of instrumentation in ICP and DC accelerometer, Fibre optic cable, charge amplifier and coaxial cable.

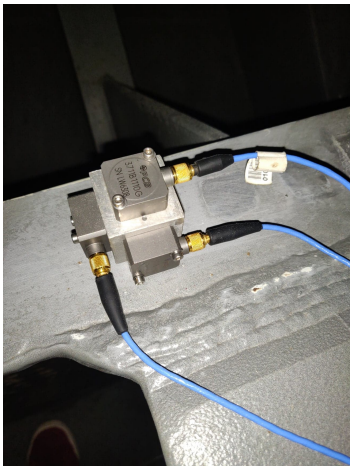

Figure 4.8: Three DC accelerometer glued to form a triaxle accelerometer. Blue wires are fibre optic cables connected to slave 2.

4.0.2 Environmental observations

The vibration research group onboard the ship carried out environmental observations covering all daylight hours as a mean to validate accelerometer data. The observations was performed in shifts of 2 hours per observer. To reduce uncertainty and bias, shifts was overlapped by 15 minutes. An example of the observation chart is shown in Table 4.4. Observations was registered in ten minute intervals. Number of significant slams was recorded as slamming events that the observer felt shook the ship from the observational post, positioned on port side of the bridge. Significant wave height and max wave height was in the beginning of the journey registered with guidance from navigational officers on the bridge. The wave direction, *Wave dir* was observed relative to ship heading, *Ship hdg*. Encounter frequency was counted and timed with a stopwatch.

Table 4.4: Environmental observation chart.

Number of significant slams	Ship Velocity	ship hdg 01-36	Beaufort number 0-12	Wind speed [kn]	Wave dir. 000-360	Avg. wave height [m]	Max wave height [m]	λ/L (0 : <L), (1 : = L), (2: >L) 0-2	Encounter frequency [s] number of periods	Encounter frequency [s] Total time	Avg.
3	14.9	218	2	4	330	1.00	1.5	0	7	42	6.0

Ice condition

During ice navigation floodlights were on during dark hours as an additional insurance to keep watch for icebergs. Therefore ice observations were made possible to perform for all hours of the day. The ice thickness was estimated by using a yardstick positioned horizontally out over the port railing. The yardstick was used a reference to make visual approximation of the ice thickness.

Figure 4.9: The yardstick used to measure ice thickness positioned horizontally from the ship. Each white and black segment is ten centimetres long. The ice thickness shown here is estimated to be approximately 40-50 centimeters.

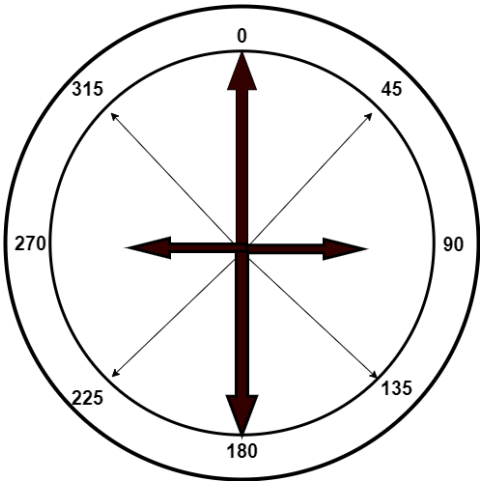

Figure 4.10: Chart used for determining wave train direction relative to ship heading.

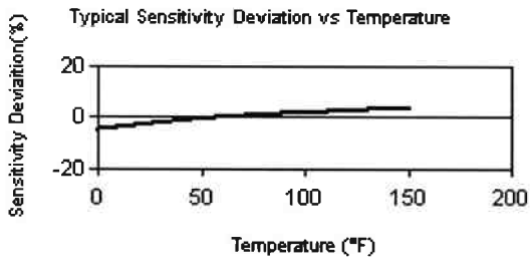

Figure 4.11: Sensitivity deviation vs temperature. 0 farenheit is equal to ca -18 Celsius. Graph is gathered from accelerometer manufacturer *PCB* product guide.

4.0.3 Uncertainty introduced in accelerometers

All measurements are introduced to some type of uncertainty. Changes in temperature alter internal parameters, consequently a change in picocoulombs produced. The ICP accelerometers used has a temperature operation range between -18 to 66 Celsius. It is seen from Figure 4.11 that there is approximately a 5% sensitivity deviation at -18 Celcius. None of the sensors was exposed to such low temperatures, and was considered low. Therefore sensitivity deviation has not been included in analysis and interpretation of the data.

Calibration

The accelerometers were originally calibrated by the manufacturer, PCB electronics. Some of the accelerometers were yearly sent to the national metrology institute of South Africa for quality control and calibration. These accelerometers were then further used as reference accelerometers for in-house calibrations checks using a Svantek SC111 vibration calibrator. All accelerometers were control checked by Stellenbosch University sounds and vibration team before the voyage.

Chapter 5

Analysis

Twelve environmental conditions were selected (see Table 5.1,5.2). Selection was based on differences in wave state, relative heading towards waves and velocity. From each environmental condition 30 min of data was extracted. The recordings are numerated from 1 to 12 based on its timestamp. Reference will be made to recording number.

Table 5.1: Environmental condition

Date/time	20/07 11:09	21/07 15:18	27/07 12:29	27/07 16:24	29/07 15:49	29/07 19:59
Recording number	1	2	3	4	5	6
Condition	Calm	Medium	Stationary in Ice	Ice	Stationary	Stationary
Beaufort Nr	2	7	NA	NA	8	8
Significant wave height	1m	4m	NA	NA	6m	3m
Max wave height	2m	5m	NA	NA	8m	5m
Relativ wave direction	320 deg	15 deg	NA	NA	0 deg	35 deg
Wave encounter frequency	7.5 s	7 s	NA	NA	9s	6.4s
Ship velocity	15 kn	11 kn	0 kn	3 kn	0 kn	0kn

Table 5.2: Environmental conditions

Date/time	30/07 13:09	30/07 14:29	31/07 13:29	31/07 16:09	04/08 07:26	05/08 10:59
Recording number	7	8	9	10	11	12
Condition	Severe	Severe	Medium	Medium	Medium	Medium
Beaufort Nr	8	8	7	6	7	6
Significant wave height	5.5m	5.5m	2m	3m	3m	2
Max wave height	7.5m	8m	5m	5m	5m	4
Relativ wave direction	330 deg	330 deg	0 deg	255 deg	265 deg	190 deg
Wave encounter frequency	9s	9.3s	8.4s	6.5s	6s	17.6
Ship velocity	8.8 kn	7.8 kn	6, 8, 10 kn	13.8kn	14 kn	17.8 kn

5.0.1 Signal processing

The accelerometers had a sampling rate of 2048Hz. Prior to evaluating statistical values of kurtosis and skewness the signal were processed in Matlab using the inbuilt function, $detrend$. Detrending removes trends in the signal by linear regression analysis. By Subtracting linear mean trends from the data. Mean values were evaluated on the raw signal. The signal was shortened to increase processing speed. This was done in Matlab using the function $decimate$. It uses a lowpass FIR filter, and essentially removes data points from the original signal. Reduction ratios are seen in Equation 5.1 and 5.2. The decimated sampling frequencies were selected based on the frequency bandwidth expected to excite the system. Thus, a sampling frequency of 128 would sufficiently describe the signal up to 64Hz without aliasing issues. Slamming events were captured with a decimated frequency of 1024Hz, high enough to capture the slamming impact and water intrusion. All time histories traced each other and no phase distortions were present. It was observed that slamming events were poorly reflected with decimated ratio of 16.

The decimated signal of 128Hz was cascade filtered with three separate bandpass filters. This helped to capture the 2-node and 3-node bending, as identified from frequency analysis. In addition a bandpass filter was used to capture the first engine harmonics at 12.5Hz, with a passband and stopband frequency of 11.5 and 13Hz, respectively. The 2-node bending mode was bandpassed with a passband frequency of 1.9Hz and stopband frequency of 2.4Hz. On the other hand the 3-node limits were set to 3.7 and 4.2Hz. To allow for an easier detection of slamming events, a highpass FIR filtered with with a passband frequency of 1Hz was applied. A FIR filter was applied to avoid phase distortion as mentioned in 3.0.8. In addition, a lowpass FIR filter was created at a stopband of 1Hz, and passband of 0.5Hz. All filters had a stopband attenuation set at 60db. Peak value analysis was performed on the filtered signals and a comparison between largest amplitude, ten and one percentage largest amplitudes between different environmental conditions and sensors. A flowchart of the signal processing steps taken is seen in Figure 5.1

$$R_{1024} = \frac{2048\ Hz}{1024\ Hz} = 2 \tag{5.1}$$

$$R_{128} = \frac{2048\ Hz}{128\ Hz} = 16 \tag{5.2}$$

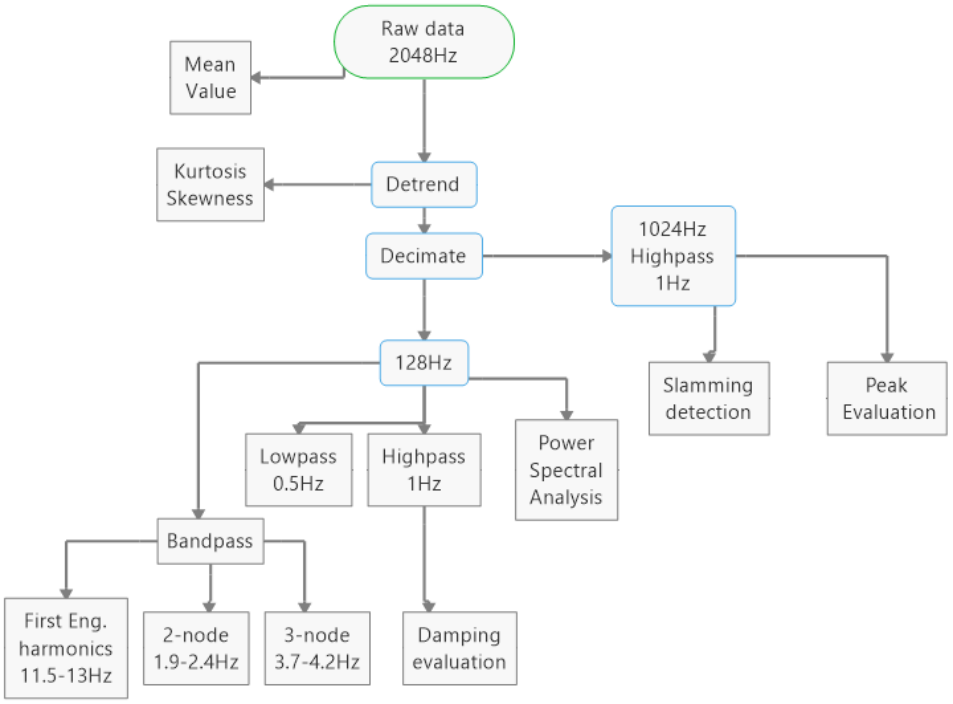

Figure 5.1: Flowchart of signal processing

5.0.2 Frequency analysis

Power spectral density was calculated by using the inbuilt Matlab function, *pwelch*, using Welch's overlapped segments in averaging an estimate.

Internal excitation

Data sample labeled as recording 3, the vessel was stationary in ice with a thickness of approximately 70 to 80 cm. There were no visual detection of waves and a assumption to neglect wave excitation is made. The data set is used as a reference of internal frequency excitation originating from main engines. The PSD for all sensors are plotted in Figure 5.2 revealing the region, direction and magnitude of excitation. There are five distinct peaks present, shown in Table 5.3. The peak seen at 12.5Hz corresponds to the ships main

engine. The engines were running continuously at 750 rpm. The main engines were four stroke, thereby, engine harmonics were noticed at half and whole multiples of the frequency. Results correspond to specifications given by the engine manufacturer, Wartsila product guide (Wartsila, 2018) listing torque variation frequency at 750rpm as 37.5Hz . The stern sensors, shown as red line with asterisk marker, shows the largest energy content for 12.5 Hz, at a peak value of 0.02. This is to be expected as the sensors are close to the excitation source, as well as the sensors are mounted on web frames directly connected to longitudinal girders, which lay the foundation for the engine bed.

Compared to the stern, the chain locker has a reduced magnitude of four. Sensors were located far away from the excitation source. This explains the lower energy content. However, several sensors were in closer proximity to the main engines than the chain locker and an even further magnitude reduction was observed. For example, sensors in engine store room, one deck directly above the main engines did not display any excitation. This depicts how engine vibrations may be transferred through decks. The sensors in the chain locker were mounted two decks above the main engines. However, installed on structural components making up the hull shell.

Table 5.3: Engine harmonic peaks seen from stationary condition.

Peak	1	2	3	4	5
Multiple	1	1.5	2	3	4
Frequency	12.5 Hz	18.75 Hz	25 Hz	37.5 Hz	50 Hz

$$12.5\,Hz = \frac{750\,rpm}{60\,s} \tag{5.3}$$

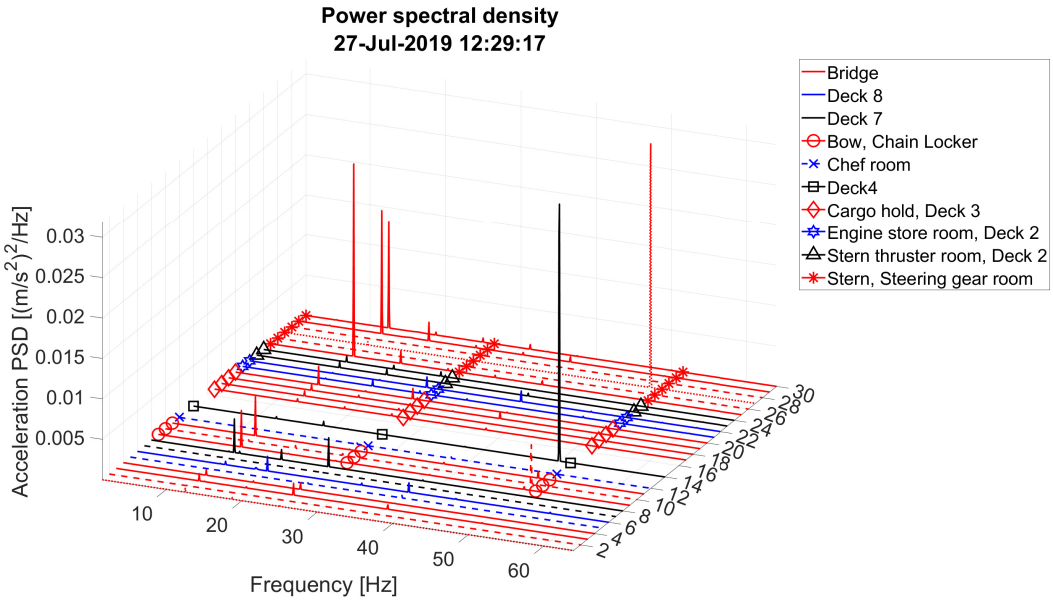

Figure 5.2: Power spectral density of all sensors during the stationary condition in ice. Solid, dashed and dotted line indicates Z, Y and X direction of sensors, respectively. Vertical excitation is dominant arcoss all frequencies with the exception for sensor 10 and 27 at 50Hz.

The fourth, third, second and first blade pass frequencies can be found respectively by Equation 5.4 to 5.7. FFT analysis from shaft line bearings was not conclusive in determining shaft rotational speed. The effect of oil whirling was observed but too many unknown variables made the results non-conclusive in relation to blade pass frequency.

$$9.31\,Hz = 4\,blade * \frac{139\,rpm}{60\,s} \tag{5.4}$$

$$6.98\,Hz = 3 * \frac{139\,rpm}{60\,s} \tag{5.5}$$

$$4.65\,Hz = 2\,blade * \frac{139\,rpm}{60\,s} \tag{5.6}$$

$$2.32\,Hz = 1\,blade * \frac{139\,rpm}{60\,s} \tag{5.7}$$

5.0.3 Vibration modes

Vertical hull girder vibration modes was identified by plotting the PSD. A comparison was made between three sensors, respectively located in the bow, stern and bridge, as seen in Figure 5.3. The PSD for all environmental conditions shows a clear agreement between the vibration modes. The frequencies for 2, 3 and 4-node mode are presented in Table 5.4.

Table 5.4: Identified vibration node modes from power spectral analysis

Vibration node mode	Frequency
2	2.18 Hz
3	3.83-4 Hz
4	5.18 Hz

Figure 5.3 displays the spectral content for each environmental observation. The magnitude of the 2-node mode is dominant with largest values seen for sensors in the bow.

A clear correlation is seen between magnitude and wave height, where the two most severe conditions measured on 30 of July show the largest values. Recording nr 9 and 10, conducted on 31 of July were performed under similar environmental conditions. However, with different relative heading of head on and port beam, respectively. Although recording nr 10 maintained a higher velocity, 2-node vibration was reduced by avoiding head on waves (See Figure 5.3. The findings indicate the importance of vessel heading compared to velocity as a means to mitigate 2-node vibration. A logarithmic scale visualization of the spectral content is shown in the appendix Figure B.1.

Ice navigation was seen to excite higher vibration modes (see recording nr 4 in Figure 5.3). From the spectral content a clear distinction is seen for the 3-node. Noting an equal size for stern 2-node and 3-node mode. Furthermore, although having a modest magnitude, excitation is also seen for 4-node vibration mode. The excitation is seen to be concentrated to the hull as bridge acceleration values are comparable to open water navigation.

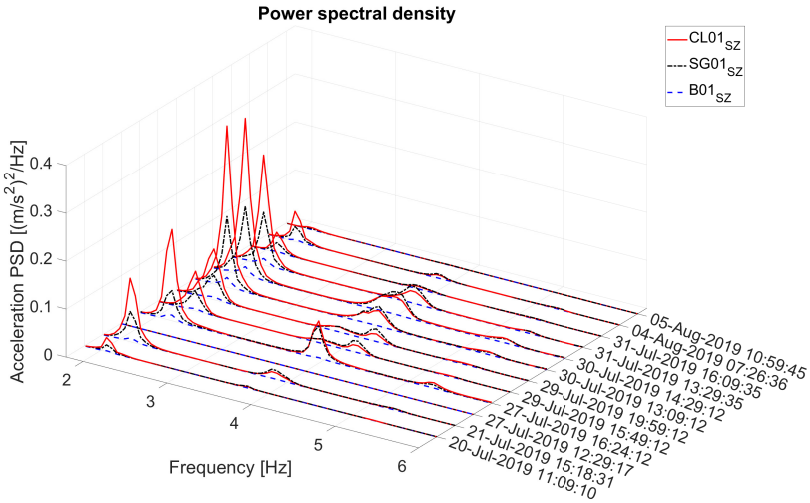

Figure 5.3: Power spectral density for the vertical bow, stern and bridge sensors.

Energy content

The energy content has been calculated for specific frequency intervals using the inbuilt Matlab function *Bandpower*. The output is the average power of the input signal or alternatively, the sum of squared r.m.s values. For the 2-node mode frequency limits was set to 1.9-2.4Hz and for the 3-node, 3.7-4.2Hz. Results for the vertical accelerometers are presented in Appendix E. Furthermore a comparison between the 2 and 3 node mode was made by evaluating the ratio as presented in Table E.1 and E.2. Most sensors displayed a significant lower energy content about the 3-node mode, as expected. However, the ice navigation measurements revealed similar quantity for sensors in the steering gear room. Where the two starboard located accelerometers contained a 2% and 6% increase in 2-node mode, while a 7% increase was noticed for the 3-node mode for the portside accelerometer. Open water navigation showed a 100-400 % increase in way of the second mode of vibration.

Hull

Energy content from 2 node and 3 node modes of vibration from all environmental conditions were compared to values obtained from recording 1. Focus was placed on data gathered from four accelerometers in the cargo hold due to their symmetric installation. Thus variations could indicate the relation between magnitude and location. Results are presented in Table E.7 and E.8. Sensors located in the aft part of cargo hold contained larger values for 2-node, while 3-node had a greater magnitude for sensors located towards the bow.

During ice navigation the 3 node vibration displayed a magnitude increase of 23 to 29

times relative to 2-node mode which increased by approximately 3.3-3.2. This further strengthened the hypothesis that ice navigation has a large influence on higher vibration modes. Furthermore an increase of 3-node was experienced in more severe sea states. In these conditions the 2-node lead to 2-3 times larger magnitude than 3-node. Further aft in the ship, sensors in the engine store room and fresh water tank depicted very little excitation, however 3 node is dominant.

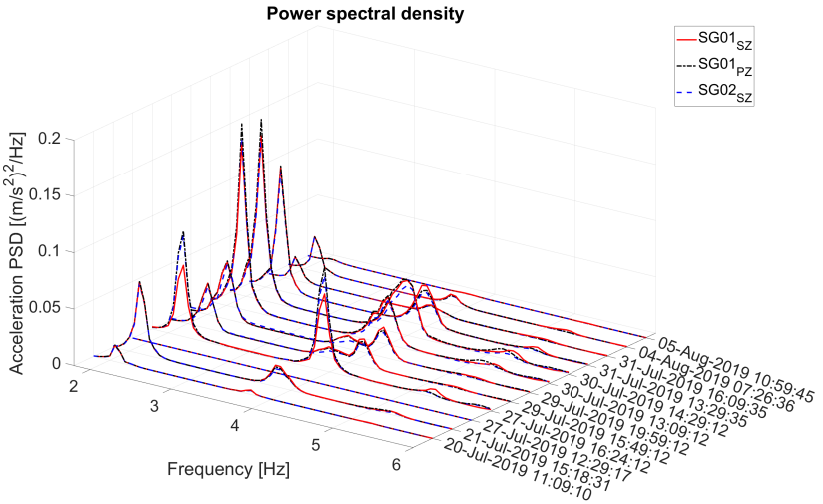

Figure 5.4: Power spectral density comparison of DC and ICP accelerometer, the three sensors are measuring in vertical direction. Sensor $SG01_{SZ}$ and $SG02_{PZ}$ is DC and ICP, respectively located on starboard side, while $SG01_{PZ}$ is an DC accelerometer located on port side.

5.0.4 PSD discussion

Results presented in Table 5.4 is compared to previous investigations of the S.A. Agulhas from Soal et al. (2019). The comparison reveal deviations. Stable modes identified by PolyMax is believed to have a better accuracy. However, it is noted that the results do not correspond to equal operational conditions. Although added mass from hydrodynamics effects, cargo and ballast would further decrease the natural frequencies. The FEM analysis has been modeled to include the effects of added mass and with an similar draught of operational conditions. Causation for the deviation is difficult to declare. A possible cause can be modeling of environmental conditions and its affect on added mass. Complexity of FEM could be flawed with regards to stiffness and mass matrix applied. The loading conditions of the vessel could be wrong. Furthermore, errors in the PSD plots could contain errors. Peaks are not necessarily representing natural modes, only frequencies with dominant power and occurrence. The averaging performed by *pwelch* is an estimate and thus inadequate frequency resolution may cause a misrepresentation of the frequency. A consistent 2 node peak was observed at a frequency of 2.18Hz for all environmental recordings. However, for the 3 node a clear peak was not as easily distinguishable. 3 node

frequency was determined based on the curves 0 gradient in the expected region. It was observed that the frequency shifted slightly.

Exact rpm chosen by ship master is not known. The ship was fitted with an controllable pitch propeller, and often velocity adjustments was made by pitch adjustments rather than rotational velocity of shaft. An assumption of 140 rpm is made. However, it can not be excluded that in certain periods rpm may have been reduced to 130 or 120. In these cases the blade pass frequencies would be in close proximity to the 2 and 3-node modes of vibration. This would affect the magnitude of spectral content based on the principle of superposition.

The spectral content for all sensors can be seen in Figure B.3 to B.14. Accelerometer location is thought to be a major factor in spectral content. Sensors mounted on longitudinal girders is hypothesized to show a larger content of 2-node. Accelerometers was not strictly placed on strength carrying members and therefore a straight forward comparison between all sensors could not be made. Some observations could not be explained, such as the spectral content from vertical accelerometers on deck 7 and 8. As both are located in the superstructure it was expected to observe similar quantities of 2 and 3 node vibration modes. However, sensor on deck 7 reveled a 2 node dominance. On the other hand deck 8 was dominated by 3 node mode. Logarithmic display of the two accelerometers is shown in Figure B.2.

Another example is the spectral content seen from the *DC* and *ICP* vertical sensors on the bridge. Where the *ICP* contains magnitudes comparable to sensors in the bow. The difference in energy contained at the frequencies is remarkable large. It could not be explained by vessel heading as it is apparent for all recordings. *ICP* and *DC* accelerometers from stern region displayed comparable magnitudes, thus difference in hardware is not responsible. The difference between these bridge sensors is seen from Figure B.3 to B.14 as sensors 3 and 4, respectively for *DC* and *ICP*.

Table 5.5: Different values of node-modes from sources

	Frequency		
Node	OMA polymax	FEM STX Finland	PSD
2	1.935	2.6	2.18
3	3.367	4.28	3.83-4
4	4.721	5.63	5.18

5.0.5 Time series analysis

Acceleration time series from stationary condition

Figure 5.5 displays time series from recording nr 4, performed stationary in ice. The signal has been bandpass filtered to maximize content at a frequency of 12.5 Hz. The figure helps visualize how the amplitude my decrease depending on accelerometer location. The amplitudes corresponds to the spectral content seen in Figure 5.3 and Figure B.5, where largest excitation, in descending order is seen for stern, bow, engine store room and bridge.

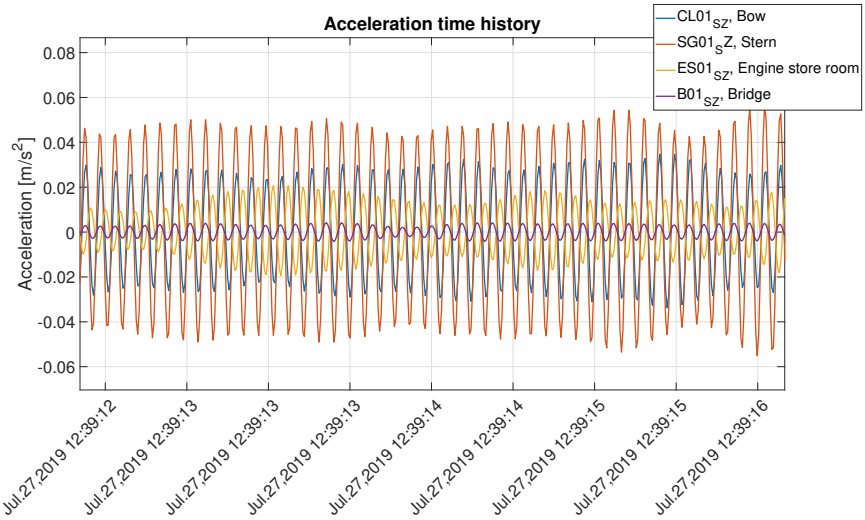

Figure 5.5: Acceleration time history of bandpassed filtered to show 12Hz component. Displaying the stationary in ice condition.

Slamming

A method for detecting slamming events was made by analysing the standard deviation. The methods were inspired by Storhaug (2007a) and the criterion applied in ABS guidance for hull condition monitoring, i.e. major slamming events detected as standard deviation exceeding $0.4g$. Appendix A shows an algorithm created to identify slamming events by scanning time series and registering time instances where the criterion was met. Severe slamming was identified in five conditions for four sensors. Of these sensors, three were located in the chain locker, two vertical and one transverse sensor. The forth sensor was located in the steering gear room. Although there were few slamming events which fulfilled the criterion, visual inspection revealed there were numerous more.

Table 5.6: Number of significant slams of sensors on specific days.

Sensors\days	21/07 15:18	30/07 13:09	30/07 14:29	31/07 13:29	04/08 07:26
$CL01_{PZ}$	1	4	7		2
$CL01_{SZ}$				2	
$CL01_{0Y}$		1	2	4	
$SG01_{SZ}$			1		

Crew observations recorded twelve major bow slamming events during the 30 min period on the 30 of July, recording nr 8. Approximate times of slamming events are seen in Table 5.7. A selection of these slamming events has been used for further characterising resulting ship vibrations. Frequency analysis of slamming events can be seen in Appendix C, section C.2

Table 5.7: Slamming observations on 30-July, recording initiated at 14:29

Time	Nr of events
14:33-14:38	3
14:49-1450	2
14:53-14:55	3
14:57-1459	4

Case 1

Figure 5.6 to 5.7 shows the acceleration time history of sensor $CL01_{SZ}$ and $SG01_{SZ}$. The two sensors plotted were located furthest apart from one another and can therefore indicate the largest phase difference between bow and aft.

A major bow slamming event was registered for recording nr 8 at 14:41:43 (see Figure 5.6). The peak value was seen to be $13.21 m/s^2$. Immediately after the slamming event, the bow and stern sensor was seen to oscillate at 3.95Hz. The bow sensors was accompanied with high frequency noise. The sensors experience a peak approximately 1.54 and 1.83 seconds after the impact, for the aft and bow sensor, respectively (see Figure 5.7). FFT analysis on reveled frequency content dominated by 3.95Hz but also contributions from 2.28Hz and 5.32Hz. These frequencies are recognized as the 3,2 and 4 node vibration modes, respectively. Peak analysis identified a phase distortion of approximately 0.88 seconds. Nine seconds after the impact it is observed that the phase distortion becomes narrower. Frequency analysis reveled the 2 node mode to be dominant, with small contributions from the 3-node frequency. By plotting the 2 and 3 node bandpassed signals the visualization of vibration modes become apparent (see Appendix C section C.1).

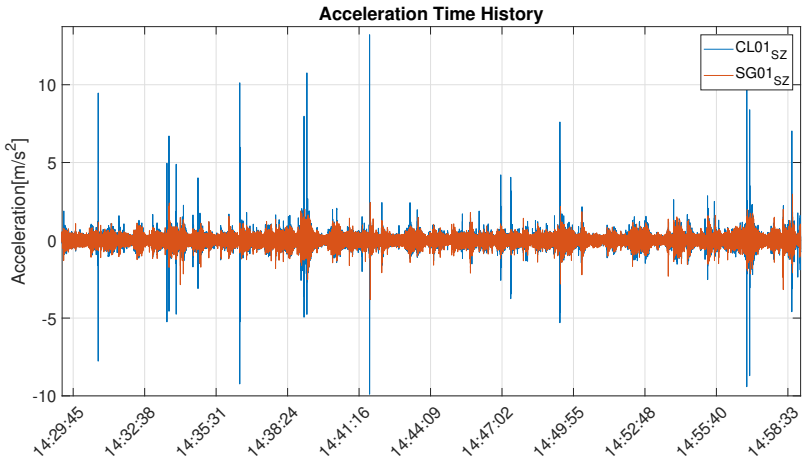

Figure 5.6: Acceleration time history of severe condition, 30 July, initiated at 14:29. Time history of sensor $CL01_{SZ}$ located starboard side in the chainlocker and $SG01_{SZ}$ located starboard side in the steering gear room

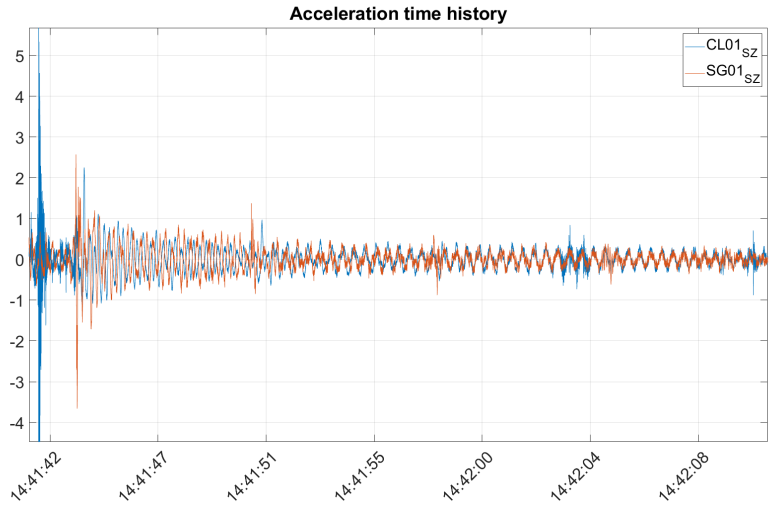

Figure 5.7: Slamming event and the aftermath structural response.

Case 2

In Figure 5.8 two successive slamming events have been captured. Highpassed and lowpassed signal for $CL01_{SZ}$ and $SG01_{SZ}$ are labeled as Hp and Lp, respectively. Immediately after the slamming events, the sensors were in equal phase at the 2-node mode. The mode was excited for ca 26 seconds before the 3-node mode became dominant. The transition between 2 and 3 node bending mode is shown in Figure 5.9 between 14:57:29 to 14:57:38. The 3-node is dominating for roughly 9 seconds before both sensors return to 2-node bending mode.

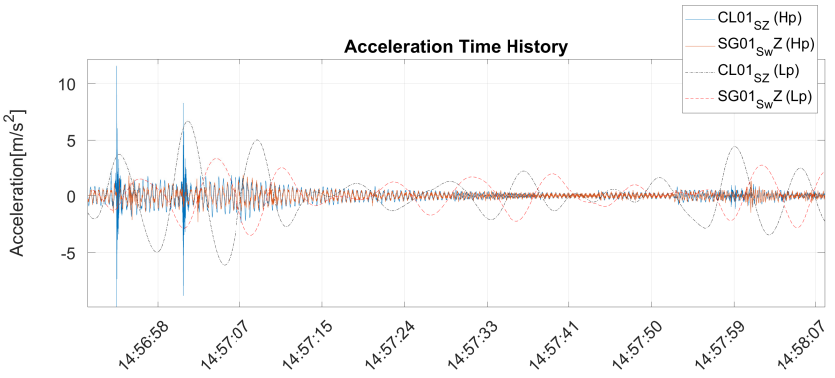

Figure 5.8: Two successive Slamming event occurring with 7 seconds of separation. signal labeled as (Hp) is highpass filtered and contains frequencies above 1.8Hz. Similarly (Lp) is lowpassed and contains frequencies below 0.5

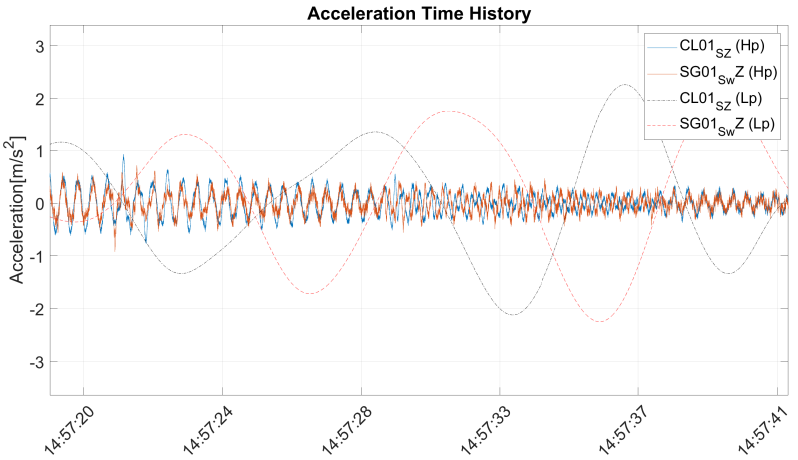

Figure 5.9: Closer inspection of the transition between 1^{st} and 2^{nd} bending modes following the two successive slamming events. 2 node is dominant up to 14:57:29. Followed by 9 seconds of 3-node mode. Lastly, oscillations return to 2-node mode.

Case 3

The third slamming event included occurred at 14:49:22. It possess many of the same characteristics as seen in case 1. For the bow sensor, close to the impact a short period of roughly 1.5 seconds with high frequency noise is registered before larger accelerations dominated by 3-node and 2-node occurs. Stern sensor displays larger excitations at the 3-node frequency before diminishing and being suppressed by 2-node frequency, approximately 6 seconds after first recognition.

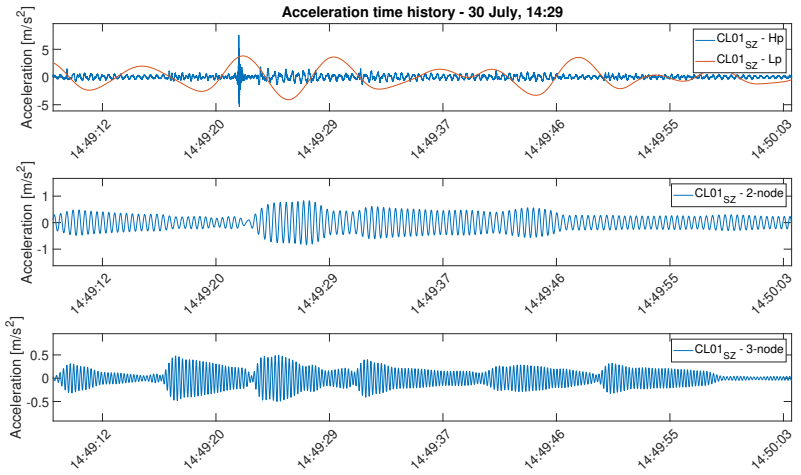

Figure 5.10: From top to bottom: Highpass and lowpass filtered signal of slam, case 3, blue and orange, respectively. Bandpass filtered signal of 2- node, Bandpass filtered signal of 3- node.

Discussion on slamming events

The slamming algorithm detected a few time instances were the standard deviation criterion was exceeded. By plotting acceleration time series and cross referencing with detected slamming events a visual confirmation of the events was made. Processing power became an issue when applying the algorithm. For evaluating the standard deviation an incremental step of 10 sample points was used. As a result processing speed was increased at the cost of precision.

Discrepancies between port and starboard chain locker accelerometers was observed. Slamming events was only registered for port sensor, while acceleration time history depicted slamming for both sensors. The port sensor also displayed extremely large values thereby raising suspicion on sensor credibility. No discrepancies was observed between the sensors for lowpass filtered signals. The cause is hypothesised to originate from differences in structural component rigidness or faulty installation.

In the case studies presented above, values originating from starboard sensor was used. As

suggested by Storhaug (2007a) a criterion based on design value could be better suited for the purpose, particularly for the basis of structural condition monitoring. Applying the developed algorithm to peak values could further reduce the number of sample points used by a factor of 500.

A common feature observed are slamming occurs at the peak of or closely before the peak of the low-passed signal. In terms of the ship global dynamic motions slamming occurs closely before pitch motion reach its max value. However it is noted that that heave motion can be a considerable factor not accounted for. Slamming events were not well captured by the ICP sensors. Nor was there any significant excitation present in the DC accelerometer located on the bridge deck.

The high frequency content immediately following the slam, containing high frequency noise with small 2-node and 3-node mode is identified as the water intrusion part, of the two contributions identified by Soares (2015). Therefore an inclination towards wave impact having greater contribution to acceleration levels from slamming is made. It should be noted that contributions to pressure can not be based sincerely on acceleration levels.

Slamming events are seen to excite both 2-node, 3-node and 4-node frequency of the vessel. A clear conclusion to how impacts affect the behavior of higher vibration modes is difficult. It is apparent from Figure 5.10 that 3-node vibration experience incremental excitation aside from impacts. Passing waves with varying wave lengths is thought to be a contributing factor. 3-node excitation is seen shortly after the bow experience a peak from wave action, although dependent on wave length, this would strengthen the belief of bending moments contribution. The slamming event in Table 5.0.5, which had a significant acceleration amplitude caused the largest excitation of 4-node vibration.

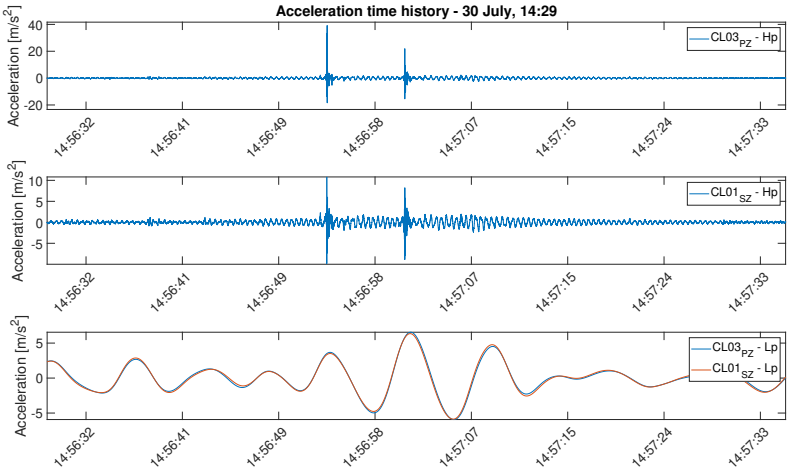

Figure 5.11: Slamming event on the 30 July, recording Nr 8. Only the slamming events from $CL03_{PZ}$ was registered with standard deviation exceeding 0.4g. However, it is observed that both sensors experience slamming. Excessive values from $CL03_{PZ}$ lead to starboard sensor being used in case studies

5.0.6 Peak Analysis

Peak amplitudes were identified by applying the inbuilt Matlab function, *findpeaks*. On average a total of 3500 peaks were identified for each accelerometer. The maximum and average of 10 % and 1% largest values are presented in Figure 5.12, 5.13 and Appendix D. Making a clear distinction between wave heights, relative heading and vessel velocities contribution to peak amplitudes is difficult due to changing parameters between recordings. However, a correlation is observed with wave height and relative heading.

A velocity manoeuvre was performed on recording nr 9 in Table 5.2. The vessel maintained a constant head on heading. The vessels velocity was varied from 6,8 to 10kn and kept constant for 10 minutes. The average of the 50 largest peak values from each 10 minute interval is shown in Figure 5.12. A clear trend was seen for a majority of the vertical sensors. That is an increased average amplitude with vessel velocity. Sensors located in cargo hold, engine store room freshwater tank and deck 8 did not display this correlation. Table D.1 contains a comparison between average peak amplitude related to velocity. An inverse relationship is observed for transverse accelerometers in the bridge, chain locker and steering gear room. It indicated that largest amplitudes was experienced at lower velocities. It is thought this may be due to increased effect of rolling motion from oblique waves at reduced velocities.

Beam wave encounters was not seen to increase transverse accelerations. Rather, head on waves are observed to increase structural transverse accelerations. Figure D.1 to D.3 gives a good illustration of the relationship between Z and Y acceleration amplitudes.

For recordings close to 0 deg. wave heading, absolute max acceleration levels are obtained from the bow section resulting from major slamming events.The recordings initiated on the 29 of July revealed the stern to be susceptible to high acceleration levels during stationary conditions. The importance of relative heading can be postulated from the two recordings. Where despite milder wave condition and with a heading of 35 deg, higher acceleration levels were experienced compared to head on waves. This could be explained by the undisturbed waves was allowed for direct impact with the stern. Ship dynamics in terms of pitch and heaving could also be disadvantageous for stern slamming when vessel is position with a bow heading. The elevated transom stern makes it susceptible to stern slamming and it was therefore expected to observe dominant stern acceleration levels during following seas.

Furthermore, transverse acceleration levels during ice navigation did not result in major acceleration values compared to open water. Although by comparing average 10% largest amplitudes, levels are comparable to severe sea states (see Figure D.8).

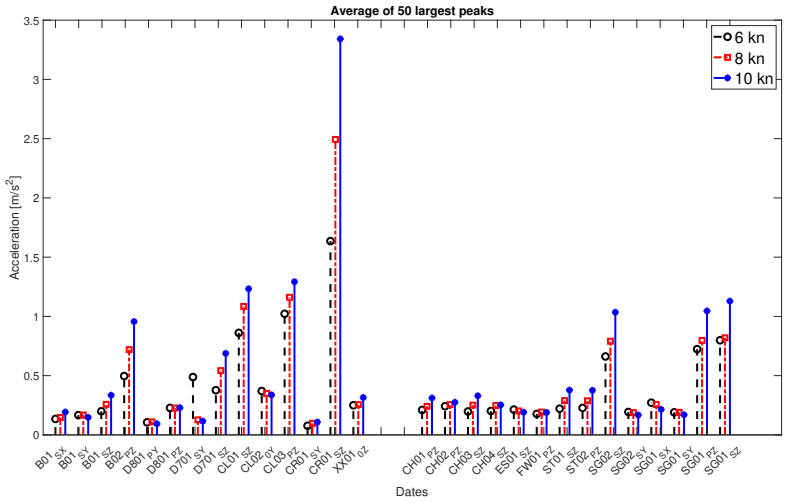

Figure 5.12: Average of 50 largest peaks during varying speed, performed on the 31/07-13:29. The vessel was maintained a constant heading, head on towards the waves, while the velocity was kept constant for 10minutes at 6,8 and 10 knots.

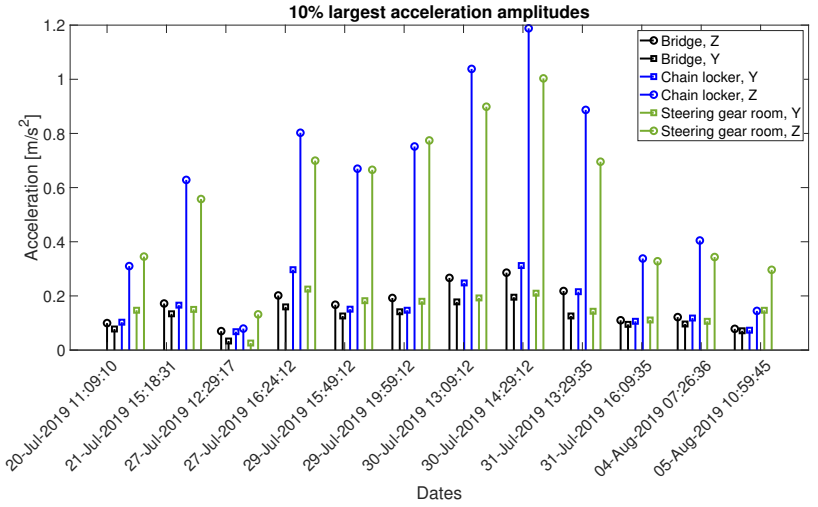

Figure 5.13: Max 10% largest acceleration amplitudes for ship sections: bow, bridge and stern. Z values shown with circles, Y with squares. A trend is seen with increased peak values with wave condition severity.

5.0.7 Damping evaluation

2nd node

By extracting peak values from acceleration time history after slamming events it was possible to evaluate structural damping by analysing the decremental decay. Locating whipping events qualified for the technique described by Casiano (2016) is an elaborate process due to interference from wave action and there were few quality responses available. A method of circumventing this issue is to apply a curve fitting on peak values and approximating the decremental decay. Figure 5.15 is an example of curve fitting made with the inbuilt Matlab application $cftool$. The original signal is seen in Figure 5.14. The curve fitting is described by Equation 5.8 and the coefficients in Table 5.8.

$$f(x) = a * x^b \tag{5.8}$$

Table 5.8: Damping curve coefficients. Lower and upper bound represents 95 % confidence bounds

Coefficient	Damping curve	Lower bound	Upper bound
a	6.576	5.413	7.739
b	-0.491	-0.5196	-0.4623

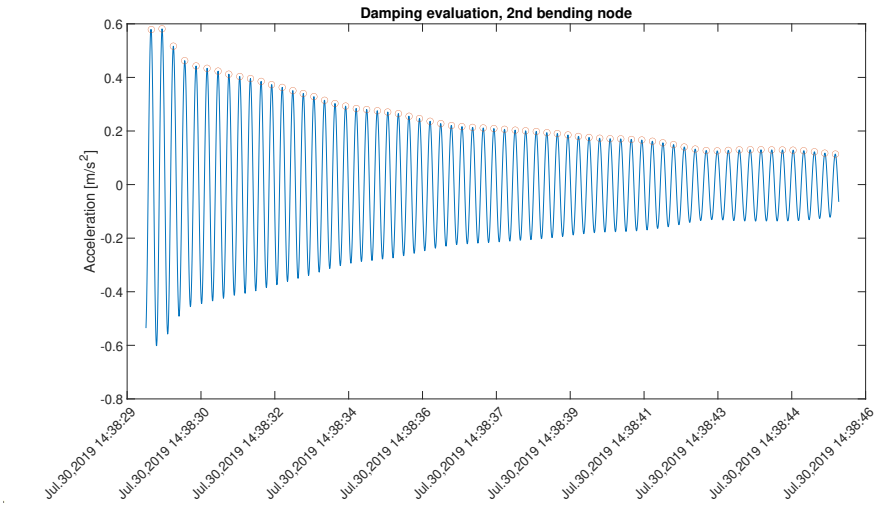

Figure 5.14: Undisturbed whipping event from vertically oriented bow sensor displaying decremental decay between peaks. Identified peaks are circled.

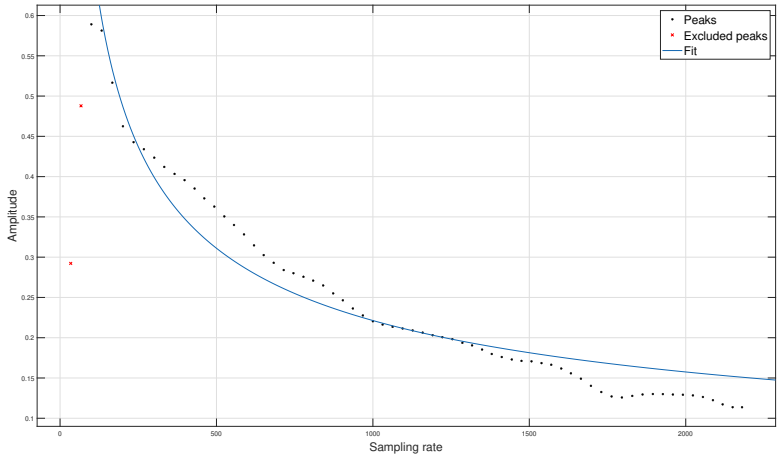

Figure 5.15: Peaks extracted from whipping event seen in Figure 5.14 used in curve fitting.

A collection of suitable responses was collected and evaluated. Results are presented in Table 5.9. The table includes the same procedure applied to a 3-node response as well. The damping ratio obtained would be locale, and is not representative of global damping values. Due to the complexity of structural damping and the simplicity of the method applied the results are not suggested as conclusive. However it should be noted that operational modal analysis performed by Soal et al. (2019) using PolyMax and CCSSI techniques identified damping ratios of 0.651% and 0.571%, respectively. A controlled damping evaluation could be performed by dropping the anchor and recording the response. Although hydrodynamic effects from velocity would not be detected (Storhaug, 2007a).

Table 5.9: Decremental decay and damping ratio based on 2-node and 3-node response.

Sensor	Decremental decay	Damping Ratio [%]
$B01_{SZ}$	0.0288	0.46
$D801_{PZ}$	0.0360	0.57
$SG02_{SZ}$	0.0325	0.52
$CL01_{SZ}$ curve fit	0.0137	0.22
$CL01_{SZ}$ 3-node	0.0437	0.7

5.0.8 Statistics

Statistical analysis can serve as a mean to validate and control data from acceleration time history and potentially reveal fault and errors. Statistical analysis has been performed in ways of, mean value, kurtosis, skewness and standard deviation. The excitations are assumed to depict the same distribution as the excitation sources. Ocean waves are considered to be the predominant source, following a Gaussian distribution.

Mean value

With the exception of vertically oriented *DC* accelerometers, a mean value of zero is expected. The mean values during all recordings are shown in Table D.6. DC accelerometers with a horizontal and longitudinal orientation displaying small deviations from $1g$ was assumed to correlate to sensor being installed with a small angle. For Vertical sensors displaying larger values than $9.81 m/s^2$ a initial angle deviation is not explanatory. Mean value analysis amplifies the necessity for signal processing by detrending and removing mean trends.

Kurtosis and standard deviation

From Table D.4 it is evident that majority of sensors experienced a kurtosis value in the proximity of 3. Higher kurtosis levels was seen for some ship section on severe conditions, e.g., deck 7 and 8. However, examining values from the stationary measurements labeled as recording 5 and 6 (see Table D.4), an marginally increased kurtosis is observed, compared to the two most severe conditions measured on the 30/07 (recording 7 and 8). It is evident from peak analysis that vessel velocity had a clear correlation to max acceleration amplitudes and mean peak value (Table D.2). This alone does not justify an increased kurtosis as it may also lead to increased standard deviation, as is seen in this circumstance. The relationship between kurtosis and standard deviation is easily observed by examining the accelerometers in the chain locker. A kurtosis level of approximately 3 is experienced on all days but the standard deviation levels are high and correlates with increase in speed, wave height and relative wave heading.

Higher kurtosis value can seem to be correlated with wave height and relative heading closer to 0. This is to be expected as it would cause higher acceleration levels and therefore a larger contribution in the tail of the distribution. It is noticed by comparing kurtosis values from ship sections that deck 7,8 and stern thruster room contain more acceleration outliers during severe wave conditions. If correlated with slamming events it can indicate a impact threshold causing high acceleration in these sections, however the observations are not deemed certain nor conclusive.

Some sensors experienced abnormal high values. This can be seen on a variety of the environmental conditions and sensors. The sensor on deck 7 with a transverse orientation experienced a kurtosis value of 20.95 on recording nr 9. From acceleration time history a consecutive time period of approximately 5 min contained large excitations before

acceleration levels return to comparable levels, relative to other conditions. FFT analysis indicated noise as all frequencies were excited. No correlation was seen with bow or stern slamming events. Further examination on cause of high kurtosis on other sensors were not conclusive.

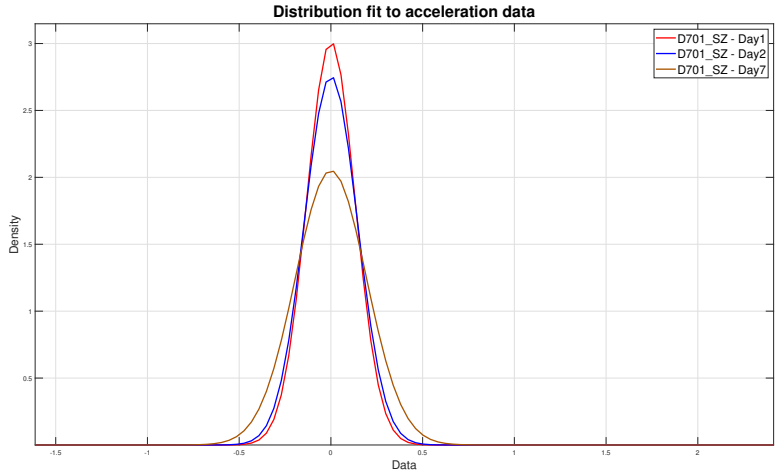

Figure 5.16: Distribution of vertically oriented accelerometer on deck 7. Kurtosis values for day 1,2 and 7 are respectively, 3.4, 4.92 and 6.27

Chapter 6

Conclusions

This thesis studied some of the current methods for performing hull condition monitoring.

The structural response from different environmental conditions experienced on the South African polar supply and research vessel, S.A. Agulhas was evaluated. Twelve recordings was selected on the basis of wave state severity, vessel velocity and ship heading. The data was subjected to post processing and analysed in frequency and time domain. Internal excitation sources from main engines was identified, but frequencies related to propulsion were not. The vibration modes were identified at 2.18, 3.83-4 and 5.18Hz for the 2nd 3rd and 4-node mode. Results were compared to previous investigations of the vessel and deviations between the OMA, FEM and power spectral analysis were observed. From frequency analysis a consistent frequency between ship section was observed for 2-node, while a larger frequency span was observed for 3-node mode. FFT analysis on slamming response identified 2nd 3rd and 4-node modes at 2.28Hz 3.95 and 5.32Hz. These frequencies are locally dominant but no conclusion to why 3-node vibration showed larger deviations could be made.

Energy content of higher vibration modes was seen to increase during ice navigation, where 3-node grew exponentially in comparison to 2-node. Larger excitation's of 3-node mode was also observed in the bow. Wave height and heading was seen to have a clear correlation to the energy content from whipping. Velocity maneuvers confirmed the relationship on peak vertical amplitudes. Furthermore it was seen that ship heading had a greater importance on peak values than velocity. Transverse accelerations were reduced at higher velocities, likely due to a reduction in rolling motion. It was observed that head waves contributed to the largest transverse accelerations.

Both frequency and time domain analysis confirmed the importance of ship heading as a mitigating measure to reduce slamming and consequently whipping and peak acceleration

levels. Stationary conditions under dynamic positioning in open water could reduce the frequency of bow slamming and acceleration levels by acquiring a slight heading of 35 degrees to the waves. However larger stern acceleration would occur with this heading. Although global ship dynamics were not analysed, bow slamming was seen to occurred close to the peak of pitch motion, indicating that slams arise from wave impact rather than bottom re-entry. Furthermore, impacts from slams transitioned to a section of high frequency content, identified as the water intrusion of the vessel. Impacts excited higher vibration modes and a possible correlation between significant slams to 4-node vibration mode were observed.

The algorithm developed and applied to detect slamming events would need to be altered and it is suggested that peak amplitudes are investigated for a multiple of mean peak amplitude. Studying the slamming was not conclusive to higher vibration modes. An inclination towards passing waves influencing the 3-node was made due to incremental sections. Investigations of global dynamic ship motions could enlighten this topic.

There was a lack of consistency seen between the sections that couldn't be explained. There was a search for a pattern which wasn't easily detected when analysing sensors located at elevated decks of the superstructure. Results from spectral analysis raised suspicion to each sensors individual credibility. Therefore focus was placed on vertical accelerometers in the hull, which allowed for confirmation through other accelerometers.

6.0.1 Recommendations for Further Work

Although the vessel instrumentation is limited by the permanent cables installed. For future measurements on the vessel, accelerometers are suggested to be fitted on stiffeners or longitudinal members to ensure consistency of structural rigidness. There was an issue with recognizing patterns from ship sections and acceleration values. Machine learning software has proven useful in these regards and it is suggested to be used for pattern recognition. Furthermore, placing accelerometers in a configuration about the transitional area between keel and bow could determine if the vessel is subjected to a larger degree of bottom slamming.

Further investigations should be focused to pin pointing the 3-node bending mode for the various ship sections and how wave state affects the frequency. Furthermore, pitch motion showed a correlation to slamming, however a global dynamic analysis should be performed to see how heaving motion is related. The relationship between acceleration values and excitation of 4 and 5-node modes is suggested

Reference is made to ISO 20283-4 for engine run up maneuvers to perform resonance investigations originating from main engines. Investigations to how increase in *MCR* is affected on ship sections should be included.

Further work could relate slamming detection algorithm to crew and passenger comfort levels. Allowing for detection of instances work was interrupted or passengers felt uncomfortable. The sound and vibration group conducted statistical analysis based on

surveys of human perception to slamming events. A bias involved is experience and adaptability of crew. However, if overcome surveys could be coupled with slamming detection algorithms. Applied to big data statistics gathered from wide usage of hull condition monitoring a probability chart can be extrapolated to link slamming with environmental condition and crew comfort.

Bibliography

ABS, 1995. Guide for hull condition monitoring systems.

Aertssen, G., 1968. Laboring of ships in rough seas with special emphasis on the fast ship. SNAME Diamond Jubilee International Meeting, June, pp. 18-21 .

Asmussen, I., Muller-Schmerl, A., 1995. Consideration Of Medium-speed Four-stroke Engines In Ship Vibration Analyses. WIT Transactions on the Built Environment; Southampton 12. URL: https://search.proquest.com/docview/2267017323/abstract/4E56C92053D24459PQ/1, doi:http://dx.doi.org/10.2495/MT950421.

Beghin, D., 2010. Ship Structural Analysis and design. The Society of Naval Architects and Marine Engineers, 601 Pavonia Avenue, Jersey City, New Jersey.

Bekker, A., Lu, L., van Zijl, C., Matthee, J., Kujala, P., 2019. Correlation between bow ice loads and operational responses during ice navigation in the weddell sea. Proceedings of the 25th International Conference on Port and Ocean Engineering under Arctic Conditions June 9-13, 2019, Delft, The Netherlands .

Bertram, V., 2012. Practical Ship Hydrodynamics (2nd Edition). Elsevier, Newark, UNITED KINGDOM. URL: https://app.knovel.com/hotlink/pdf/id:kt00B8MYU1/practical-ship-hydrodynamics/excitation-propellers.

Brandt, A., 2011. Noise and vibration signal analysis and experimental procedures. A John Wiley and Sons, Ltd., Publication,.

Braun, S., Ewins, D., Rao, S., 2002. Encyclopedia of Vibration, Volumes 1-3. Cambridge University press.

Casiano, M., 2016. Extracting damping ratio from dynamic data and numerical solutions. URL: https://ntrs.nasa.gov/archive/nasa/casi.ntrs.nasa.gov/20170005173.pdf.

DNVGL, 2011. Dnv vibration class, newbuildings, special equiptment and systems additional class. URL: https://rules.dnvgl.com/docs/pdf/dnv/rulesship/2011-01/ts615.pdf.

DNVGL, 2017. Part 4. systems and components chapter 9 control and monitoring systems. URL: https://rules.dnvgl.com/docs/pdf/dnvgl/ru-ship/2017-01/DNVGL-RU-SHIP-Pt4Ch9.pdf.

DNVGL, 2019. Digital twins and sensor monitoring. URL: https://www.dnvgl.com/expert-story/maritime-impact/Digital-twins-and-sensor-monitoring.html.

Faltinsen, 2005. Hydrodynamics of high-speed marine vehicles. Cambridge University Press, Cambridge.

Fonseca, N., Soares, G., 2006. Whipping response of vessels with large amplitude motions. Proceedings of the International Conference on Offshore Mechanics and Arctic Engineering .

Ghalishooyan, M., Shooshtari, A., 2015. Operational modal analysis techniques and their theoretical and practical aspects: A comprehensive review and introduction. 6th International Operational Modal Analysis Conference, IOMAC 2015 .

Gianpiero, R., Peeters, B., Ota, R., 2016. Experimental ship hull dynamic characterization using operational modal analysis. IOMAC'11 – 4th International Operational Modal Analysis Conference .

Gunnar Lian, S.K.H., 2016. Estimating long-term extreme slamming from breaking waves. Ocean, Offshore, and Arctic Engineering Division of ASME .

Hirdaris, S., Temarel, P., 2009. Hydroelasticity of ships: recent advances and future trends. Proc. IMechE Vol. 223 Part M: J. Engineering for the Maritime Environment .

ISO 20283-2, 2008. Mechanical vibration - measurement of vibration on ships - measurement of structural vibration - part 2.

ISO 20283-4, 2012. Mechanical vibration — measurement of vibration on ships — part 4: Measurement and evaluation of vibration of the ship propulsion machinery.

ISO 20283-5, 2016. Measurement of vibration on ships — part 5: Guidelines for measurement, evaluation and reporting of vibration with regard to habitability on passenger and merchant ships.

ITTC, 2017. The seakeeping committee, Final Report and Recommendations to the 28th ITTC Conferance.

Lillemäe-Avi, I., Liinalampi, S., Lehtimäki, E., Remes, H., Lehto, P., Romanoff, J., Ehlers, S., Niemelä, A., 2018. Fatigue strength of high-strength steel after shipyard production process of plasma cutting, grinding, and sandblasting .

Lloyds register, 2006. Ship vibration and noise. URL: https://www.cdinfo.lr.org/information/Documents/LRGuidance/Vibration%20&%20Noise%20Guidance%20Notes%202.pdf#page=31.

Matlab, 2019. Pwelch. URL: https://se.mathworks.com/help/signal/ref/pwelch.html.

Naess, A., Gaidai, O., Storhaug, G., Ye, R., Cheng, Y., Xu, X., 2019. Efficient fatigue assessment of ship structural details. Ships and Offshore Structures 0, 1–8. URL: https://doi.org/10.1080/17445302.2019.1661623, doi:10.1080/17445302.2019.1661623.

Naess, A., Moan, T., 2012. Stochastic Dynamics of Marine Structures. Cambridge University Press. doi:10.1017/CBO9781139021364.

Newland, D., 1993. An introduction to random vibrations, spectral and wavelet analysis. CDover publications, inc.

Ochi, M., 1964. Extreme behavior of a ship in rough seas : - slamming and shipping green water. SNAME.

Omer, H. Bekker, A., 2016. Detection of wave slamming sites from ship deflections URL: :https://www.researchgate.net/publication/309040742.

P. Lacey, H.C., 1995. Improved passage planning using weather forecasting maneuvering guidance, and instrumentation feedback .

Peeters, B., Van der Auwerer, H., 2005. Polymax: A revolution in operational modal analysis. In Proceedings of the 1st International Operational Modal Analysis Conference, Copenhagen, Denmark, 26-27 April 2005 .

Randall, R., 2011. Vibration-Based Condition Monitoring : Industrial, Aerospace and Automotive Applications. John Wiley Sons, Incorporated, Hoboken, New Jersey.

Rina, 2019. International standards for ship vibration. URL: https://www.rina.org.uk/International_standards_for_ship_vibration.html.

Shan Wang, C.G.S., 2015. Experimental and numerical study of the slamming load on the bow of a chemical tanker in irregular waves. Centre for Marine Technology and Ocean Engineering (CENTEC), Instituto Superior Técnico, Universidade de Lisboa, Portugal .

Soal, K., Bekker, A., 2014. Whole-body vibration comfort on the S.A. Agulhas II Polar Supply and Research Vessel During a voyage to Antarctica.

Soal, K., Bienert, J., Bekker, A., 2019. Operational Modal Analysis on The Polar Supply and Research Vessel the S.A. Agulhas II During ice Navigation in The Weddell Sea .

Soares, C.G., 2015. Transient response of ship hulls to wave impact .

Storhaug, G., 2007a. Experimental investigation of wave induced vibrations and their effect on the fatigue loading of ships. Dr.Sc. NTNU.

Storhaug, G., 2007b. Measurements of wave induced hull girder vibrations of an ore carrier in different trades. Journal of Offshore Mechanics and Arctic Engineering, Vol. 129, ASME .

Wang, S., Soares, G., 2017. Review of ship slamming loads and responses .

Wartsila, 2018. Wartsila 32 product guide. URL: https://www.wartsila.com/docs/default-source/product-files/engines/ms-engine/product-guide-o-e-w32.pdf?utm_source=engines&utm_medium=dieselengines&utm_term=w32&utm_content=productguide&utm_campaign=msleadscoring.

Appendix A

Matlab scripts

For further questions regarding Matlab scripts, contact the author.

Slam detection

Slamming detection of all sensors on one environmental conditions.

```
%if std > 0.4*9.81 index position is saved in indexstruct. run seperatly
%for each environmental condition and saved as variable.
%indexpoints saved for each Col_X where X is sensor
% from 1 to 30.

%x= Yhp_1024(1).sensors(:,:); Acceleration data
indexstruct=struct;
indexvec=[];
j=1;
index=1;
runloop=true;
i=0;

while runloop
    i=i+1;
    if index+100>length(x)
        index=1;
        ind_col=['col_' num2str(j)];%make new struct field name
        indexstruct.(ind_col)=indexvec;% Make new field in struct for indexvec with column number
        indexvec=[]; %make indexvec empty for new column
        j=j+1;
        if j>size(x,2)%If j is larger than numbers of columns, break loop
            break
        end
    end
    vec1=x(index:index+100,j);
    if  std(vec1) > 0.4*9.81  % criterion to be exceeded
        indexvec=[indexvec,index];
        index=index+100;
    else
        index=index+10;  % step increase from 1 to 10 to increase analysis speed.

    end

end
```

Figure A.1: Matlab script of algorithm used to detect slamming events.

Appendix B

Power spectral analysis

Figures display power spectral density of all accelerometers. Accelerometer number from 1 to 30, corresponding to sensor identification numbers as seen in figures of instrumentation layout.

B.0.1 Logarithmic Plot

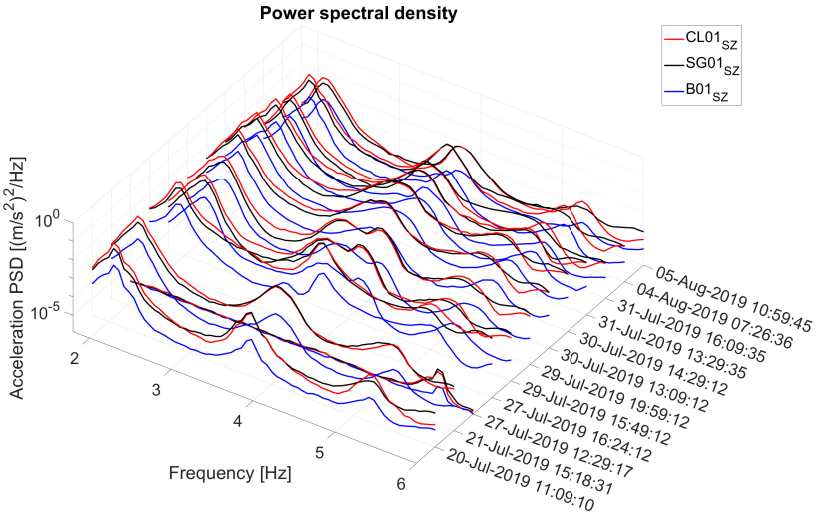

Figure B.1: Power spectral density of selected vertical sensors in Chain locker, steering gear room and bridge. The plots shows a logarithmic scale. It is seen that the two stationary conditions on the 29 July has a double peak for in the proximity of the 3-node vibration mode

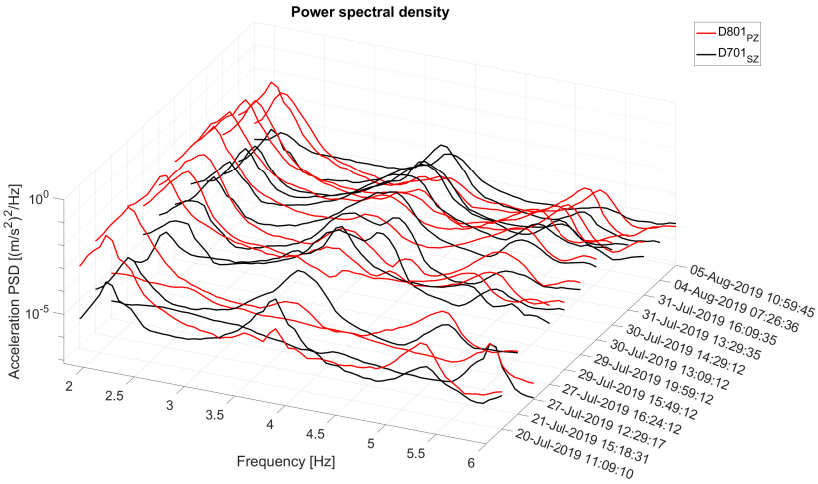

Figure B.2: Logarithmic plot of accelerometers on deck 7 and 8

B.0.2 Power Spectral Density of All Accelerometers From Recordings

Dotted line indicate longitudinal direction. Stippled line indicate transverse direction. Consolidated line indicate vertical direction of accelerometers. Plotted lines have further been marked corresponding to ship section locality.

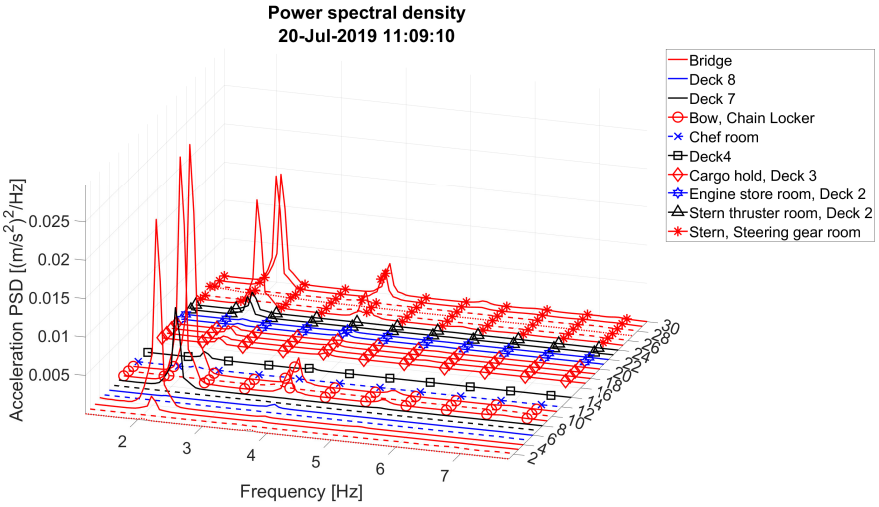

Figure B.3: Power spectral density from 20-July.Recording Nr 1.

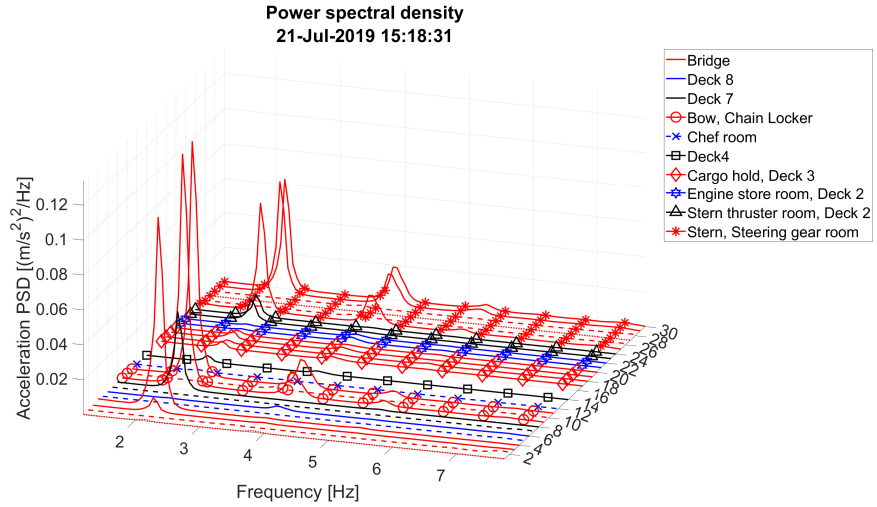

Figure B.4: Power spectral density from 21-July. Recording Nr 2.

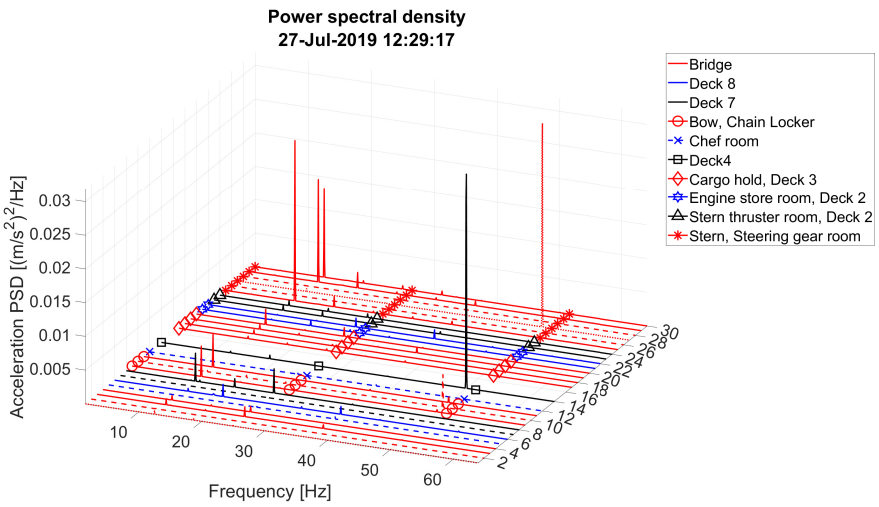

Figure B.5: Power spectral density from 27-July - Stationary, Recording Nr 3.

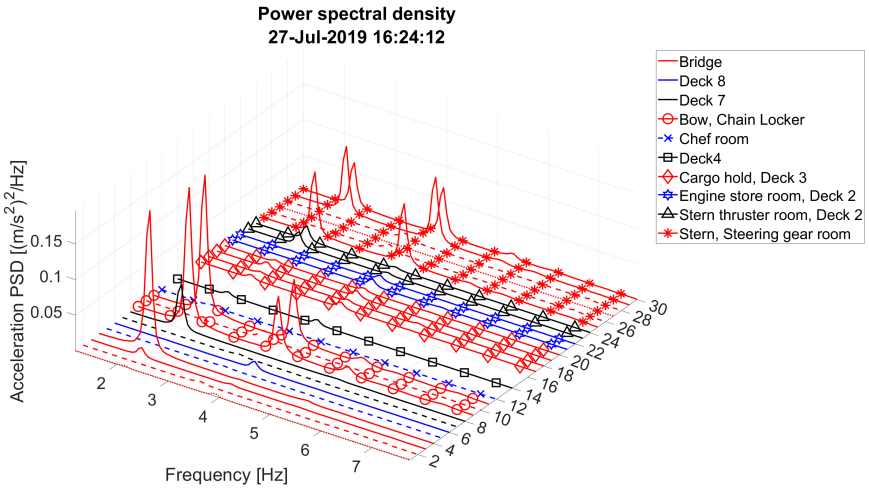

Figure B.6: Power spectral density from 27-July - Ice navigation, Recording Nr 4.

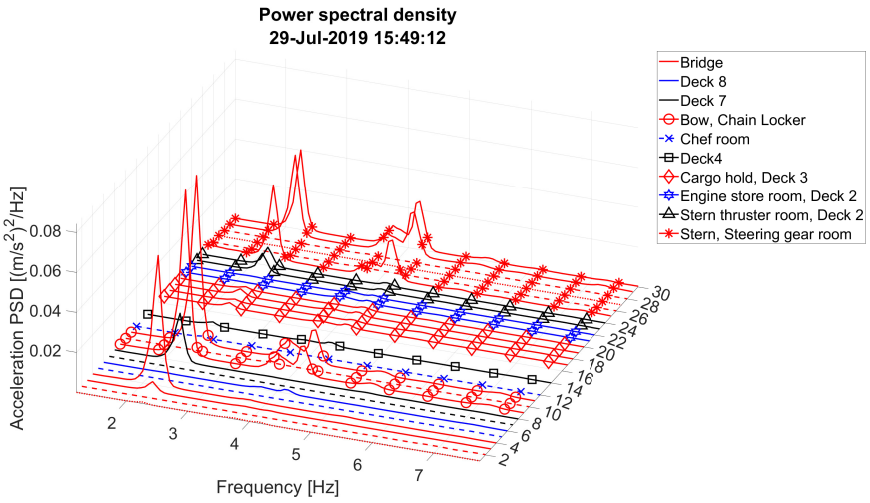

Figure B.7: Power spectral density from 29-July - Recording Nr 5.

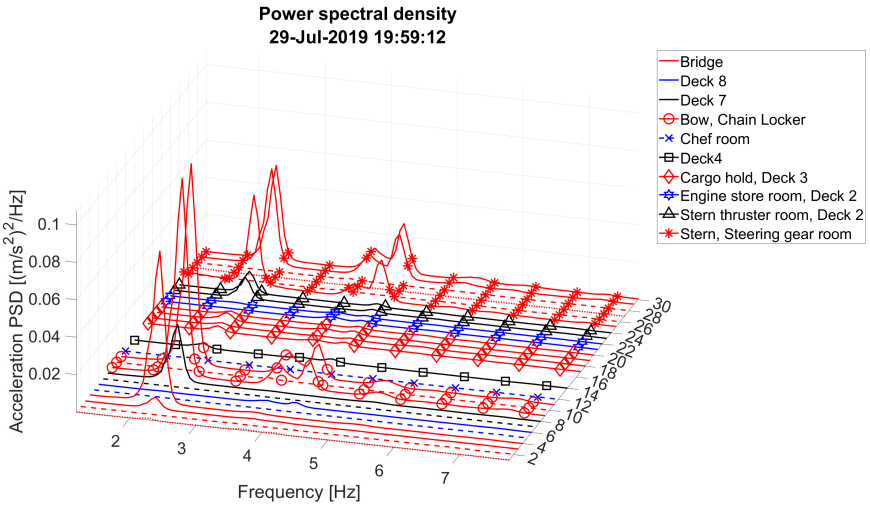

Figure B.8: Power spectral density from 29-July - Recording Nr 6.

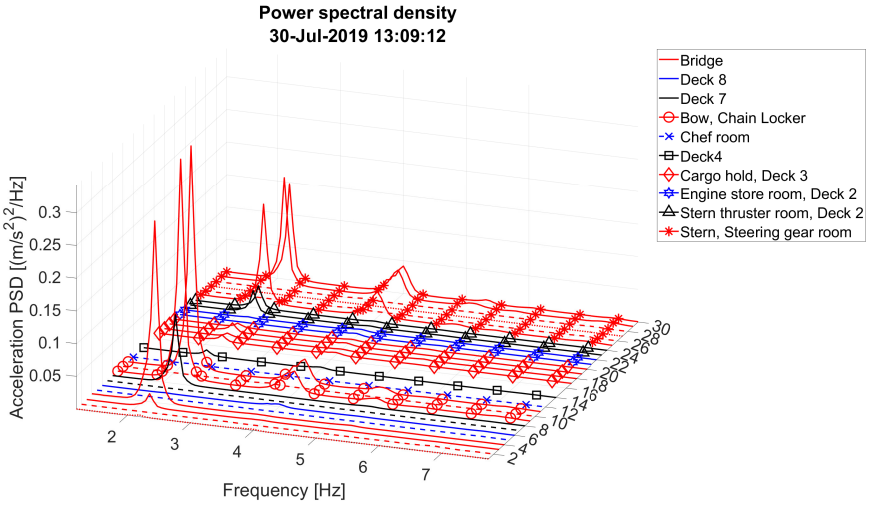

Figure B.9: Power spectral density from 30-July. Recording Nr 7.

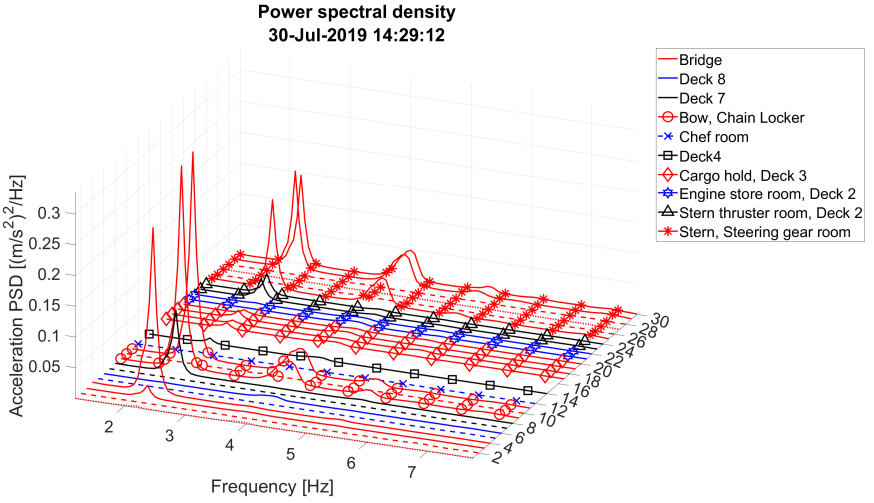

Figure B.10: Power spectral density from 30-July. Recording Nr 8.

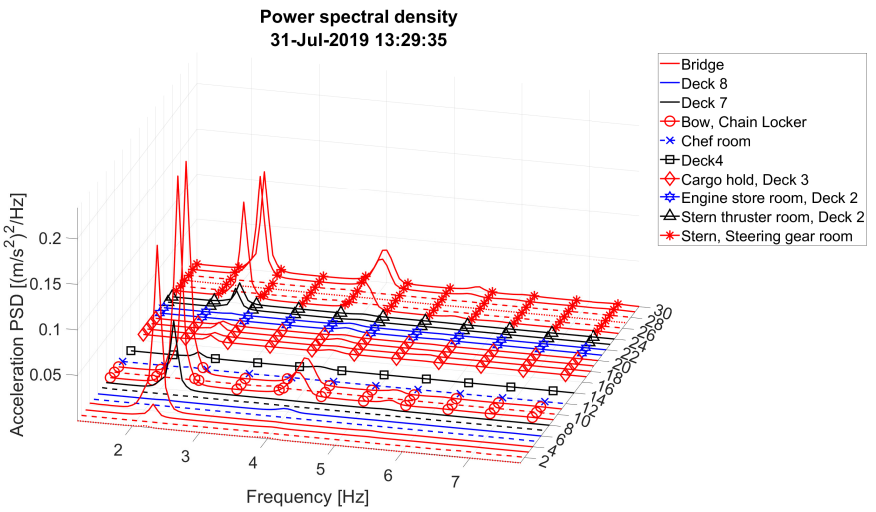

Figure B.11: Power spectral density from 31-July. Recording Nr 9.

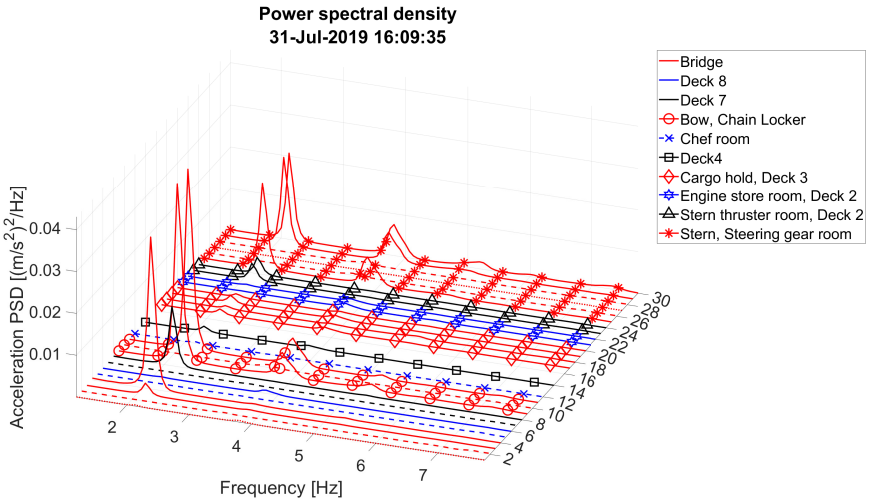

Figure B.12: Power spectral density from 31-July. Recording Nr 10.

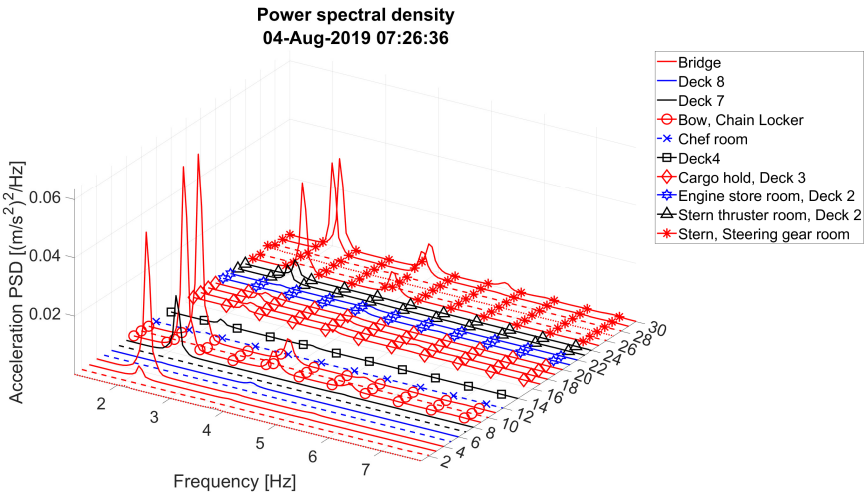

Figure B.13: Power spectral density from 04-August. Recording Nr 11.

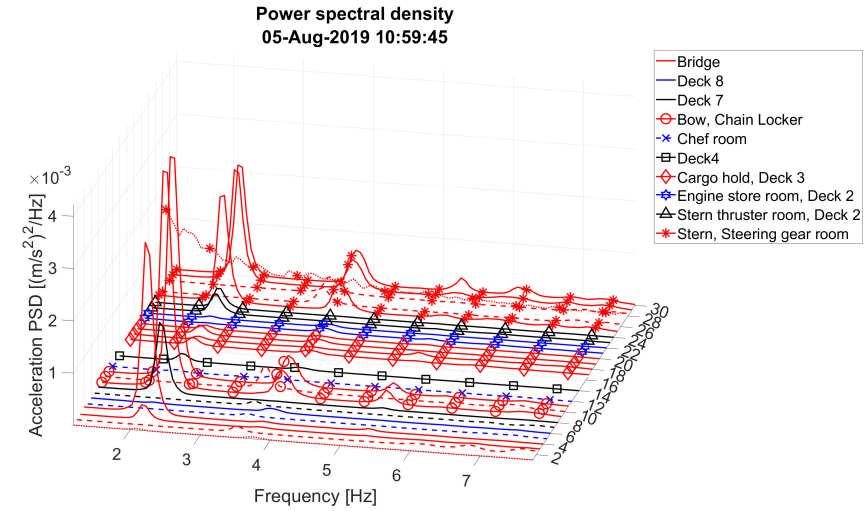

Figure B.14: Power spectral density from 05-August. Recording Nr 12.

Appendix C

Slamming

Slamming event seen in Case 1

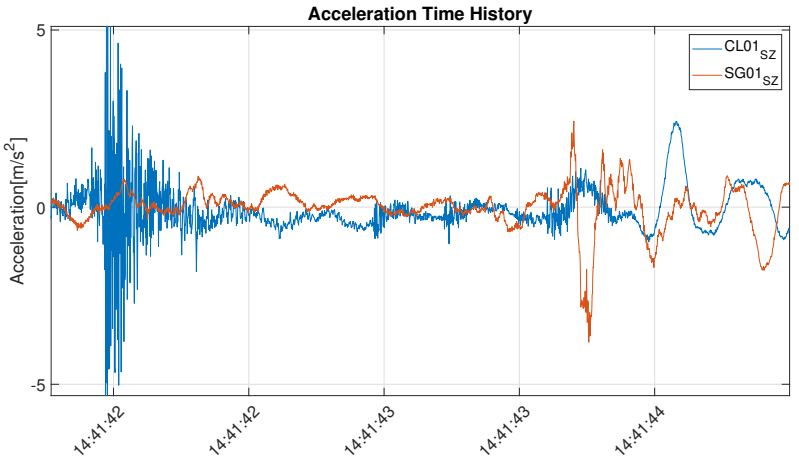

Figure C.1: Close up of slam seen at 14:41:42. $CL01_{SZ}$ oscillates at the frequency of 3-node mode, with high frequency noise. The high frequency part is believed to come from water intrusion of the bow.

C.1 2 and 3-node vibration modes

Case 1

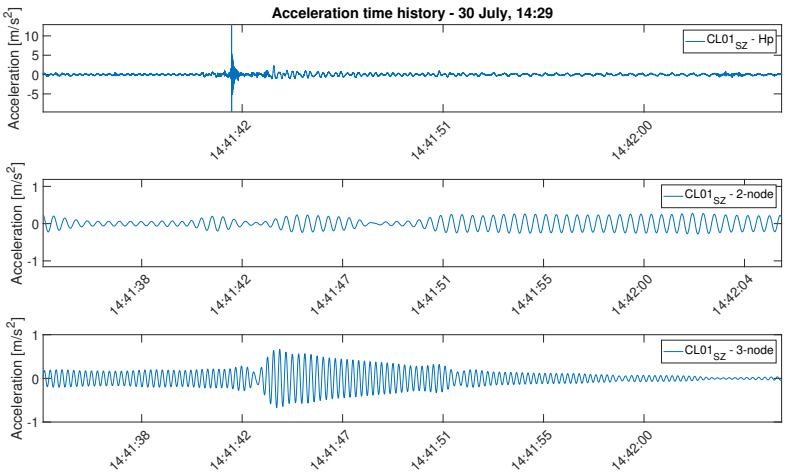

Figure C.2: From top to bottom: Highpass, 2-node and 3-node bandpass filtered signal of chain locker sensor from slamming event in Case 1.

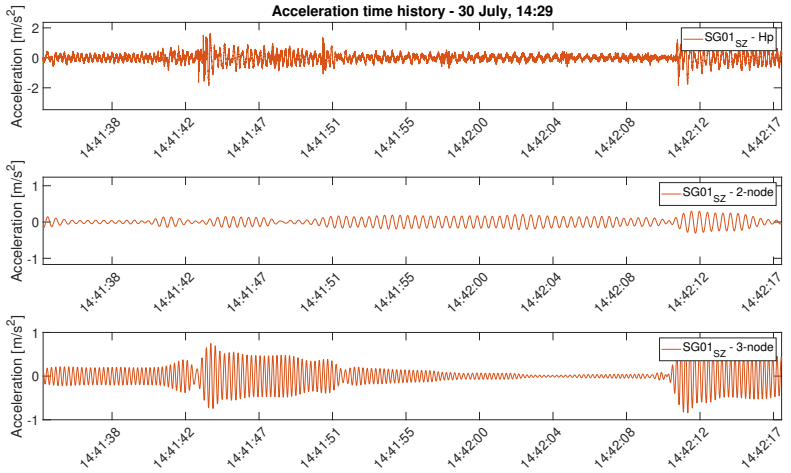

Figure C.3: From top to bottom: Highpass, 2-node and 3-node bandpass filtered signal of steering gear room sensor from slamming event in Case 1.

Case 3

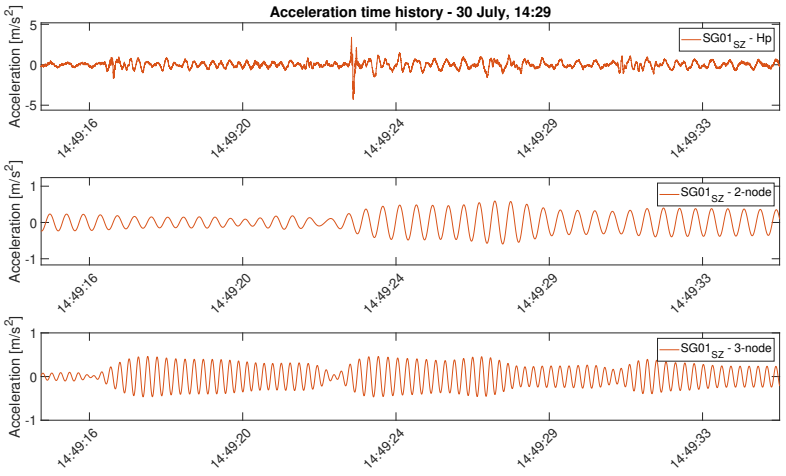

Figure C.4: From top to bottom: Highpass, 2-node and 3-node bandpass filtered signal of steering gear room sensor from slamming event in Case 3.

C.2 FFT Slamming

Case 1

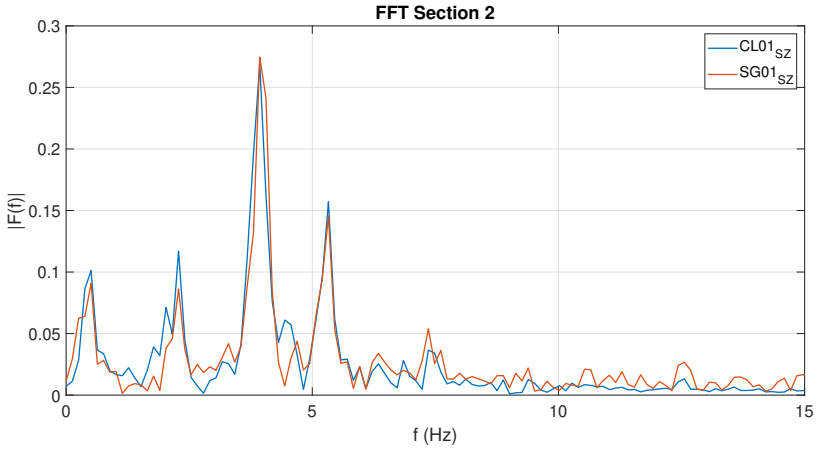

Figure C.5: FFT from approximately 3 seconds after the slamming event in case 1. lasting 7 seconds.

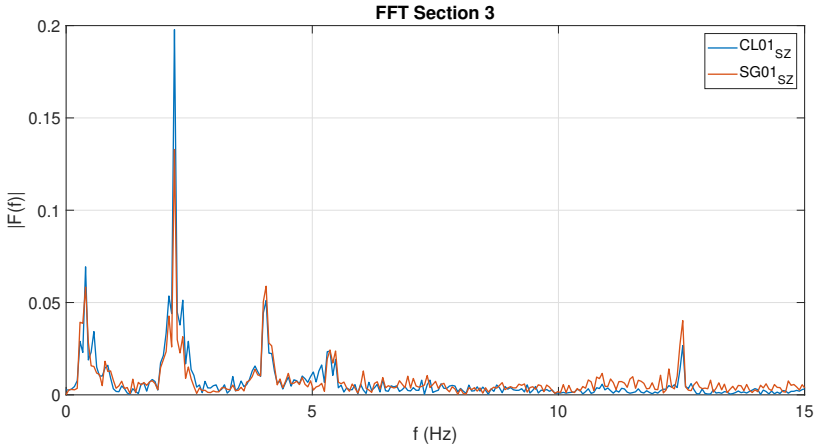

Figure C.6: FFT from approximately 10 seconds after the slam in case 1. lasting 17 seconds.

Case 2

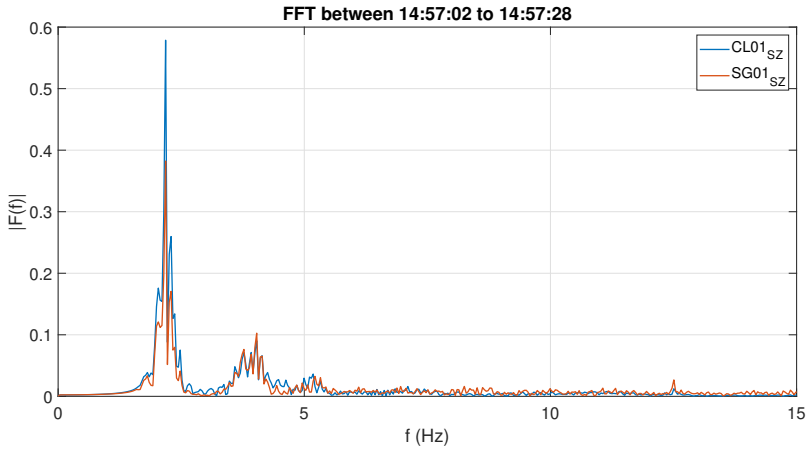

Figure C.7: FFT of section immediately after second slamming event in case 2. Response lasts approximately 26 seconds. from 14:57:02 to 14:57:28. The frequency of the second bending mode is excited at 2.18Hz

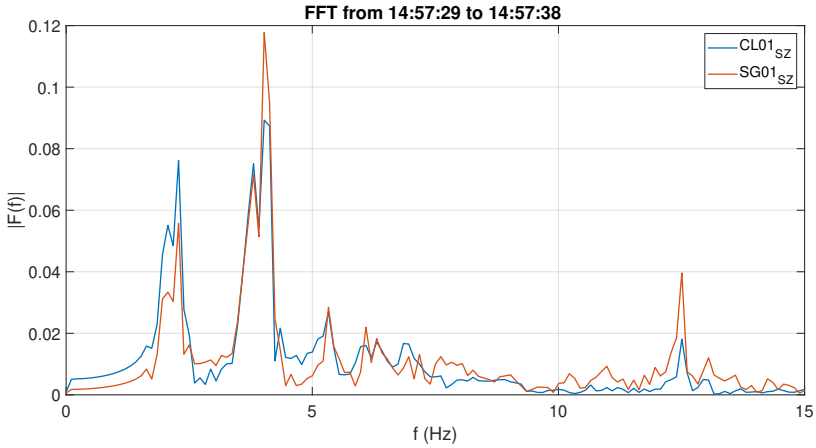

Figure C.8: FFT of section between 14:57:29 to 14:57:38. The FFT reveals components at 2.28Hz and 4.024Hz

Appendix D

Peak amplitude evaluation

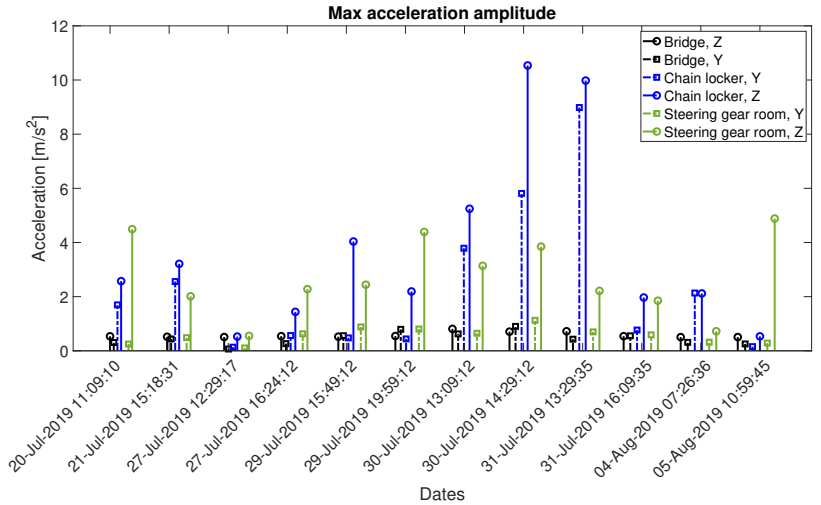

Figure D.1: Maximum amplitude for bow, bridge and stern sensors. Circle indicate vertical orientation. Square indicates transverse direction.

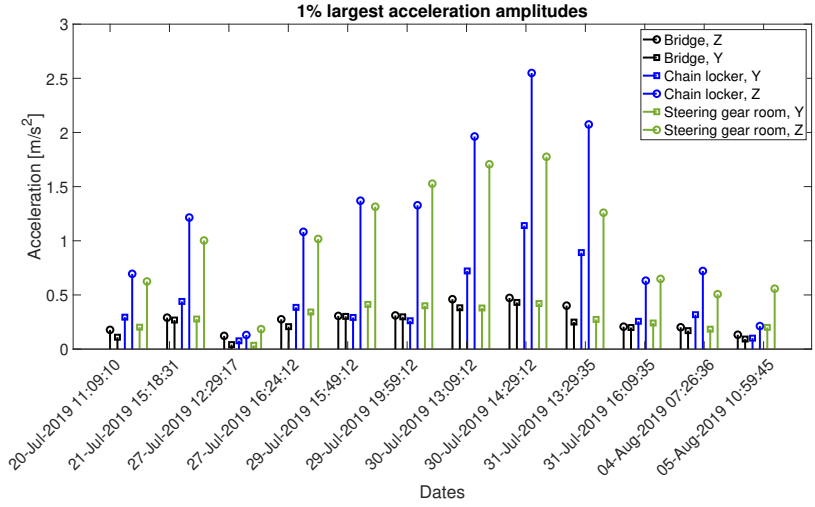

Figure D.2: Maximum 1% amplitude for bow, bridge and stern sensors. Circle indicate vertical orientation. Square indicates transverse direction.

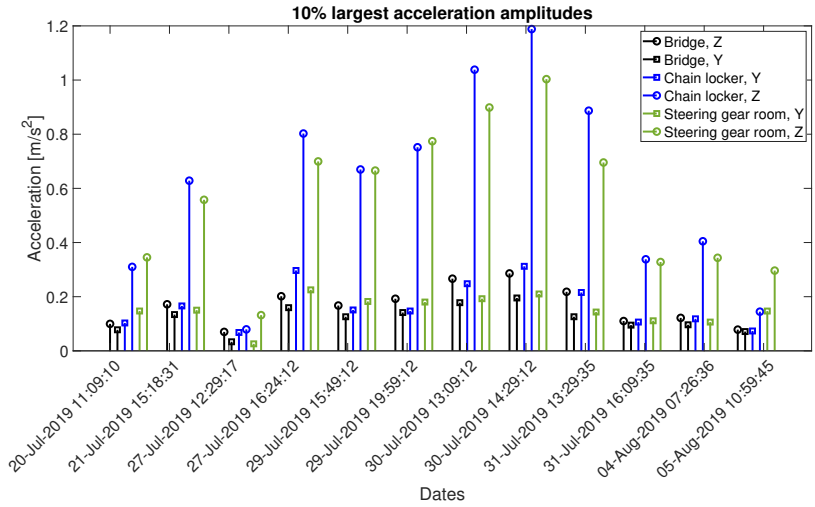

Figure D.3: Max 10% largest amplitudes for bow, bridge and stern sensors. Circle indicate vertical orientation. Square indicates transverse direction.

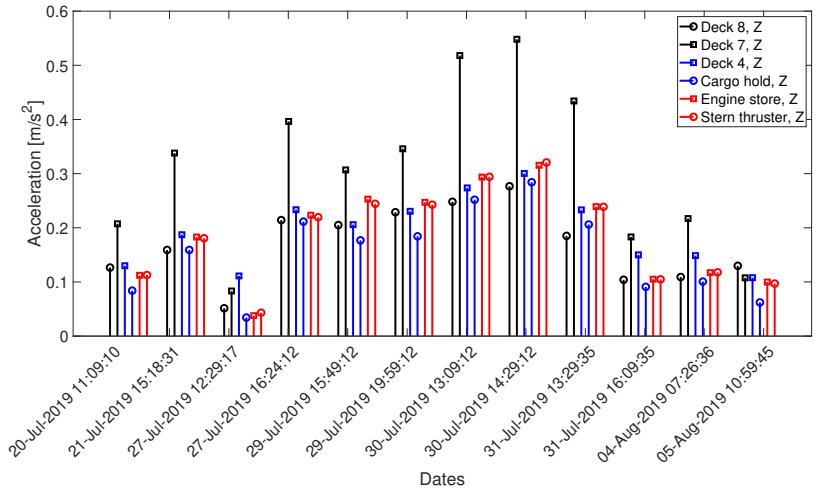

Figure D.4: Maximum amplitude for superstructure. All sensors are vertically oriented.

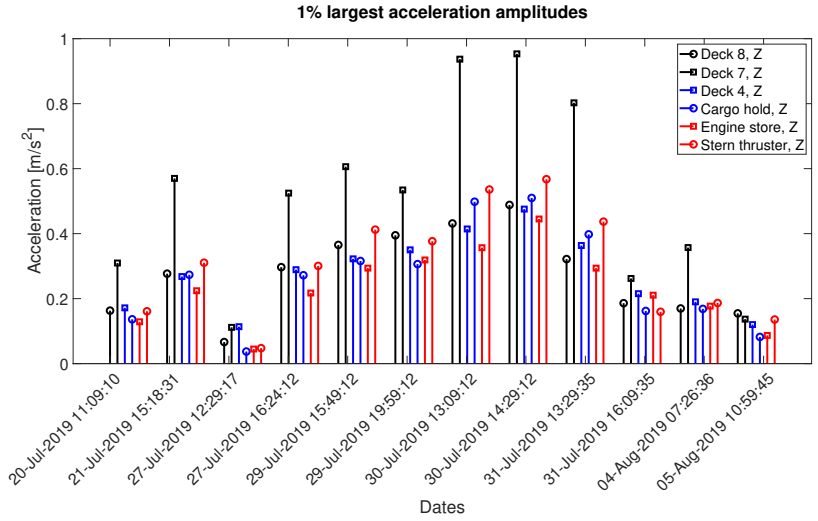

Figure D.5: Maximum 1% largest amplitudes for superstructure. All sensors are vertically oriented.

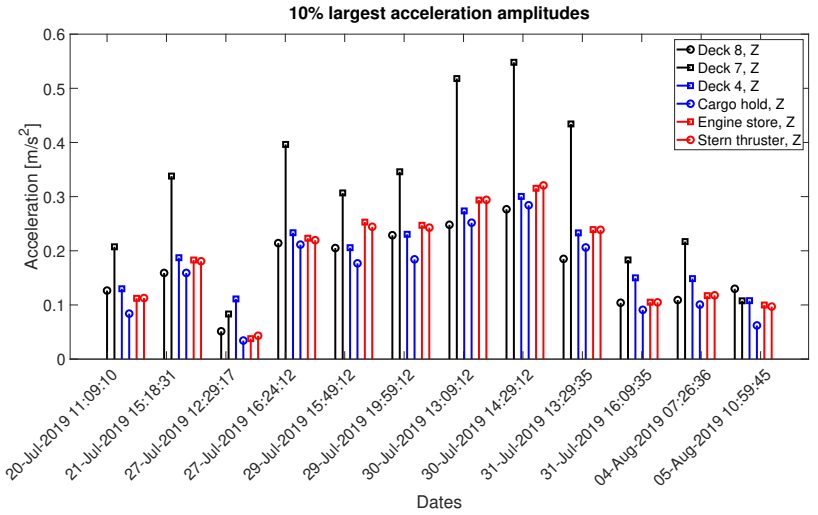

Figure D.6: Max 10% largest amplitudes for superstructure. All sensors are vertically oriented

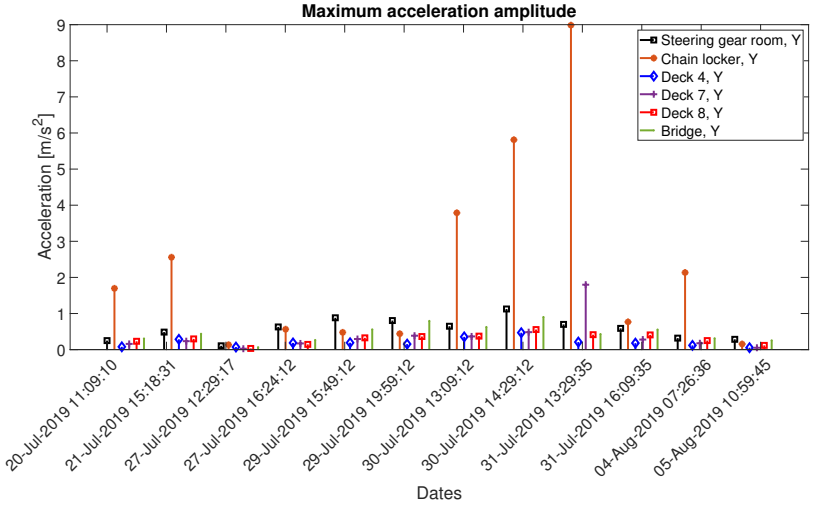

Figure D.7: Maximum acceleration peak amplitudes. All sensors are in transverse direction.

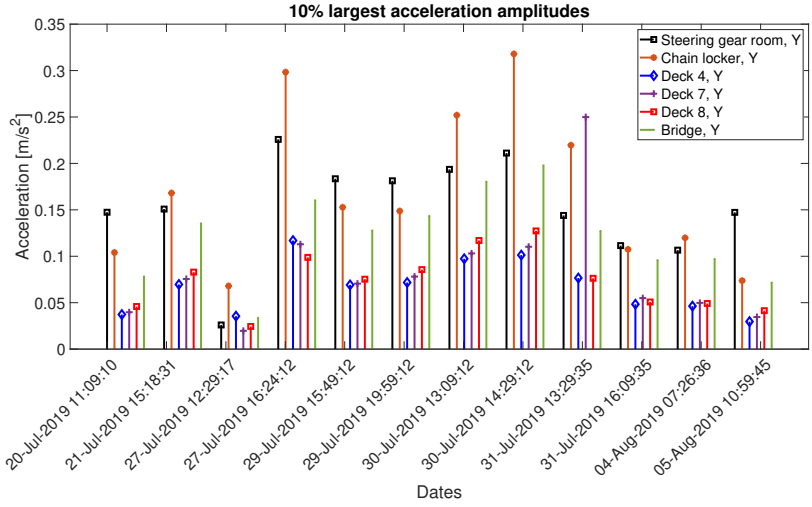

Figure D.8: Average 10% largest acceleration peak amplitudes. All sensors are in transverse direction

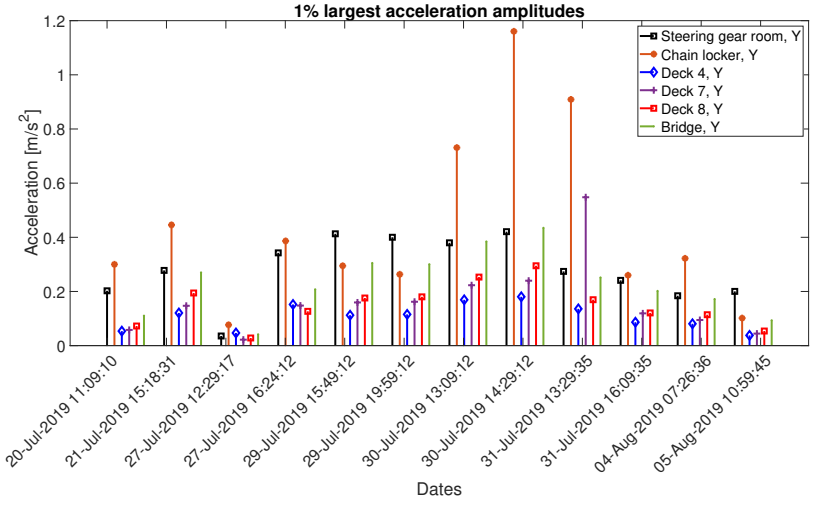

Figure D.9: Average 1% largest acceleration peak amplitudes. All sensors are in transverse direction.

Table D.1: Peak amplitude ratio between the average of the 50 largest amplitudes, made between 10kn, 8kn and 6kn

Sensors	10 kn/8 kn	10 kn/6 kn	8 kn/6 kn
$B01_{SX}$	1.31	1.43	1.09
$B01_{SY}$	0.88	0.89	1.01
$B01_{SZ}$	1.30	1.68	1.29
$B02_{PZ}$	1.33	1.92	1.45
$D801_{PY}$	0.85	0.88	1.04
$D801_{PZ}$	1.01	1.00	0.99
$D701_{SY}$	0.91	0.24	0.26
$D701_{SZ}$	1.27	1.82	1.44
$CL01_{SZ}$	1.14	1.43	1.26
$CL02_{0Y}$	0.96	0.91	0.95
$CL03_{PZ}$	1.11	1.26	1.14
$CR01_{SY}$	1.11	1.40	1.26
$CR01_{SZ}$	1.34	2.04	1.52
$XX01_{0Z}$	1.23	1.26	1.02
$CH01_{PZ}$	1.29	1.48	1.14
$CH02_{PZ}$	1.08	1.14	1.06
$CH03_{SZ}$	1.31	1.67	1.27
$CH04_{SZ}$	1.02	1.26	1.23
$ES01_{SZ}$	0.95	0.90	0.95
$FW01_{PZ}$	0.98	1.07	1.09
$ST01_{SZ}$	1.31	1.71	1.31
$ST02_{PZ}$	1.31	1.65	1.26
$SG02_{SZ}$	1.31	1.56	1.19
$SG02_{SY}$	0.89	0.87	0.97
$SG01_{SX}$	0.84	0.79	0.94
$SG01_{SY}$	0.89	0.89	1.00
$SG01_{PZ}$	1.31	1.44	1.10
$SG01_{SZ}$	1.38	1.41	1.03

D.1 Mean peak value

Table D.2: Mean value of all peak values

	Sensors	Environemental condition											
		1	2	3	4	5	6	7	8	9	10	11	12
Bridge	$B01_{SX}$	0.034	0.048	0.031	0.079	0.051	0.055	0.069	0.074	0.059	0.034	0.036	0.033
	$B01_{SY}$	0.047	0.061	0.023	0.083	0.044	0.047	0.068	0.071	0.054	0.047	0.049	0.044
	$B01_{SZ}$	0.053	0.084	0.048	0.114	0.079	0.087	0.116	0.124	0.097	0.060	0.063	0.049
	$B02_{PZ}$	0.094	0.187	0.026	0.279	0.150	0.180	0.268	0.285	0.224	0.111	0.122	0.055
Deck 8	$D801_{PY}$	0.028	0.034	0.016	0.052	0.026	0.029	0.042	0.044	0.031	0.025	0.023	0.026
	$D801_{PZ}$	0.082	0.081	0.037	0.126	0.108	0.121	0.106	0.115	0.092	0.062	0.068	0.086
Deck 7	$D701_{SY}$	0.023	0.034	0.015	0.055	0.024	0.026	0.036	0.038	0.080	0.027	0.023	0.020
	$D701_{SZ}$	0.116	0.159	0.063	0.219	0.135	0.148	0.211	0.222	0.175	0.097	0.104	0.068
Chain locker	$CL01_{SZ}$	0.125	0.265	0.041	0.430	0.247	0.280	0.385	0.415	0.324	0.148	0.165	0.085
	$CL02_{0Y}$	0.051	0.061	0.053	0.149	0.058	0.058	0.077	0.088	0.062	0.048	0.049	0.044
	$CL03_{PZ}$	0.131	0.274	0.059	0.433	0.255	0.287	0.391	0.422	0.331	0.149	0.165	0.087
Chefs room deck 7	$CR01_{SY}$	0.021	0.032	0.018	0.059	0.030	0.033	0.042	0.044	0.034	0.024	0.023	0.019
Deck 4	$CR01_{SZ}$	0.290	0.648	0.035	0.849	0.479	0.584	0.876	0.925	0.727	0.358	0.400	0.152
	$XX01_{0Z}$	0.100	0.124	0.103	0.160	0.130	0.138	0.158	0.163	0.143	0.112	0.105	0.089
Cargo hold	$CH01_{PZ}$	0.039	0.068	0.024	0.122	0.076	0.079	0.095	0.104	0.081	0.044	0.048	0.035
	$CH02_{PZ}$	0.036	0.065	0.018	0.134	0.074	0.075	0.086	0.095	0.073	0.039	0.041	0.037
	$CH03_{SZ}$	0.046	0.074	0.027	0.120	0.071	0.075	0.100	0.109	0.087	0.044	0.047	0.039
	$CH04_{SZ}$	0.041	0.068	0.031	0.112	0.072	0.077	0.091	0.099	0.077	0.035	0.037	0.036
Engine store	$ES01_{SZ}$	0.051	0.058	0.028	0.091	0.060	0.064	0.077	0.086	0.069	0.043	0.046	0.048
Fresh water	$FW01_{PZ}$	0.048	0.061	0.037	0.084	0.062	0.064	0.076	0.083	0.067	0.050	0.045	0.046
Stern thruster room	$ST01_{SZ}$	0.066	0.087	0.029	0.117	0.100	0.106	0.120	0.128	0.103	0.054	0.058	0.060
	$ST02_{PZ}$	0.066	0.086	0.034	0.115	0.099	0.105	0.122	0.130	0.104	0.055	0.059	0.058
Steering gear room	$SG02_{SZ}$	0.172	0.243	0.100	0.355	0.248	0.279	0.341	0.367	0.297	0.149	0.161	0.148
	$SG02_{SY}$	0.085	0.073	0.017	0.108	0.059	0.059	0.072	0.076	0.059	0.057	0.054	0.086
	$SG01_{SX}$	0.078	0.070	0.101	0.099	0.055	0.053	0.049	0.054	0.053	0.049	0.053	0.108
	$SG01_{SY}$	0.088	0.076	0.026	0.108	0.061	0.062	0.075	0.079	0.062	0.061	0.057	0.088
	$SG01_{SZ}$	0.185	0.254	0.099	0.374	0.261	0.293	0.362	0.393	0.308	0.160	0.170	0.165
	$SG01_{PZ}$	0.189	0.262	0.081	0.344	0.279	0.299	0.354	0.390	0.329	0.164	0.175	0.172

D.2 Standard deviation

Table D.3: Acceleration standard deviation from all environmental condition

	Sensors	Environemental condition											
		1	2	3	4	5	6	7	8	9	10	11	12
Bridge	$B01_{SX}$	0.313	0.319	0.014	0.043	0.285	0.324	0.424	0.464	0.350	0.211	0.285	0.090
	$B01_{SY}$	0.371	0.380	0.023	0.066	0.314	0.275	0.741	0.691	0.515	0.425	0.513	0.404
	$B01_{SZ}$	0.430	0.412	0.021	0.064	0.290	0.324	0.569	0.592	0.468	0.322	0.454	0.180
	$B02_{PZ}$	0.159	0.208	0.018	0.203	0.142	0.168	0.284	0.297	0.239	0.130	0.157	0.047
Deck 8	$D801_{PY}$	0.032	0.034	0.019	0.035	0.034	0.034	0.053	0.053	0.040	0.035	0.043	0.022
	$D801_{PZ}$	0.070	0.056	0.022	0.066	0.059	0.065	0.091	0.095	0.075	0.066	0.082	0.050
Deck 7	$D701_{SY}$	0.036	0.038	0.008	0.036	0.031	0.032	0.063	0.061	0.078	0.042	0.053	0.025
	$D701_{SZ}$	0.132	0.145	0.032	0.127	0.101	0.112	0.195	0.203	0.166	0.106	0.133	0.052
Chain locker	$CL01_{SZ}$	1.013	1.024	0.024	0.250	0.845	0.950	1.362	1.480	1.124	0.675	0.931	0.297
	$CL02_{0Y}$	0.318	0.348	0.033	0.097	0.346	0.306	0.664	0.642	0.468	0.407	0.463	0.389
	$CL03_{PZ}$	1.017	1.023	0.027	0.254	0.853	0.950	1.362	1.480	1.125	0.691	0.938	0.296
Chefs room deck 7	$CR01_{SY}$	0.042	0.049	0.052	0.088	0.054	0.065	0.088	0.081	0.080	0.058	0.056	0.032
Deck 4	$CR01_{SZ}$	0.587	0.791	0.017	0.670	0.496	0.590	0.959	1.003	0.824	0.424	0.519	0.162
	$XX01_{0Z}$	0.079	0.081	0.063	0.082	0.077	0.081	0.105	0.107	0.094	0.082	0.088	0.058
Cargo hold	$CH01_{PZ}$	0.109	0.104	0.012	0.063	0.073	0.077	0.139	0.148	0.118	0.083	0.106	0.035
	$CH02_{PZ}$	0.137	0.128	0.011	0.067	0.090	0.094	0.168	0.181	0.144	0.102	0.130	0.041
	$CH03_{SZ}$	0.088	0.090	0.016	0.066	0.061	0.066	0.117	0.125	0.101	0.067	0.086	0.031
	$CH04_{SZ}$	0.134	0.127	0.028	0.059	0.083	0.090	0.162	0.174	0.139	0.098	0.126	0.041
Engine store	$ES01_{SZ}$	0.070	0.069	0.038	0.057	0.062	0.065	0.089	0.095	0.080	0.065	0.078	0.043
Fresh water	$FW01_{PZ}$	0.064	0.063	0.020	0.047	0.057	0.059	0.089	0.093	0.075	0.064	0.077	0.037
Stern thruster room	$ST01_{SZ}$	0.100	0.104	0.015	0.071	0.088	0.098	0.144	0.151	0.124	0.087	0.107	0.045
	$ST02_{PZ}$	0.099	0.103	0.017	0.071	0.088	0.097	0.143	0.150	0.124	0.087	0.107	0.045
Steering gear room	$SG02_{SZ}$	0.153	0.191	0.052	0.204	0.179	0.215	0.270	0.290	0.228	0.132	0.157	0.082
	$SG02_{SY}$	0.060	0.057	0.067	0.095	0.084	0.076	0.107	0.109	0.094	0.082	0.069	0.049
	$SG01_{SX}$	0.118	0.093	0.062	0.049	0.170	0.105	0.106	0.122	0.174	0.061	0.220	0.219
	$SG01_{SY}$	0.309	0.353	0.023	0.078	0.259	0.251	0.549	0.499	0.401	0.396	0.454	0.362
	$SG01_{SZ}$	0.639	0.707	0.045	0.213	0.665	0.753	0.919	0.983	0.764	0.477	0.630	0.259
	$SG01_{PZ}$	0.659	0.696	0.041	0.623	0.683	0.769	0.961	1.024	0.823	0.501	0.674	0.249

D.3 Kurtosis

Table D.4: Kurtosis value from acceleration data

	Sensors	Environemental condition											
		1	2	3	4	5	6	7	8	9	10	11	12
Bridge	$B01_{SX}$	2.788	3.114	2.827	3.340	3.201	3.158	2.741	2.832	3.049	3.248	2.810	3.049
	$B01_{SY}$	2.969	2.900	3.054	4.151	3.227	3.030	3.138	2.723	2.874	2.753	2.892	2.891
	$B01_{SZ}$	2.987	2.947	2.846	3.381	2.998	2.970	2.891	3.046	3.190	3.091	3.099	2.997
	$B02_{PZ}$	3.541	4.787	65.820	3.540	6.959	5.336	6.059	5.246	8.221	3.582	3.920	2.996
Deck 8	$D801_{PY}$	3.079	5.383	3.065	3.225	6.307	5.433	5.064	5.995	4.887	4.504	3.478	3.178
	$D801_{PZ}$	3.149	5.073	3.074	3.742	6.440	5.745	4.639	5.479	4.476	3.471	3.349	3.010
Deck 7	$D701_{SY}$	2.990	3.857	2.548	3.617	5.434	5.844	4.319	4.236	20.954	3.400	3.299	3.086
	$D701_{SZ}$	3.402	4.922	4.744	3.628	14.446	5.428	6.272	5.983	7.925	3.482	3.844	3.018
Chain locker	$CL01_{SZ}$	2.813	3.060	2.002	3.561	3.256	2.995	2.822	2.960	3.213	3.263	2.910	2.865
	$CL02_{0Y}$	2.984	2.792	2.606	3.624	3.250	3.372	3.326	2.917	3.539	2.977	2.865	2.963
	$CL03_{PZ}$	2.814	3.108	2.685	3.559	3.294	2.993	2.824	3.045	3.296	3.350	2.900	2.887
Chefs room deck 7	$CR01_{SY}$	3.016	3.399	4.258	3.024	3.217	3.132	2.956	3.164	3.024	3.402	3.127	3.402
Deck 4	$CR01_{SZ}$	3.656	4.871	2.897	3.478	7.380	5.969	6.833	5.710	9.482	3.711	4.222	3.185
	$XX01_{0Z}$	2.736	2.892	1.648	2.567	2.971	3.107	3.354	3.715	3.306	2.704	3.009	2.216
Cargo hold	$CH01_{PZ}$	3.087	4.060	3.315	3.511	4.540	3.942	4.154	3.965	5.100	3.623	3.339	2.950
	$CH02_{PZ}$	2.984	3.947	2.513	3.762	3.926	3.543	3.657	3.516	4.567	3.668	3.249	2.898
	$CH03_{SZ}$	3.082	4.009	2.650	3.440	5.489	4.491	4.658	4.281	5.859	3.469	3.307	2.937
	$CH04_{SZ}$	3.002	3.933	2.773	3.454	3.836	3.452	3.750	3.660	4.810	3.343	3.196	2.836
Engine store	$ES01_{SZ}$	3.193	3.603	2.836	3.391	5.088	5.918	4.249	4.840	3.908	3.947	3.394	3.105
Fresh water	$FW01_{PZ}$	3.114	3.674	2.517	3.417	5.064	6.124	4.237	4.604	3.995	3.659	3.410	3.007
Stern thruster room	$ST01_{SZ}$	3.146	3.751	2.341	3.596	4.884	4.848	4.362	4.008	4.578	3.383	3.291	3.060
	$ST02_{PZ}$	3.177	3.789	3.292	3.616	6.717	4.751	4.342	4.041	4.616	3.310	3.281	3.071
Steering gear room	$SG02_{SZ}$	3.716	6.354	1.917	3.594	14.977	42.555	7.728	7.250	7.291	4.105	3.619	3.505
	$SG02_{SY}$	3.218	4.056	3.906	3.512	4.814	4.557	4.413	4.959	4.060	3.350	3.396	3.299
	$SG01_{SX}$	14.792	16.932	1.705	3.192	9.014	18.577	4.659	6.982	7.176	3.601	4.350	2.665
	$SG01_{SY}$	3.099	3.070	3.108	4.007	3.011	2.829	3.388	2.916	2.731	3.041	3.234	3.235
	$SG01_{SZ}$	2.927	3.153	2.385	3.618	3.157	3.377	2.955	2.932	3.129	3.149	2.973	2.992
	$SG01_{PZ}$	2.982	3.244	2.256	2.482	3.087	3.339	3.046	2.913	3.108	3.228	2.988	2.997

D.4 Skewness

Table D.5: Skweness value from acceleration data

	Sensors	Environemental condition											
		1	2	3	4	5	6	7	8	9	10	11	12
Bridge	$B01_{SX}$	-0.02	-0.15	0.21	-0.09	-0.37	-0.37	-0.18	-0.20	-0.16	-0.03	-0.03	-0.14
	$B01_{SY}$	-0.03	-0.02	-0.20	-0.04	0.01	-0.03	-0.08	-0.02	0.00	-0.16	-0.10	-0.10
	$B01_{SZ}$	-0.08	-0.02	0.40	0.05	0.01	0.02	-0.03	0.02	-0.07	-0.05	-0.04	0.00
	$B02_{PZ}$	0.18	0.10	0.91	0.01	-0.03	-0.10	-0.12	-0.08	-0.02	0.04	0.08	0.01
Deck 8	$D801_{PY}$	0.05	-0.11	-0.16	0.00	0.05	-0.12	0.13	0.10	0.26	0.04	0.03	-0.05
	$D801_{PZ}$	-0.04	-0.12	-0.69	0.04	-0.12	-0.02	-0.23	-0.37	-0.22	-0.02	-0.02	0.05
Deck 7	$D701_{SY}$	0.09	-0.01	0.10	0.00	0.25	0.03	0.26	0.15	-0.03	0.07	0.05	-0.01
	$D701_{SZ}$	0.15	0.13	0.14	0.05	-0.01	-0.21	0.02	0.02	0.09	0.13	0.20	0.02
Chain locker	$CL01_{SZ}$	-0.08	0.03	-0.13	-0.01	0.26	0.24	0.05	0.08	0.04	-0.08	-0.04	0.03
	$CL02_{0Y}$	-0.10	-0.09	-0.07	-0.02	0.09	-0.01	-0.01	0.02	0.10	-0.25	-0.18	-0.08
	$CL03_{PZ}$	-0.08	0.03	0.28	-0.02	0.24	0.24	0.02	0.07	0.04	-0.07	-0.04	0.06
Chefs room deck 7	$CR01_{SY}$	0.12	0.13	0.07	0.03	0.22	-0.10	0.11	0.22	0.09	0.25	0.15	0.37
	$CR01_{SZ}$	0.03	0.08	0.17	-0.01	-0.08	-0.22	-0.10	-0.10	-0.01	-0.07	-0.06	0.01
Deck 4	$XX01_{0Z}$	0.00	-0.01	0.02	0.00	-0.04	-0.03	-0.06	-0.13	-0.06	0.02	0.02	0.02
Cargo hold	$CH01_{PZ}$	0.30	0.31	-0.26	0.02	-0.17	-0.21	0.07	0.01	0.24	0.16	0.18	0.06
	$CH02_{PZ}$	0.32	0.38	-0.05	-0.02	-0.19	-0.24	0.19	0.12	0.35	0.19	0.19	0.06
	$CH03_{SZ}$	0.27	0.14	-0.06	0.03	-0.11	-0.11	-0.08	-0.10	0.09	0.14	0.15	0.03
	$CH04_{SZ}$	0.33	0.37	-0.10	-0.02	-0.19	-0.25	0.18	0.16	0.41	0.28	0.24	0.05
Engine store	$ES01_{SZ}$	0.02	-0.11	-0.01	0.03	-0.14	0.00	-0.23	-0.34	-0.12	-0.02	-0.06	0.03
Fresh water	$FW01_{PZ}$	0.06	-0.10	0.09	-0.01	-0.23	-0.02	-0.06	-0.23	-0.13	0.07	0.11	0.03
Stern thruster room	$ST01_{SZ}$	0.16	0.24	-0.07	0.00	0.23	0.38	0.33	0.28	0.24	0.18	0.19	0.08
	$ST02_{PZ}$	0.16	0.24	0.12	0.00	0.16	0.39	0.35	0.29	0.25	0.19	0.20	0.07
Steering gear room	$SG02_{SZ}$	0.23	0.33	0.10	0.07	0.57	1.99	0.44	0.28	0.24	0.06	0.19	0.07
	$SG02_{SY}$	0.07	0.05	0.12	-0.02	0.33	0.22	0.36	0.26	0.32	0.07	0.22	0.02
	$SG01_{SX}$	2.75	2.25	-0.03	-0.03	2.55	3.07	0.34	0.90	2.08	0.04	1.62	1.15
	$SG01_{SY}$	-0.04	0.02	-0.24	-0.07	-0.02	-0.07	-0.21	-0.21	-0.03	-0.05	-0.07	-0.31
	$SG01_{SZ}$	-0.07	-0.11	0.27	0.07	-0.25	-0.29	-0.16	-0.11	-0.11	-0.08	-0.07	-0.09
	$SG01_{PZ}$	-0.06	-0.12	0.19	-0.08	-0.23	-0.29	-0.18	-0.11	-0.11	-0.04	-0.10	-0.12

D.5 Mean value

Table D.6: Mean value from accelerometers

	Sensors	Environemental condition											
		1	2	3	4	5	6	7	8	9	10	11	12
Bridge	$B01_{SX}$	0.1	0.1	0.0	0.0	0.0	0.0	0.1	0.0	0.1	0.0	0.1	0.1
	$B01_{SY}$	-0.3	-0.2	-0.3	-0.4	-0.4	-0.2	-0.2	-0.3	-0.4	-0.1	-0.2	-0.3
	$B01_{SZ}$	10.0	10.0	9.9	9.9	10.0	9.9	9.9	10.0	9.9	10.0	10.0	10.0
	$B02_{PZ}$	0.0	0.0	0.0	0.0	0.0	0.0	0.0	0.0	0.0	0.0	0.0	0.0
Deck 8	$D801_{PY}$	0.0	0.0	0.0	0.0	0.0	0.0	0.0	0.0	0.0	0.0	0.0	0.0
	$D801_{PZ}$	0.0	0.0	0.0	0.0	0.0	0.0	0.0	0.0	0.0	0.0	0.0	0.0
Deck 7	$D701_{SY}$	0.0	0.0	0.0	0.0	0.0	0.0	0.0	0.0	0.0	0.0	0.0	0.0
	$D701_{SZ}$	0.0	0.0	0.0	0.0	0.0	0.0	0.0	0.0	0.0	0.0	0.0	0.0
Chain locker	$CL01_{SZ}$	9.9	9.9	9.9	9.9	9.9	9.9	9.9	9.9	9.9	9.9	9.9	9.9
	$CL02_{0Y}$	-0.3	-0.2	-0.3	-0.3	-0.4	-0.2	-0.2	-0.3	-0.4	-0.1	-0.2	-0.3
	$CL03_{PZ}$	10.2	10.1	10.0	10.0	10.1	10.1	10.1	10.1	10.1	10.1	10.1	10.2
Chefs room deck 7	$CR01_{SY}$	0.0	0.0	0.0	0.0	0.0	0.0	0.0	0.0	0.0	0.0	0.0	0.0
	$CR01_{SZ}$	0.0	0.0	0.0	0.0	0.0	0.0	0.0	0.0	0.0	0.0	0.0	0.0
Deck 4	$XX01_{0Z}$	0.0	0.0	0.0	0.0	0.0	0.0	0.0	0.0	0.0	0.0	0.0	0.0
Cargo hold	$CH01_{PZ}$	0.0	0.0	0.0	0.0	0.0	0.0	0.0	0.0	0.0	0.0	0.0	0.0
	$CH02_{PZ}$	0.0	0.0	0.0	0.0	0.0	0.0	0.0	0.0	0.0	0.0	0.0	0.0
	$CH03_{SZ}$	0.0	0.0	0.0	0.0	0.0	0.0	0.0	0.0	0.0	0.0	0.0	0.0
	$CH04_{SZ}$	0.0	0.0	0.0	0.0	0.0	0.0	0.0	0.0	0.0	0.0	0.0	0.0
Engine store	$ES01_{SZ}$	0.0	0.0	0.0	0.0	0.0	0.0	0.0	0.0	0.0	0.0	0.0	0.0
Fresh water	$FW01_{PZ}$	0.0	0.0	0.0	0.0	0.0	0.0	0.0	0.0	0.0	0.0	0.0	0.0
Stern thruster room	$ST01_{SZ}$	0.0	0.0	0.0	0.0	0.0	0.0	0.0	0.0	0.0	0.0	0.0	0.0
	$ST02_{PZ}$	0.0	0.0	0.0	0.0	0.0	0.0	0.0	0.0	0.0	0.0	0.0	0.0
Steering gear room	$SG02_{SZ}$	0.0	0.0	0.0	0.0	0.0	0.0	0.0	0.0	0.0	0.0	0.0	0.0
	$SG02_{SY}$	0.0	0.0	0.0	0.0	0.0	0.0	0.0	0.0	0.0	0.0	0.0	0.0
	$SG01_{SX}$	-0.6	-0.7	-0.7	-0.7	-0.6	-0.7	-0.7	-0.7	-0.6	-0.7	-0.6	-0.6
	$SG01_{SY}$	-0.1	0.0	-0.1	-0.1	-0.2	0.0	0.0	-0.1	-0.2	0.1	-0.1	-0.1
	$SG01_{SZ}$	9.8	9.8	9.8	9.8	9.8	9.8	9.8	9.8	9.8	9.8	9.8	9.8
	$SG01_{PZ}$	9.4	9.4	9.4	7.7	9.4	9.0	9.1	9.4	9.5	9.4	9.4	9.4

Appendix E

Energy content

E.0.1 Ratio Between 2-node and 3-node Vibration Mode

Table E.1: Energy ratio between 2-node and 3-node bending mode. 2-node bending mode is calculated with the frequency range 1.9 to 2.4 and the 3-node bending between 3.7 to 4.2Hz

Sensors	Date					
	20/07 11:09	21/07 15:18	27/07 16:24	29/07 15:49	29/07 19:59	30/07 13:09
$B01_{SZ}$	15.08	11.03	5.79	7.49	9.60	9.63
$B02_{PZ}$	170.66	169.30	153.20	109.28	127.51	134.01
$D801_{PZ}$	0.26	0.10	0.02	0.09	0.11	0.08
$D701_{SZ}$	394.78	425.60	232.74	149.01	184.43	217.23
$CL01_{SZ}$	10.48	6.37	2.41	4.26	5.24	4.80
$CL03_{PZ}$	9.48	5.77	2.22	3.81	4.70	4.39
$CR01_{SZ}$	255.97	204.14	113.95	135.36	167.62	173.08
$XX01_{0Z}$	3.92	1.90	0.73	1.16	1.50	1.32
$CH01_{PZ}$	2.45	1.64	0.69	1.11	1.32	1.30
$CH02_{PZ}$	4.09	1.94	0.76	1.52	1.87	1.39
$CH03_{SZ}$	3.03	1.97	0.94	1.38	1.69	1.69
$CH04_{SZ}$	4.00	1.87	0.72	1.26	1.62	1.31
$ES01_{SZ}$	0.48	0.17	0.01	0.08	0.11	0.04
$FW01_{PZ}$	0.73	0.33	0.12	0.22	0.31	0.22
$ST01_{SZ}$	94.79	23.70	7.06	10.59	12.86	13.53
$ST02_{PZ}$	92.60	22.28	6.79	10.08	12.28	13.15
$SG02_{SZ}$	4.33	2.63	1.07	1.72	2.17	2.05
$SG01_{PZ}$	4.26	2.47	1.04	1.66	2.05	1.89
$SG01_{SZ}$	3.93	2.21	0.95	1.47	1.83	1.77

Table E.2: Energy ratio between 2-node and 3-node bending mode. 2-node bending mode is calculated with the frequency range 1.9 to 2.4 and the 3rd bending mode between 3.7 to 4.2Hz

Sensors	Date				
	30/07 14:29	31/07 13:29	31:07 16:09	04/08 07:26	05/08 10:59
$B01_{SZ}$	6.35	9.74	6.96	12.83	10.85
$B02_{PZ}$	85.73	165.35	94.52	155.34	129.92
$D801_{PZ}$	0.05	0.10	0.10	0.17	0.42
$D701_{SZ}$	133.01	337.17	253.24	442.43	206.93
$CL01_{SZ}$	3.19	5.32	4.10	8.18	8.42
$CL03_{PZ}$	2.93	4.72	3.73	7.41	7.62
$CR01_{SZ}$	110.41	193.74	124.06	235.67	214.03
$XX01_{0Z}$	0.90	1.49	1.32	2.79	3.17
$CH01_{PZ}$	0.84	1.44	0.95	1.92	2.15
$CH02_{PZ}$	1.01	1.67	1.33	2.70	2.68
$CH03_{SZ}$	1.10	1.74	1.23	2.36	2.39
$CH04_{SZ}$	0.95	1.44	1.18	2.44	2.41
$ES01_{SZ}$	0.03	0.04	0.04	0.08	0.15
$FW01_{PZ}$	0.16	0.26	0.22	0.46	0.60
$ST01_{SZ}$	8.99	15.76	21.26	46.44	54.78
$ST02_{PZ}$	8.72	14.65	20.85	43.82	49.77
$SG02_{SZ}$	1.36	2.22	1.71	3.50	3.78
$SG01_{PZ}$	1.26	2.14	1.67	3.39	3.68
$SG01_{SZ}$	1.20	1.86	1.54	3.14	3.28

Table E.3: Power ratio of 1st bending mode/all frequencies. Signal is highpass filtered.

Sensors	Dates					
	20/07 11:09	21/07 15:18	27/07 16:24	29/07 15:49	29/07 19:59	30/07 13:09
$B01_{SZ}$	29.6	48.4	55.1	48.9	54.0	55.1
$B02_{PZ}$	69.4	81.0	86.4	89.3	87.5	83.8
$D801_{PZ}$	1.2	2.9	0.9	1.9	2.2	2.7
$D701_{SZ}$	41.1	71.1	71.0	69.4	73.9	73.7
$CL01_{SZ}$	59.1	68.1	54.1	61.4	63.0	65.3
$CL03_{PZ}$	55.2	66.2	53.7	59.9	61.7	64.2
$CR01_{SZ}$	67.9	78.0	89.1	90.8	89.0	82.3
$XX01_{0Z}$	5.1	15.0	14.2	9.2	12.0	17.7
$CH01_{PZ}$	21.3	32.6	26.0	25.3	29.2	32.7
$CH02_{PZ}$	11.9	16.8	11.5	15.0	19.4	17.6
$CH03_{SZ}$	25.1	39.0	35.1	35.4	39.5	42.1
$CH04_{SZ}$	13.0	19.5	17.5	20.0	23.2	20.6
$ES01_{SZ}$	6.4	8.1	0.5	2.8	3.6	2.2
$FW01_{PZ}$	7.0	10.9	7.0	6.3	8.2	8.7
$ST01_{SZ}$	38.2	70.3	71.1	53.5	60.8	70.1
$ST02_{PZ}$	37.9	70.1	71.5	55.1	61.2	69.8
$SG02_{SZ}$	32.8	49.3	39.1	32.5	30.7	47.0
$SG01_{PZ}$	29.5	47.0	37.7	32.9	35.4	44.1
$SG01_{SZ}$	28.1	45.8	30.2	31.4	35.0	42.8

E.0.2 Power ratio of node mode vs all frequencies

Table E.4: Power ratio of 1st bending mode/all frequencies. Signal is highpass filtered.

Sensors	Dates				
	30/07 14:29	31/07 13:29	31/07 16:09	04/08 07:26	05/08 10:59
$B01_{SZ}$	51.0	54.1	38.8	45.1	8.8
$B02_{PZ}$	82.3	82.2	79.0	81.6	65.7
$D801_{PZ}$	2.3	4.1	2.2	2.5	0.4
$D701_{SZ}$	71.1	77.0	66.0	70.5	23.4
$CL01_{SZ}$	58.3	66.9	62.2	69.9	42.6
$CL03_{PZ}$	56.8	64.8	62.0	68.6	42.8
$CR01_{SZ}$	81.5	79.6	79.4	80.3	75.0
$XX01_{0Z}$	16.6	16.8	5.4	8.8	1.0
$CH01_{PZ}$	26.6	34.1	21.9	29.0	9.4
$CH02_{PZ}$	15.5	18.4	12.0	16.7	4.1
$CH03_{SZ}$	34.6	41.0	32.4	40.3	9.4
$CH04_{SZ}$	18.3	21.9	18.6	24.0	4.3
$ES01_{SZ}$	1.8	2.0	1.6	2.4	0.4
$FW01_{PZ}$	7.3	11.2	5.2	10.3	1.3
$ST01_{SZ}$	65.9	72.3	59.6	66.9	10.1
$ST02_{PZ}$	65.4	72.2	60.8	66.9	10.7
$SG02_{SZ}$	40.6	50.8	44.2	55.8	8.8
$SG01_{PZ}$	37.9	48.8	39.5	51.0	7.4
$SG01_{SZ}$	36.4	45.7	35.5	47.0	7.0

Table E.5: Power ratio of 2nd bending mode/all frequencies. Signal is highpass filtered.

Sensors	Dates					
	20/07 11:09	21/07 15:18	27/07 16:24	29/07 15:49	29/07 19:59	30/07 13:09
$B01_{SZ}$	2.0	4.4	9.5	6.5	5.6	5.7
$B02_{PZ}$	0.4	0.5	0.6	0.8	0.7	0.6
$D801_{PZ}$	4.7	29.3	45.7	21.7	18.8	35.3
$D701_{SZ}$	0.1	0.2	0.3	0.5	0.4	0.3
$CL01_{SZ}$	5.6	10.7	22.4	14.4	12.0	13.6
$CL03_{PZ}$	5.8	11.5	24.2	15.7	13.1	14.6
$CR01_{SZ}$	0.3	0.4	0.8	0.7	0.5	0.5
$XX01_{0Z}$	1.3	7.9	19.4	7.9	8.0	13.4
$CH01_{PZ}$	8.7	19.9	37.4	22.8	22.2	25.2
$CH02_{PZ}$	2.9	8.7	15.2	9.9	10.4	12.7
$CH03_{SZ}$	8.3	19.8	37.2	25.6	23.4	24.9
$CH04_{SZ}$	3.3	10.5	24.1	15.8	14.3	15.8
$ES01_{SZ}$	13.4	48.0	62.6	36.2	33.4	48.6
$FW01_{PZ}$	9.6	32.7	57.7	28.2	26.9	39.2
$ST01_{SZ}$	0.4	3.0	10.1	5.1	4.7	5.2
$ST02_{PZ}$	0.4	3.1	10.5	5.5	5.0	5.3
$SG02_{SZ}$	7.6	18.8	36.6	18.9	14.1	22.9
$SG01_{PZ}$	6.9	19.1	36.5	19.7	17.2	23.4
$SG01_{SZ}$	7.1	20.7	31.7	21.4	19.2	24.2

Table E.6: Power ratio of 2nd bending mode/all frequencies. Signal is highpass filtered.

Sensors	Dates				
	30/07 14:29	31/07 13:29	31:07 16:09	04/08 07:26	05/08 10:59
$B01_{SZ}$	8.0	5.6	5.6	3.5	0.8
$B02_{PZ}$	1.0	0.5	0.8	0.5	0.5
$D801_{PZ}$	42.9	40.7	21.6	14.6	1.0
$D701_{SZ}$	0.5	0.2	0.3	0.2	0.1
$CL01_{SZ}$	18.3	12.6	15.2	8.5	5.1
$CL03_{PZ}$	19.4	13.7	16.6	9.3	5.6
$CR01_{SZ}$	0.7	0.4	0.6	0.3	0.4
$XX01_{0Z}$	18.5	11.3	4.1	3.1	0.3
$CH01_{PZ}$	31.8	23.7	23.1	15.1	4.4
$CH02_{PZ}$	15.3	11.0	9.0	6.2	1.5
$CH03_{SZ}$	31.4	23.6	26.3	17.1	3.9
$CH04_{SZ}$	19.3	15.2	15.8	9.8	1.8
$ES01_{SZ}$	51.7	51.9	37.7	28.8	2.6
$FW01_{PZ}$	45.9	43.6	23.4	22.1	2.1
$ST01_{SZ}$	7.3	4.6	2.8	1.4	0.2
$ST02_{PZ}$	7.5	4.9	2.9	1.5	0.2
$SG02_{SZ}$	29.9	22.8	25.8	15.9	2.3
$SG01_{PZ}$	30.2	22.9	23.7	15.1	2.0
$SG01_{SZ}$	30.4	24.5	23.0	15.0	2.1

E.0.3 Cargo Hold Comparison

Table E.7: Power ratio of 2-node for each recording compared to reference condition, set as recording 1.

	Sensor			
Environmental Condition	$CH01_{PZ}$	$CH02_{PZ}$	$CH03_{SZ}$	$CH04_{SZ}$
2/1	4.65	3.90	4.47	3.98
4/1	6.70	5.54	7.03	5.42
5/1	3.36	3.18	3.37	3.12
6/1	4.50	4.55	4.60	4.44
7/1	8.79	7.44	8.80	7.17
8/1	8.66	7.90	8.72	7.67
9/1	6.83	5.88	6.64	5.80
10/1	1.37	1.29	1.41	1.24
11/1	1.90	1.82	1.86	1.75
12/1	0.17	0.14	0.15	0.13

Table E.8: Power ratio of 3-node for each recording compared to reference condition, set as recording 1.

	Sensor			
Environmental Condition	$CH01_{PZ}$	$CH02_{PZ}$	$CH03_{SZ}$	$CH04_{SZ}$
2/1	6.93	8.23	6.90	8.53
4/1	23.65	29.93	22.56	29.91
5/1	7.41	8.56	7.41	9.87
6/1	8.38	9.96	8.26	10.94
7/1	16.59	21.85	15.80	21.85
8/1	25.35	32.06	23.99	32.20
9/1	11.64	14.35	11.60	16.08
10/1	3.54	3.98	3.47	4.20
11/1	2.43	2.75	2.39	2.87
12/1	0.19	0.21	0.19	0.22

Tor Magnus Konradsen Aarskog

NTNU
Norwegian University of
Science and Technology